UNIVERSITY OF SOUTHAMPTON
Faculty of Engineering, Science and Mathematics
School of Engineering Sciences

Thermoelastic stress analysis of laminated composite materials

by

Shamala Sambasivam

Thesis for the degree of Doctor of Philosophy

October 2009

UNIVERSITY OF SOUTHAMPTON

ABSTRACT

FACULTY OF ENGINEERING, SCIENCE AND MATHEMATICS
SCHOOL OF ENGINEERING SCIENCES

Doctor of Philosophy

THERMOELASTIC STRESS ANALYSIS OF LAMINATED COMPOSITE MATERIALS

by Shamala Sambasivam

In this work thermoelastic stress analysis (TSA) is used to obtain quantitative stress/ strain data from a variety of multi-directional laminated composites. In order to interpret the thermoelastic signal correctly the source of the thermoeleastic response has been investigated in detail. In this thesis four possible routines to extract quantitative stress/strain information from thermoelastic data have been explored. A set of carefully selected glass/epoxy composite specimens with designated stacking sequences provided a scheme to identify the source and nature of the thermoelastic response. All of the material properties of the composite laminate were obtained experimentally, to aid an accurate assessment of each routine. The variation in the stress experienced by the laminate in the surface resin layer and ply by ply there after leads to large variations in the temperature change through the thickness. The thermoelastic measurements from different laminates revealed a local non-adiabatic condition within the layered medium. Therefore, the implication of applied loading frequency on the heat conduction properties of the laminates was studied. Based on the experimental observation from a representative specimen, numerical models have been developed to understand the nature of the heat transfer in the glass/ epoxy material considered in this work. An analysis of the effect of holes in a variety of laminated components is presented to provide stress concentration factors (SCF's) based on TSA data. The conventional, orthotropic surface ply model most often used for thermoelastic stress analysis of composite material is revisited in order to elucidate the invariant nature of the equation. This is an important base for the analysis of structures which are better notated in coordinate system other than Cartesian, or as ratio of thermoelastic measurements in two different coordinate systems. The nature of the thermoelastic response in the presence of the in-plane stress gradient is investigated with the aid of numerical and analytical models. An introductory work for quantifying the SCF's around pin-loaded holes in laminated composite based on TSA measurements is also presented. The work presented in this thesis provides a step forward in the application of TSA to the composite materials in a quantitative manner.

Contents

List of Figures

List of Tables

Declaration of Authorship

I, Shamala Sambasivam, declare that this thesis titled, 'Thermoelastic stress analysis of laminated composite materials' and the work presented in the thesis are both my own, and have been generated by me as the result of my own original research. I confirm that:

- this work was done wholly or mainly while in candidature for a research degree at this University;
- where any part of this thesis has previously been submitted for a degree or any other qualification at this University or any other institution, this has been clearly stated;
- where I have consulted the published work of others, this is always clearly attributed;
- where I have quoted from the work of others, the source is always given. With the exception of such quotations, this thesis is entirely my own work;
- I have acknowledged all main sources of help;
- where the thesis is based on work done by myself jointly with others, I have made clear exactly what was done by others and what I have contributed myself;
- parts of this work have been published as: (Appendix A).

Signed:

Date:

Acknowledgements

First and foremost I offer my sincere gratitude to my supervisor, Prof. Janice Barton, who has supported me throughout my thesis with her advice and knowledge. One simply could not wish for a friendlier supervisor than Dr. Simon Quinn, without his continuous encouragement and support, this thesis would not have been completed.

In the various laboratories I have been assisted in many ways by technicians, Eric Roszkowiak, David Beckett and Chris for producing test specimens with consistent quality. The School of engineering sciences has provided the financial support and facilities that needed to produce and complete my thesis and the EPSRC has funded my studies.

I am thankful to the TSA users for organising group meetings and generating fruitful ideas and discussion on using 'Cedip system'; special thanks to Richard Fruehmann. In my daily work I have been blessed with a friendly and cheerful group of fellow students; who provided healthy discussions about science and engineering in general and helped me regain some sort of fitness: healthy mind and body.

I wish to thank all my family members and close friends for providing a loving and caring environment. Special thanks to Sairam, Sevvearl, Dilan, Lingesh and Hashanthy for helping me get through the difficult times and for all the emotional support, entertainment and care they provided.

Lastly, and most importantly, I wish to thank my parents. They raised me, supported me, taught me, and loved me. To them I dedicate this thesis.

Thanks everyone.

Abbreviations

AP	**A**ngle **P**ly
ASTM	**A**merican **S**ociety for **T**esting **M**aterial
CFRP	**C**arbon **F**ibre **R**einforced **P**olymer
CLPT	**C**lassical **L**aminate **P**late **T**heory
CP	**C**ross **P**ly
CTE	**C**oefficient of **T**hermal **E**xpansion
DIC	**D**igital **I**mage **C**orrelation
DSC	**D**igital **S**canning **C**alorimetry
ESPI	**E**lectronic **S**peckle **P**attern **I**nterferometry
FDM	**F**inite **D**ifference **M**ethod
FEM	**F**inite **E**lement **M**ethod
FFT	**F**ast **F**ourier **T**ransform
FRP	**F**ibre **R**einforced **P**olymer
GFRP	**G**lass **F**ibre **R**einforced **P**olymer
IR	**I**nfra **r**ed
MATLAB	**MAT**rix **LAB**oratory
NDT	**N**on **D**estructive **T**esting
QI	**Q**uasi **I**sotropic
SCF	**S**tress **C**oncentration **F**actor
SPATE	**S**tress **P**attern **A**nalysis by measurement of **T**hermal **E**missions
TSA	**T**hermoelastic **S**tress **A**nalysis
UD	**U**ni **D**irectional

Symbols

$[a]$	Extensional compliance matrix	-
c	Speed of light	ms^{-1}
n	Temperature correction power index	-
k	Stress concentration factor	-
A	Isotropic calibration constant	MPaU^{-1}
$[A]$	Extensional stiffness matrix	-
B'	Stefan Boltzmann constant	$\mathrm{Wm}^{-2}\mathrm{K}^{-2}$
C_1	First radiation constant	Wm^2
C_2	Second radiation constant	mK
C_ϵ	Specific heat at constant strain	$\mathrm{Jkg}^{-1}\mathrm{K}^{-1}$
C_p	Specific heat at constant pressure	$\mathrm{Jkg}^{-1}\mathrm{K}^{-1}$
E	Young's modulus	MPa
G	Shear modulus	MPa
K	Thermoelastic constant	MPa
M	Mass	Kg
N_b	Photon flux	$\mathrm{phs}^{-1}\mathrm{m}^{-2}\mathrm{sr}^{-1}$
P	Load	N
Q_{ij}	Reduced stiffness terms	-
R	Temperature correction factor	-
S	Thermoelastic signal	U
T	Ambient temperature	K
V_o	Volume	m^3
α	Coefficient of linear thermal expansion	$^o\mathrm{C}^{-1}$
ε	Direct strain	-
η	Emissivity	-
γ	Shear strain	-
κ	Thermal diffusivity	$\mathrm{m}^2\mathrm{s}^{-1}$
λ	Wavelength	m

ρ	Density	kgm^{-3}
σ	Stress	MPa
$\sigma_x + \sigma_y$	Sum of principal stresses	MPa
$\sigma_1 + \sigma_2$	Sum of stresses in the principal material direction	MPa
τ	Shear stress	MPa
ν	Poisson's ratio	-
Δ	Change in	-
Φ_b	Spectral radiant power	Wm^{-2}

Dedicated to my parents...

Chapter 1

Introduction

1.1 Background

As composite manufacturing technologies have advanced, the use of composites for engineering components has increased significantly. The introduction of composite components can reduce weight and has the potential to reduce the through life cost of the component. Although corrosion is less pronounced in structures made of composites, it should be considered that repairing these structures can be costly. In using composite materials, a typical design objective is to meet the mechanical performance (i.e. strength and stiffness) of the same structure made of other materials (e.g. metals) with improved characteristics such as weight reduction. Advanced polymer composite systems composed of various fibre forms and matrix types, are used to meet specific service requirements. Their overall performance is influenced by the constituent materials, their distribution and the interaction between them. To fully exploit the potential of composite material, it is extremely important to understand and develop procedures for analysing the mechanical behaviour of composite material.

Most of the composite laminates used today are symmetrical and have orthotropic lay ups. The differently oriented layers are stacked in a specific sequence to tailor the properties of the laminate to best withstand the applied load, therefore enhancing weight reduction. Composite materials also can be formed into single, continuous parts (unlike their metallic counterparts), therefore not only reducing the number of parts required for a component, but also reducing the need for fasteners and joints. The unique characteristics of composite materials also provide some significant challenges in developing safe, strong structures. While the primary concerns in metallic structures typically relate to crack growth and corrosion, damage such as delamination and fibre breakage are major concern in fibre reinforced polymer (FRP) matrix composites.

FRP composites laminates have been successfully incorporated into the design of lightweight, high-performance structures (e.g. marine and aircraft components) in recent years, enabled by extensive laboratory testing and advances in computational methods. Efforts continue to increase the need for designs with better performance, reliability, and durability requirements and drive composite design to higher levels of structural efficiency. Conventional strain measurement techniques, such as resistance strain gauges and photoelastic coatings provide a means for characterisation of composite materials for design purposes. In addition, more recent full-field stress and strain analysis techniques such as digital image correlation (DIC) and Electron Speckle Pattern Interferometry (ESPI) are being used increasingly in a variety of fields including assessment of composite material. Thermoelastic stress analysis (TSA) can be used to give equivalent full-field data and is the technique being studied in the current work. Compared to numerous applications involving isotropic solids, the practical problems solved in composite material by TSA are mostly limited to qualitative applications. This is due generally to a lack of a thorough understanding of the thermoelastic behaviour of composite material. Therefore, this work is aimed at identifying the source and prominent factors influencing the thermoelastic response from laminated composites for successfully implementing a routine for extracting quantitative full-field stress data from the thermal measurements.

Virtually every large-scale primary composite structure contains joints. Joints are required to adhere to manufacturing constraints and to meet requirements related to functionality of the structure and part replacement. Mechanically fastened joints have been found to be well suited to composite structures as these joints are relatively inexpensive to manufacture and can be easily disassembled [1]. The design and testing of joints is therefore important because the load bearing capacity of a joint is critical for full exploitation of high performance composite structures. The presence of discontinuities, such as cut-outs and joints, which are common in actual structures, increase the difficulty in accurately predicting detailed local stress distributions, especially when the component is manufactured from a composite material. However, this information is vital as it provides the strategy for efficient design, as well as providing insight into damage and fracture initiators. In most instances numerical techniques are preferred because experimental approaches are expensive in comparison. However, full-field experimental techniques are vital to assess the validity and accuracy of numerical approaches.

TSA is an experimental technique based on IR thermography, where the small temperature changes resulting from a change in elastic stress are obtained by measuring the change in infrared photon emission [2]. It has advantages over other experimental techniques since only minimal surface preparation (i.e. coatings, grids or speckle patterns are not needed) is required for obtaining full-field stress data with spatial resolution of 4 μm [3]. The resulting temperature variations at the component surface are measured with

commercially available infrared (IR) cameras, which have sensitivities in the order of 1 mK. The underlying physics is that under adiabatic conditions, changes in the stresses within the elastic region produce reversible conversion between mechanical and thermal forms of energy. The standard TSA procedure utilises a cyclic load to prevent heat transfer within test parts to ensure the temperature change occurs adiabatically [4]. The near real time nature of TSA also makes it suitable for monitoring the fatigue behaviour of composite joints [5]. It is convenient to apply the method to structures experiencing dynamic loading and it has great potential as a design or theoretical model validation tool because there are a limited amount of full-field experimental data available for this complex and difficult stress analysis problem [6, 7].

Investigations into applying TSA to composites were instigated by Stanley and Chan [8], who modified the original thermoelastic equation for isotropic material for orthotropic materials and showed the temperature change as a function of stress change to be:

$$\Delta T = -\frac{T}{\rho C_p}(\alpha_1 \Delta\sigma_1 + \alpha_2 \Delta\sigma_2) \tag{1.1}$$

where C_p is the specific heat at constant pressure, T is the ambient temperature, ρ is the density, α_1 and α_2 are the coefficients of thermal expansion in the principal material directions and σ_1 and σ_2 are the direct stresses in the principal material directions.

Later, the possibility of a influence from the surface resin rich layer as a consequence of the manufacturing process in glass fibre reinforced composite (GFRP) was suggested by Cunningham et al. [9]. Some authors have identified the possibility of using the surface layer as strain witness and to obtain quantitative TSA data [10, 11, 12]. In this work, a full evaluation of the strain witness approach is carried out and it is shown that this may not be appropriate for the type of material used [13] and alternative approaches are identified and investigated further.

The findings have been incorporated in developing an experimental procedure for assessing the stresses in the vicinity of holes and pin loaded joints in laminated composite components.

1.2 Aims and Objectives

The overall aim of this work is to develop the TSA technique so that it can be used quantitatively in the analysis of laminated composite structures. Of particular interest are the stress distribution of circular cut-outs that facilitate mechanical fasteners. To

achieve this aim significant challenges need to be overcome; these form the objectives of this work and are as follows:

- Determine the source of the thermoelastic response and assess the prominent factors influencing the thermoelastic response from a multi-directional laminated composite material.
- Devise a technique or routine to extract quantitative stress/strain data from TSA data obtained from composite laminates.
- Investigate the non-adiabatic thermoelastic effect and the influence of the periodic heat diffusion through a layered medium on the thermoelastic temperature change measured on the surface of a laminated composite material.
- Complete characterisation of the mechanical and physical material properties of multi-directional laminated composite material to theoretically define its thermoelastic response.
- Obtain experimentally the stress/ strain distribution around holes in laminated composite plates using thermoelastic stress analysis.
- Investigate effects of both in-plane and through thickness temperature gradients on the thermoelastic response in the neighbourhood of holes in composite laminate.
- Devise approaches to relate the thermoelastic data to finite element models and analytically derived results to provide a means for direct comparison and validation.
- Provide an initial insight into application of TSA to composite pin loaded joints by defining an experimental approach that is validated using isotropic metallic materials.

1.3 Novelty

After conducting a thorough literature review, it is evident that studies conducted using TSA for quantitative stress analysis of realistic composite components are limited. There is no prior work on mechanically fastened composite joints and most studies are limited to composite coupons/strips. It is also notable that in many cases the anisotropic properties of composite materials contributing to differences in mechanical and thermoelastic properties have not been fully considered. Although large variations arise as a result of the material palettes available for composite materials no real effort has been taken

to characterise these materials in order to obtain the physical properties that are vital in verifying the thermoelastic theory. Most importantly, is the means of obtaining the coefficient of thermal expansion.

In this work, all the factors that influence the thermoelastic response of composite materials are considered. This includes consideration of extension shear coupling which has been neglected in the previous quantitative work on orthotropic composites.

The influence of the periodic heat diffusion between the layered medium on the thermoelastic response is explored using the finite difference method. All the necessary material properties are obtained experimentally, including the definition of procedures to obtain the coefficient of thermal expansion. The findings of this work provide a complete, definitive and clearer procedure for quantitative stress data for composite components.

This procedure is then applied to laminate with cut-outs, sucessfully quantifying the stress concentration factor (SCF) around circular holes. A new way of presenting SCF is formulated in order to use TSA as a validation tool of numerical and analytical models. Also, initial investigation on pin-loaded joints in isotropic and composite structures are conducted.

1.4 Content of thesis

Chapter 2 provides a detailed review of the state of the art in TSA. A clear description of the current standing of the theory, equipment, operational procedure, developments of the technique and practical applications of TSA is provided. The advantages and suitability of the experimental technique are highlighted in this chapter. The evolution of the conception, theories and applications of TSA to isotropic, orthotropic and woven composites are described, along with identification of the gaps in knowledge that require further exploration.

Chapter 3 concentrates on the specific theoretical consideration required to apply TSA successfully to composite materials. Two clear routes adopted by previous researchers to develop calibration techniques based on the orthotropic nature of the composite material are described. One utilises the orthotropic surface ply and the other considers the presence of a surface resin rich region (isotropic behaviour). Additionally two further cases are considered, the first in which the CTE's and laminate stresses are assumed to provide the thermoelastic response from the laminate as a whole (i.e. global response) and in the second case CTE's of the laminate are coupled with the stresses in the surface ply. The choice of material selection required to capture the distinct assumptions made in deriving each theoretical model is described in this chapter.

Chapter 4 outlines the experimental procedures to fully characterise the mechanical and physical properties of composite materials. The associated error analysis is presented to show the uncertainty in the measurements.

The comparison between the proposed theoretical models and thermoelastic measurements are given in Chapter 5. The suitability and limitations of the calibration techniques are highlighted in this chapter. The applied loading frequency and the associated heat transfer problem is discussed based on heat transfer analysis conducted using a simple FE model and periodic heat transfer analysis performed using the Finite Difference Method.

In Chapter 6 details of the stress concentrations in laminated composites, focusing on circular cut-outs is provided. The underlying theory and development of the research on laminated composites with holes is presented. A comparison of the SCF_{TSA} obtained from experimental, analytical and FEA data for laminates with different fibre lay-ups is reported in this section.

Chapter 7 gives detail of the factors that influence the design and analysis of mechanical fasteners in composite joints. The detailed literature review demonstrates the crucial need for further full-field experimental data to enable the development of more reliable design procedures and further development of analytical and computational models. TSA of both isotropic and composite pin-loaded joints are presented. Finite element analysis has been used to assist the interpretation and validation of the experimental data.

Future work and the overall conclusions derived from this research work are provided in Chapter 8.

Chapter 2

Thermoelastic stress analysis

2.1 Theory

Thermoelastic stress analysis (TSA) is based on the measurement of the temperature changes that occur when an external load is applied to a component as a result of a reversible effect [14]. When a structure is loaded within the elastic range the resulting temperature profile can be related to the surface stress state. To acquire this, the standard TSA procedure utilises a cyclic load to prevent heat transfer within test parts and ensure the temperature change is reversible (adiabatic).

Themoelasticity is a general term used to describe the change in stresses within the elastic limit that occur as a result of reversible conversions between mechanical and thermal forms of energy. The theoretical basis for thermoelasticity was established in the 19th century [14, 15], although it did not find practical application in experimental stress analysis until the advent of highly sensitive IR detectors, which have the ability to measure the small temperature changes resulting from the thermoelastic effect [16]. For isotropic materials the use of TSA is well documented, i.e. [17, 18, 19]. The relationship between the small temperature changes, caused by the change in the stress state of a homogeneous, linear elastic, isotropic solid can be derived [16] from the laws of the thermodynamics in the form:

$$\Delta T = -\frac{T}{\rho C_\varepsilon}\frac{\partial \sigma}{\partial T}\varepsilon + \frac{Q}{\rho C_\varepsilon} \tag{2.1}$$

where T is the absolute temperature of the material, C_ε is the specific heat at constant strain, ρ is the density, σ is the stress change tensor, ε is the strain change tensor and Q is the heat input.

The partial derivatives in Equation 2.1 can be obtained from the stress strain temperature relationships for an isotropic material and the second term in the equation can be neglected for adiabatic conditions (Q=0). By assuming that E and ν are independent of temperature the equation reduces to:

$$\Delta T = -\frac{E\alpha T}{\rho C_\epsilon (1-2\nu)}(\epsilon_x + \epsilon_y + \epsilon_z) \tag{2.2}$$

where E is Young's modulus, α is the coefficient of linear thermal expansion and ν is Poisson's ratio.

The relationship between thermal stress and strains in an isotropic elastic solid is given by the following equation [20]:

$$\epsilon_x = \frac{1-2\nu}{E}(\sigma_x + \sigma_y + \sigma_z) + 3\alpha\Delta T \tag{2.3}$$

The relationship between the specific heat at constant strain (C_ε) and the specific heat at constant pressure (C_p) is given in [21] as:

$$C_\epsilon = C_p - \frac{3E\alpha^2 T}{\rho(1-2\nu)} \tag{2.4}$$

Substituting for $\sum \epsilon$ from Equation 2.3 and C_ϵ from Equation 2.4 into Equation 2.2 gives:

$$\Delta T = -\frac{\alpha}{\rho C_p} T(\sigma_x + \sigma_y + \sigma_z) \tag{2.5}$$

$\Delta\sigma_z$ can be considered as zero because the measurements are taken using an IR detector, which is a surface technique where plane stress conditions apply. The quantity $\frac{\alpha}{\rho C_p}$ is known as the thermoelastic constant, K, so that the temperature change, ΔT, can be expressed as:

$$\Delta T = -KT\Delta(\sigma_x + \sigma_y) \tag{2.6}$$

where $\Delta\sigma_x$ and $\Delta\sigma_y$ are the changes in the principal stresses.

In a similar manner the thermoelastic temperature change for an anisotropic material can be derived and this is discussed in detail in Chapter 3. Equation 2.6 is the familiar form of the thermoelastic equation and has been used as the basis of many TSA

studies. The temperature change has been assumed to be linearly dependent on the stress amplitude. As a result, the temperature amplitude resulting from an applied cyclic stress is assumed to be independent of the mean stress. This is as a consequence of the assumption that the elastic constants are independent of temperature. Wong et al. [22] re-examined the theoretical basis and provided an explanation for the observed mean stress dependence of aluminium and titanium alloys on the temperature change [23]. The re-derived temperature and stress relationship incorporates the temperature dependence of the elastic constants, $\frac{\partial E}{\partial T}$ and $\frac{\partial \nu}{\partial T}$ includes the effect of the mean stress, σ_m. For a uniaxial case this gives:

$$\Delta T = -\frac{\alpha T}{\rho C_\epsilon}(1 - \frac{1}{\alpha E^2}\frac{\partial E}{\partial T}\sigma_m)\Delta\sigma_x \tag{2.7}$$

However, the change in the thermoelastic temperature change due to the temperature dependence of the modulus of elasticity is very small for common engineering materials [2]. For the case of steel, it was shown that for a 1% error in the derived $\Delta\sigma$, the contribution of σ_m needs to be 29% of the yield stress of steel, which is within the noise threshold of the measurement. Although it has been shown that the effect of the mean stress may be neglected in isotropic metallic materials, this will be considered in the analysis of the orthotropic composites in Chapter 3.

Where there is a temperature difference between different volumes in proximity, heat diffusion can never be stopped; it can only be slowed. The typical non-adiabatic behaviour that can influence the TSA measurements are critically reviewed in Ref. [24]. This behaviour can cause attenuation of the thermoelastic signal. High stress gradients that lead to high temperature gradients cause internal heat conduction. This is particularly important for layered materials such as laminated composites because materials with high thermal conductivity (e.g. carbon fibre composites) or high thermal diffusivity can induce these effects. McKelvie [25] studied the surface temperature oscillation induced thermoelastically by cyclic loading through solutions of heat conduction equations. In this study the effects of the paint coating that is typically used on the surface of the specimen was discussed and it was shown how variation in the paint coating thickness attenuate the thermoelastic signal (paint coating is discussed in detail in section 2.4). In Ref. [24] it was also shown that the thermoelastic signal varies with change in the loading frequency (between 5 and 15 Hz), highlighting possible heat loss to the environment or heat transfer at lower frequencies. In Ref. [26] point by point correction for non-adiabatic thermoelastic measurement to obtain the true stress values for a specimen under fatigue loading (loaded below the adiabatic frequency) was presented. In the current work, possible errors due to non-adiabatic effects are considered carefully.

2.2 Infrared systems

2.2.1 Infrared radiation detectors

Infrared thermography techniques use an infrared detector to measure invisible infrared energy being emitted from an object. Everything with a temperature above absolute zero emits infrared electromagnetic energy. The infrared spectrum is divided into three different wavelength regions: far infrared (> 25 μm), mid infrared (2.5 to 25 μm) and near infra-red (0.75 to 2.5 μm) [27]. In the last few decades a number of infrared detection systems have been launched in the commercial market. These imagers are highly sensitive to small temperature changes and can produce faster frame rates and at better resolution [28]. The combination of reduced cost and better performance has led to an increased use of infrared equipment for thermography and TSA.

Infrared detectors are based on two main categories namely selective detectors (photon detectors) and non-selective detectors (thermal detectors) [27]. For selective detectors the output signal is dependent on the intensity of the incident radiation and its wavelength. However, the signal from thermal detectors is independent of the wave length of the incident radiation and therefore can be used over the entire range of the infrared spectrum. The response from the selective detectors in the selective ranges is substantially higher than the response from the non-selective detectors. Therefore, photon detectors are necessary for TSA as the thermoelastic temperature change is very small, of the order of a few mK.

The first commercial TSA system was produced by Ometron Ltd, which was named SPATE (Stress Pattern Analysis by the measurement of Thermal Emisions)[29]. The single cadmium-mercury-telluride (CMT) detector scans point to point in a raster fashion over a pre-defined area. Depending on the selected system parameters and the number of pixels (size of region) TSA data could take several hours (typically 2 or 3) to accumulate. In 1994, DeltaTherm, a thermoelastic stress analysis system built with an Indium Antimonide (InSb) focal plane array (128 x 128) detector was introduced [30]. DeltaTherm replaced the analogue signal processing of the SPATE system with more modern digital signal processing, which together with its detector array, rather than a single detector, reduced TSA data collection time to a matter of minutes.

In the present work, a high performance InSb focal plane array camera developed by Cedip Infrared Systems, described in detail in Section 2.2.3, is used.

2.2.2 Photon detectors

A photon detector responds to the number of photons absorbed by the detector over a given period. If an atom is to emit radiation, it must first be excited so that its peripheral electron must pass to an orbit of higher energy. The radiation is visualised as a flux of individual particles, called photons. According to quantum theory, a photon of electromagnetic radiation with frequency $\widehat{u}$ has energy h$\widehat{u}$, where h is Planck's constant. If this quantum radiation, of magnitude = h $\widehat{u}$, is greater than E_g (the energy band width separating the valence and conduction band of a semiconductor) it is absorbed by the semiconductor. This causes an electron to be excited, which contributes to the conductivity of the semiconductor and is translated to a temperature response [27].

A photon detector converts the photon strikes into a proportional voltage signal. The spectral emissive power ($\Phi_{\lambda,b}$) for a blackbody in a hemisphere can be obtained using Planck's law [31]:

$$\Phi_{\lambda,b} = \frac{C_1}{\lambda^5(e^{\frac{C_2}{\lambda T}} - 1)} \tag{2.8}$$

where C_1 and C_2 are the first and second radiation constants, and given as:

$$C_1 = 2\pi c^2 h \tag{2.9}$$

$$C_2 = \frac{ch}{k} \tag{2.10}$$

where c is the speed of light, λ is the wavelength and k is the Boltzmann constant.

Integration of Equation 2.8 between 0 and ∞ gives the well-known fourth-power Stefan-Boltzmann relationship for evaluating the radiant emittance over all wavelengths:

$$\Phi_b = \frac{2\pi^5 k^4}{15C^2h^3}T^4 \tag{2.11}$$

Equation 2.11 is suitable for thermal detectors as it covers the entire infrared wavelength range. However, in this work photon detectors are used. Noting that the photon detector functions in a discrete manner, it is important to obtain a discrete formulation for the number of photons, N_b, emitted by a blackbody at a specific temperature. By considering the complete wavelength range between zero and infinity, the photon flux can be derived

for the total number of photons per unit area and time by producing a closed form integral of the equation for spectral radiant emmitance:

$$N_b = \int_0^\infty \frac{2\pi c}{\lambda^4 (e^{\frac{hc}{\lambda k T}} - 1)} \partial\lambda \tag{2.12}$$

The InSb array based photon detectors typically used in modern approaches to TSA do not operate over the entire IR spectrum but rather in a window from 2-5 μm. Therefore, it is necessary to integrate Equation 2.12 between 2 μm and 5 μm. This is only possible numerically and therefore an approximate approach is suggested for detectors in which the response of the detector to temperature changes follows an approximate power law ($N_b \propto T^n$) [32]. By adopting this procedure is possible to propose an equation that relates the surface temperature of a body to the total number of photons emitted over a particular wavelength range as follows:

$$N_{b,\lambda} = B' T^3 \tag{2.13}$$

where B′ is Stefan Boltzmann constant for photodetectors (1.52 x 10^{15} photons s^{-1} m^{-3} sr^{-1} K^{-3}).

Introducing the surface emissivity, η gives the following:

$$N_\lambda = \eta B' T^n \tag{2.14}$$

By differentiating Equation 2.14 with respect to T the following expression is obtained:

$$\Delta T = \frac{\Delta N_\lambda}{nBT^{n-1}\eta} \tag{2.15}$$

By assuming that ΔN_λ is proportional to the detector response, S (i.e. S = ZN_λ, where Z is the detector response factor) Equation 2.15 becomes:

$$\Delta T = \frac{S}{nBZT^{n-1}\eta} \tag{2.16}$$

The relation between temperature change and the change in the principal stress as is given in Equation 2.6. When this is incorporated into Equation 2.16 the relationship between S and stress sum is given as:

$$\Delta(\sigma_x + \sigma_y) = \frac{1}{nBZT^{n-1}} \left(\frac{1}{T\eta K} \right) S \tag{2.17}$$

The first term on the right-hand side of the equation is the detector responsivity, D:

$$\Delta(\sigma_x + \sigma_y) = \left(\frac{D}{T\eta K} \right) S \tag{2.18}$$

where $\frac{D}{T\eta K}$ can be defined as the thermoelastic calibration constant, A, to give the familiar thermoelastic equation:

$$\Delta(\sigma_x + \sigma_y) = AS \tag{2.19}$$

It is clear from Equation 2.18 that the calibration constant is a function of the temperature of the specimen. In Ref. [33], a correction factor, R, was developed to account for any departure in the absolute temperature of the specimen and accumulation of generated heat during cyclic loading. This phenomenon is particularly important for composite materials where viscoelastic heating plays a role in heat generation in the specimen. However, the infrared system used in this work has the capability of processing the data directly as ΔT, the thermoelastic temperature change, since it is radiometrically calibrated. This is a distinct advantage over other system and the operation of the instrument is detailed in the following section.

2.2.3 Silver 480M infrared system

The Silver 480M infrared system is a high performance InSb focal plane array camera developed by Cedip Infrared Systems (now FLIR). Although its primary use is for thermography, the system also has TSA capabilities. A summary of the technical specification of the Silver 480M system is given in Table 2.1 [34].

The operation of the camera includes variable integration settings that give flexibility for different temperature ranges and different data acquisition speeds. The camera can also accommodate interchangeable lenses that allow specific spatial resolution requirements to be met and provide finer resolution in areas of rapidly changing stress. The InSb detector requires cooling to about 77 K, to avoid thermal ionisation of the impurity levels in the semiconductor. Different types of dedicated software are used to control and operate the system, which are summarised below:

Table 2.1: Technical specification of the Silver 480M infrared system

Wavelenth band	2-5μm
Frame rate	5-380 Hz
Number of pixels	320 x 256
Pitch	30 μm x 30 μm
Cooling type	Integral stirling cycle cooling engine
Integration time	10 μs to 20000 μs programmable, in 1 μs steps
Noise equivalent difference temperature	$<$ 30 mK (25 mK typical)
Operational temperature range	-20 ^{o}C to +55 ^{o}C

Cirrus software: The Cirrus software is used to set various camera configuration settings such as focusing using a motorized lens, uploading the non-uniformity correction and setting the frame rate and integration time in the flash memory. Since the camera is equipped with multiple independent detectors it is possible to capture images at high frame rates. However, the slight differences between the responsivity of the individual detectors of the IR focal plane array (FPA) affect the quality of the image and non-uniformity correction of the image needs to be performed following the procedures detailed in Ref. [34]. The software also controls the FPA frame rate and the exposure time (integration).

Altair: The camera is equipped with a 'CAMLINK' interface, compatible with the Windows computer operating environment that allows video data to be recorded or viewed live using the Altair software. This, combined with Cirrus, can be used to manage video specifications and viewing the post-processed data.

Motion: In the case where large displacements exist ($>$ 1 pixel), usually when higher resolution lens are used, the raw data can be motion compensated using the random motion software. This is particularly important when looking at areas of high stress gradient at high resolution, where mismatches in the positions of the individual pixels from frame to frame can corrupt the data.

Altair-LI: The Altair-LI software is used to produce full-field stress images of structures under cyclic loading based upon the principles given in section 2.2. An intuitive colour coded pattern is displayed and graphs of stress profiles, temperature change or uncalibrated signal units (also known as Digital Level, DL) can be produced.

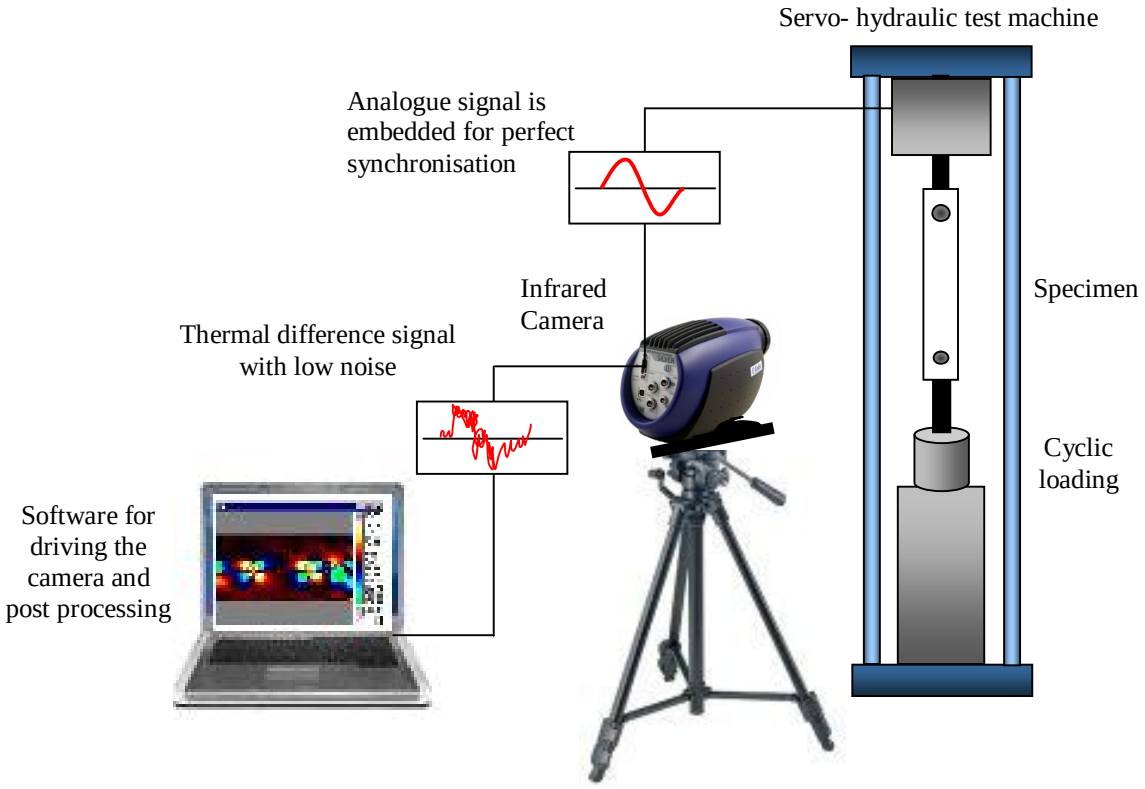

Figure 2.1: Typical operational setup of Silver 480M infrared system for TSA

2.2.4 Data acquisition and post processing

Cedip have developed a multiplex digital synchronised detection technique for their infrared systems, where all the pixels are dealt with in parallel in their signal processing routines. The signal corresponding to each pixel is time sampled and then digitally signal processed.

The raw thermoelastic signal (DL) is created by combining of large number of sine waves (each with a unique frequency) at various amplitude. All of the acquired signal (recorded as video data) in the time domain is converted into its frequency domain using Fast Fourier Transform (FFT) to break the signal back down to the frequencies that it is composed of in order to eliminate non-synchronous components with the acquired reference signal.

The raw signal, DL, for each pixel is converted to ΔT using a predetermined calibration curve. The outputs from the radiometrically calibrated system can be obtained in DL and as well as temperature difference, ΔT. A typical operational setup of the Silver 480M infrared system is shown in Figure 2.1.

2.3 Full-field stress analysis

TSA is a versatile and rapid, non-contacting technique that can provide the stresses in full-scale structures and requires minimal surface preparation. To obtain reliable quantitative stress data, prior knowledge of the component material properties is usually required. However there are standard methods for calibrating thermoelastic data [35] that can be applied, which are described in section 2.3.2.

2.3.1 Specimen preparation

As the thermoelastic signal is dependent on the emissivity of the surface of the component, it is important that this is uniform across the surface. For common engineering metals this is achieved by applying a matt black paint coating to the surface. A typical example is RS matt black spray paint which has an emissivity of 0.92 [36]. It has been shown that a thin coating of paint is thermoelastically inert for low loading rates. However, at higher frequencies attenuation in the thermoelastic signal can occur. This is because there is insufficient time for the heat to diffuse through the paint and the strain induced in the paint layer provokes a secondary thermoelastic effect [37]. In Refs. [4, 24, 38] it has been shown that the thickness of the paint coating also has an, often adverse, effect on the thermoelastic response. Materials with a high natural emissivity in the IR wavelength range, such as polymers, often do not require the prior application of a surface paint coating.

2.3.2 Calibration techniques

There are three standard methods of calibrating thermoelastic data from isotropic materials (for the cases where Equation 2.6 is valid), namely:

i direct calibration from the properties of the detector, system variables, surface emisivity, and the thermoelastic constant of the test specimen material

ii calibration against a measured stress

iii calibration against a calculated stress

To employ the first method both the material properties and infrared detector parameters are required to calculate the calibration factor A (as shown in section 2.3.3). The second method of calibration uses an independent measure of the stress responsible for

the thermoelastic signal by utilising a strain gauge rosette attached to an identical specimen to the test specimen in an area of uniform stress. For the case of an isotropic material under plane stress conditions, the sum of the principal stresses at the surface of the components can be related to the principal strains obtained from the strain gauges, can be related by applying Hooke's law to give:

$$\Delta(\sigma_x + \sigma_y) = \frac{E}{1-\nu}\Delta\left(\epsilon_x + \epsilon_y\right) \tag{2.20}$$

This can be related to Equation 2.19, to give an expression for the calibration constant, A, as follows:

$$A = \frac{E}{(1-\nu)\,S}\Delta\left(\epsilon_x + \epsilon_y\right) \tag{2.21}$$

This equation can be further simplified by using a uniaxial strain gauge on a tensile specimen, which reduces Equation 2.21 to:

$$A = \frac{E\Delta\epsilon}{S} \tag{2.22}$$

The final method involves relating a measured thermoelastic signal to a known stress value produced in a specimen by a known applied load. If an expression for the principal stress values, σ_x and σ_y is available for a point on a specimen then these expressions can be substituted into Equation 2.19, and relate it to A. For the case of a tensile specimen (where $\sigma = 0$), the signal will be directly proportional to the applied stress. Therefore the calibration constant can be found by:

$$A = \frac{\Delta\sigma_{applied}}{S} \tag{2.23}$$

A similar procedure can be applied to other closed form stress analysis cases such as a Brazilian disk specimen, or a beam in four-point bending. It should be noted that these calibration technique will not be used in this work as the Cedip System provides the thermoelastic response in ΔT directly.

2.4 Application of TSA to composite material

The proven methodology for application of TSA in metallic structures cannot directly be applied to composite materials, as these materials are anisotropic in their mechanical and

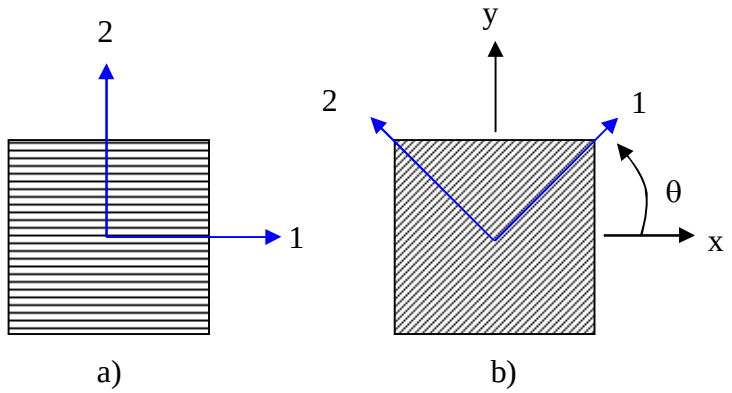

Figure 2.2: a) On-axis b) Off-axis configurations of a composite

physical properties. In this section, developments of theoretical and practical approaches for application to orthotropic composites material are reviewed.

Two orthogonal planes of symmetry exist for a unidirectional laminate: one plane is parallel to the fibres (1); and the other is transverse to the fibres (2). The two orthogonal planes are shown in Figure 2.2(a). When the reference axis (x,y) coincides with the material symmetry axes, this is called on-axis orientation. When the ply orientation is different from 0 or 90 degrees, the ply configuration is known as off-axis (shown in Figure 2.2(b)). Transformation equations can be used to find the off-axis stresses from the applied strain or vice versa. The literature review is presented based on this notation and will be followed throughout the thesis.

Stanley and Chan [39] developed the TSA theory for composite material and derived calibration equations in terms of stress. The theory for an orthotropic material is outlined by going a through a similar process to section 2.1 but incorporating changes required for orthotropic materials. For orthotropic materials the temperature change as a function of stress increment is given as [39]:

$$\Delta T = -\frac{T}{\rho C_p}(\alpha_1\sigma_1 + \alpha_2\sigma_2 + \alpha_6\sigma_6) \tag{2.24}$$

It is notable that the differences in the coefficients of thermal expansion in the different directions of the composite material need to be accounted for, where α and $\Delta\sigma$ are in the principal material axes for an off axis laminate (shown in Figure 2.2(b)). However, both approaches, principal stress or material axes have been used by works in TSA. A good example of this is the work done by Dulieu-Smith and Stanley in Refs. [40, 41]. The general thermoelastic equation which relates the change in the temperature to a

given change in strain was derived by Potter [42]. Reformulation of Equation 2.24 in terms of strain (based on the principal material directions) was given as [42]:

$$\Delta T = -\frac{T}{\rho C_p}[\alpha]^T_{1,2}[Q]_{1,2}[T][\Delta\epsilon]_{x,y} \tag{2.25}$$

where Q is the stiffness, T is a transformation matrix relating the local material (1,2) and principal stress axes (x,y) and $\Delta\epsilon$ is the change in the in-plane strain in the principal stress axes.

Bakis et al. [43] combined the plane stress solution with micromechanics for carbon fibre laminates to account for the non homogeneous strains in the fibre and matrix inorder to compute the average temperature change in the surface ply of a laminate. The results showed that the material parameters such as volume fraction, thermoelastic properties of the micro constituents and orientation of the lamina on the surface of observation affect the thermoelastic signal. Wong [44], investigated the effects of thermal conduction on the thermoelastic temperature changes for carbon fibre composite materials where large stress gradients exist between the fibres and matrix and between adjacent plies orientated at different orientations in a laminate. Later, assuming that heat transfer can be neglected in glass fibre reinforced composite (GFRP) the possibility of an influence from the surface resin rich layer present as a consequence of the manufacturing process on thermoleastic response was suggested by Cunningham et al. [9]. Potter and Greaves [45] highlighted that if the observed infrared emission were generated only at the outermost surface, significant differences in thermoelastic output should be observed if the surface resin were removed entirely. However, only small effects due to changes of resin layer thickness were observed and further work was required to define the relationship between the thermoelastic response and resin layer thickness.

Zhang et al. [46] reported that for resin thickness greater than 0.03 mm the signal is constant and independent of thickness. El Hajjar et al. [10] took advantage of the transversely isotropic surface and related the measured temperature change to the sum of the surface strains. Pitarresi et al. [12] investigated the source of the thermoelastic signal from different laminate lay-ups for orthotropic composites and created a model that accounts for the presence of the resin rich layer. This provided closer predictions for a wider range of lay-ups; these results were confirmed by Emery et al. [11]. It is apparent that a full understanding of the effect of the fundamental uncertainties for quantitative TSA work from the different approaches given in the literature, such as the thermal-mechanical behaviour, source of the thermoelastic signal, non-adiabatic behaviour and the influence of the applied loading conditions does not exist.

The quantitative studies on the application of TSA to composite materials have always been for a specific material or a particular structure and there is no general methodology of applying TSA to composite materials.

2.5 Practical applications of TSA

Thermoelastic stress analysis is a technology that has and is still developing rapidly. One of its advantages is that it can produce experimental data that is the basis for reliable design, which leads to optimum structural efficiency. For isotropic materials under adiabatic conditions the use of TSA is well defined. It has been used to characterise stress concentration factors (SCFs) around a variety of hole configurations in flat plates, cylinders and pin-loaded lugs [47, 48, 49] (explained further in Chapter 4).

As the thermoelastic output is insensitive to shear stresses for isotropic materials; it must be combined with other experimental or theoretical methods when shear stresses need to located and quantified. Although the data from TSA is in the form of the sum of the principal stresses, it can be integrated with theoretical analysis for stress separation. The review of different approaches that can be used to evaluate the individual stress components from the TSA data and potential areas for further research are proposed in Ref. [50].

The developments of analytical methods for the interpretation of data acquired from composite materials have also lead to the use of TSA for structural characterisation of composite components [39, 44, 51, 52, 53](explained further in Chapter 3). Characterisation of the fatigue damage process in composites is important in developing fatigue and fracture criteria. Theories have also been developed to characterise damage evolution using TSA [33, 54].

Previous work has also focused on the use of TSA in identifying high-stress regions in prototypes in a qualitative manner [55, 56, 57] in an attempt to apply TSA to realistic structures. In conjunction with this type of work, there are proposed methods that do not need a reference signal [58] or use a random reference signal [59] that reduces the amount of noise in the thermoelastic signal. This allows TSA to be applied to real industrial components under service loads.

2.6 Justification for current work

TSA has been used in numerous applications involving isotropic solids. However, application to composite structures are limited, almost none are applied in a quantitative

manner to assess the detailed local stress distributions in realistic structures. However, this is where experimental data are crucial and there is often a need to validate results from the ever increasing use of numerical techniques. The use of composite materials requires special consideration due to the anisotropic nature of the material system and the complexity of the failure modes. For TSA to be applied successfully, a definite and robust stress analysis routine based on the thermoelastic response need to be devised. Composite technologies have progressed a great deal in the last decade and encouraged the incorporation of composite material in load bearing structures. This has resulted in the use of different material system and manufacturing techniques that need to be considered in TSA. However, the focus of this work is the application of TSA to composite materials in a general manner. The validity of a stress analysis routine needed to be demonstrated experimentally, which this work provides by quantifying the stress/ strain distribution for standard features in realistic structures, such as around the holes and joints. This will allow the advantages of TSA, as a quantitative NDT technique, to be exploited fully to develop design methodologies for composite members that are lighter in weight and have greater structural efficiencies. TSA can be used to validate FEA results, which often require the use of full-field experimental techniques. A detailed study of the theoretical considerations required to apply TSA to composite materials in a general quantitative manner are presented in following chapters.

Chapter 3

Thermoelastic theory for laminated composites

3.1 Introduction

Analysis of laminated composite materials can be grouped into different classes, depending on the degree of detail required for analysis. The following classes are of practical interest:

i Micro level: distinct, continuous phases of fibre, matrix and in some cases, the interface and voids.

ii Ply or lamina level: homogeneity within each ply and no longer recognised as distinct phases.

iii Laminate level: average values of ply properties through the thickness of the laminate.

At the micromechanical level, the fibre and matrix stresses vary within each constituent phase. However, in composite materials it is virtually impossible to know exactly the inhomogeneity in each constituent and the distribution and locations of the fibres, so the average of these constituents is usually homogenised as the ply. Therefore, in this work (i) is disregarded and the treatments focus on (ii) and (iii) only. In a laminate, or at the macromechanical level, each ply (or ply group) has its own ply stress. As the primary objective is to devise a general treatment for laminates, distinction must be made between (ii) and (iii). TSA is a surface measurement technique; therefore the influence of the inner laminate on the surface ply is uncertain. In this chapter, a detailed

appraisal of the possible origins of the thermoelastic response focusing on the surface thermoelastic temperature changes of orthotropic fibre reinforced laminates is presented.

The chapter starts by establishing the nature of the thermoelastic response from a single orthotropic lamina. This has been the basis of most of the previous thermoelastic work on laminated orthotropic composite materials. Complete definition of the notation associated with this treatment and clarification of its previous use are included. This provides a firm basis to understand the behaviour of laminated materials. To interpret the thermoelastic response from an orthotropic laminated composite material, the usual approach is to assume that the response is a function of the orthotropic surface ply stresses and their associated coefficients of thermal expansion (CTE), this approach is presented along with the stress-strain transformation. Two further theoretical approaches to define the thermoelastic response of a laminate are then explored; (i) consideration of the global mechanical and thermal properties, and (ii) consideration of a combination of the ply by ply mechanical properties with the global thermal properties. A full description of each approach is provided in the chapter, along with a justification for the consideration of these two new treatments.

Next, the 'strain witness' assumption used by previous researchers, [11, 12] is also described and the formulation established for a resin rich surface layer presence on an orthotropic substrate.

Finally a means of establishing the validity of the four approaches is described in terms of the types of the laminates that enable a straightforward interpretation and comparison of the thermoelastic data.

3.2 Thermoelastic response from a single lamina

The starting point for practically all thermoelastic studies on orthotropic/ anisotropic composite material has been Equation 1.1. This was defined in the mid 1980s and is often referred to through two key publications [39, 42]. Before embarking on a study of the response of a laminated material, it is necessary to understand fully the origin of Equation 1.1 and its validity. It is clear that ΔT is a scalar quantity and that the thermoelastic response from any point in an orthotropic material is independent of the reference axes used on the right hand side of the Equation 1.1. In Equation 1.1 the principal material axes have been used as the reference, which is entirely logical as the material properties, e.g. α_1 and α_2, are most easily defined when referred to the material directions. In this work, all the treatments will be based on a plane stress assumption.

Therefore for a single orthotropic lamina there are three axes of interest, as shown on Figure 3.1:

- The principal material axes denoted 1,2
- The principal stress axes denoted x,y
- An arbitrary set of axes denoted i,j

The corresponding stress tensors (in contacted notation [60]) are:

$$[\sigma]_{1,2} = \begin{pmatrix} \sigma_1 \\ \sigma_2 \\ \sigma_6 \end{pmatrix} ; \; [\sigma]_{x,y} = \begin{pmatrix} \sigma_x \\ \sigma_y \\ \sigma_s \end{pmatrix} ; \; [\sigma]_{i,j} = \begin{pmatrix} \sigma_i \\ \sigma_j \\ \sigma_{ij} \end{pmatrix} \tag{3.1}$$

The other tensor property in Equation 1.1 is the coefficient of thermal expansion (CTE), which are defined with reference to the three different axes as follows:

$$[\alpha]_{1,2} = \begin{pmatrix} \alpha_1 \\ \alpha_2 \\ \alpha_6 \end{pmatrix} ; \; [\alpha]_{x,y} = \begin{pmatrix} \alpha_x \\ \alpha_y \\ \alpha_s \end{pmatrix} ; \; [\alpha]_{i,j} = \begin{pmatrix} \alpha_i \\ \alpha_j \\ \alpha_{ij} \end{pmatrix} \tag{3.2}$$

The change in the dimensions under free thermal stress of a lamina in the principal stress direction and material directions are shown in Figure 3.2. In Figure 3.2(a) where the system is referred to the principal stress axes, shear coupling occurs in any arbitrary direction and will exhibit extension shear coupling. In Figure 3.2(b) the system is refered to the principal material axes and it is clear that α_6 is always zero. This explains why the common expression given in Equation 1.1 does not include the coupling term that is given in Equation 2.24. The CTE is a second-order tensor therefore transforms like the strain components, (i.e. $\alpha_s = 2\alpha_{xy}$) as shown in Figure 3.3. Here α_{xy} is the shear CTE on the x axis along the y direction and α_{yx} is in the y axis along the x direction ($\alpha_{xy} = \alpha_{yx}$) and α_s is the total measure of the shear CTE in the x-y plane (also known as the engineering shear CTE). So more correctly, the CTE tensors should be expressed as follows:

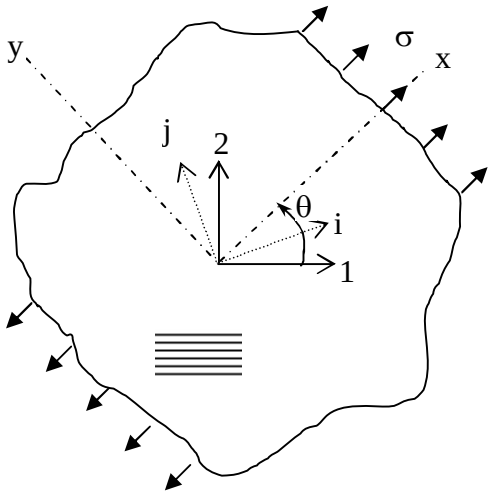

Figure 3.1: Schematic diagram of the coordinate system and nomenclature

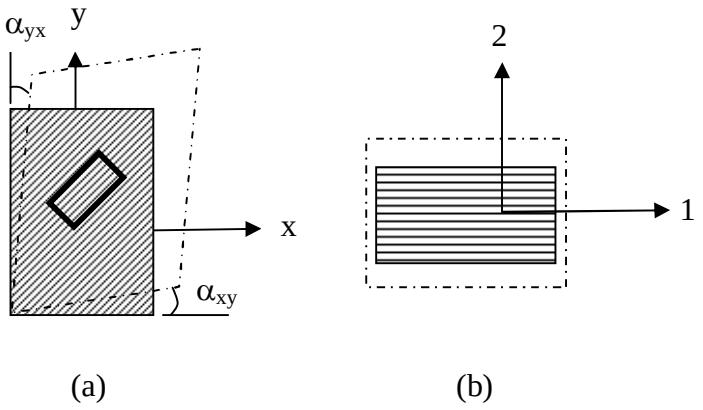

Figure 3.2: Thermal expansion of composite lamina under free thermal stress (a) principal stress axes (exhibit extension shear coupling) (b) principal material axes

$$[\alpha]_{x,y} = \begin{pmatrix} \alpha_x \\ \alpha_y \\ \frac{\alpha_s}{2} \end{pmatrix} \; and \; [\alpha]_{i,j} = \begin{pmatrix} \alpha_i \\ \alpha_j \\ \frac{\alpha_{ij}}{2} \end{pmatrix} \tag{3.3}$$

From the above it can be seen that the only tensor quantities in Equation 2.24 are the CTEs and the stresses. Therefore as ΔT is a scalar quantity, the product of these terms in any three axes systems defined in Figure 3.1 must be equal:

$$[\alpha]^T_{i,j}[\sigma]_{i,j} = [\alpha]^T_{x,y}[\sigma]_{x,y} = [\alpha]^T_{1,2}[\sigma]_{1,2} \tag{3.4}$$

where the superscript T denotes the transpose of a matrix

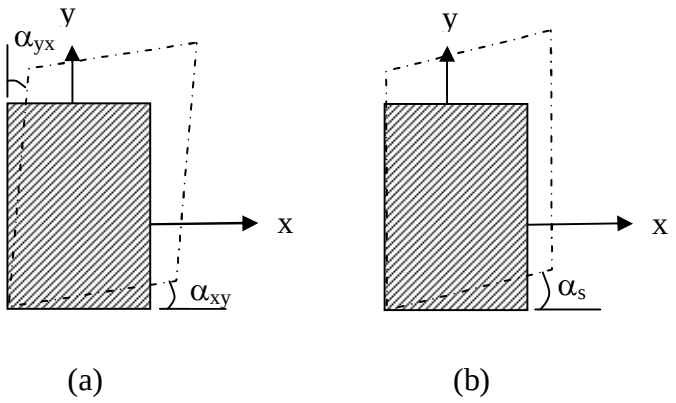

Figure 3.3: Shear thermal expansion of composite lamina (a) as shear thermal expansion tensor (b) total shear thermal expansion (known as engineering shear thermal expansion)

To prove the validity of the assumption given in Equation 3.4, it is necessary to demonstrate that the quantities given in Equation 3.4 are equal. Here the x,y quantities will be examined as an example. The starting point is to transform the values in the x,y direction through the angle, θ, shown in Figure 3.1, so they can be expressed with reference to the i,j axes. The transformation of the CTE and the stress is as follows:

$$[\alpha]_{i,j}^{T}[\sigma]_{i,j} = [[T][\alpha]_{x,y}]^{T}\,[[T][\sigma]_{x,y}] \tag{3.5}$$

where T is the transformation matrix given by:

$$[T] = \begin{bmatrix} \cos^2\theta & \sin^2\theta & 2\cos\theta\sin\theta \\ \sin^2\theta & \cos^2\theta & -2\cos\theta\sin\theta \\ -\cos\theta\sin\theta & \cos\theta\sin\theta & \cos^2\theta - \sin^2\theta \end{bmatrix} \tag{3.6}$$

The transformation of the CTE tensor is as follows:

$$[T][\alpha]_{x,y} = \begin{bmatrix} \cos^2\theta & \sin^2\theta & 2\cos\theta\sin\theta \\ \sin^2\theta & \cos^2\theta & -2\cos\theta\sin\theta \\ -\cos\theta\sin\theta & \cos\theta\sin\theta & \cos^2\theta - \sin^2\theta \end{bmatrix} \quad \begin{bmatrix} \alpha_x \\ \alpha_y \\ \frac{\alpha_s}{2} \end{bmatrix} \tag{3.7}$$

which simplifies to:

$$[\alpha]_{i,j} = [T][\alpha]_{x,y} = \begin{bmatrix} \alpha_x \cos^2\theta + \alpha_y \sin^2\theta + \alpha_s \cos\theta \sin\theta \\ \alpha_x \sin^2\theta + \alpha_y \cos^2\theta - \alpha_s \cos\theta \sin\theta \\ -2\alpha_x \cos\theta \sin\theta + 2\alpha_y \cos\theta \sin\theta + \alpha_s \left(\cos^2\theta - \sin^2\theta\right) \end{bmatrix} \tag{3.8}$$

Similarly the transformation of stress is given as:

$$[\sigma]_{i,j} = [T][\sigma]_{x,y} \begin{bmatrix} \sigma_x \cos^2\theta + \sigma_y \sin^2\theta + 2\sigma_s \cos\theta \sin\theta \\ \sigma_x \sin^2\theta + \sigma_y \cos^2\theta - 2\sigma_s \cos\theta \sin\theta \\ -\sigma_x \cos\theta \sin\theta + \sigma_y \cos\theta \sin\theta + \sigma_s \left(\cos^2\theta - \sin^2\theta\right) \end{bmatrix} \tag{3.9}$$

$[\alpha]^T_{i,j}\,[\sigma]_{i,j}$ can be obtained by multiplying the transpose of Equation 3.8 with Equation 3.9. By multiplying the first column and first row it can be shown that ($\sin\theta$=s and $\cos\theta$=c):

$$\begin{aligned}(c^2\alpha_x + s^2\alpha_y + sc\alpha_s)(c^2\sigma_x + s^2\sigma_y + 2sc\sigma_s) = c^4\alpha_x\sigma_x + c^2s^2\alpha_x\sigma_y + \\ 2sc^3\alpha_x\sigma_s + s^2c^2\alpha_y\sigma_x + s^4\alpha_y\sigma_y + 2s^3c\alpha_y\sigma_s + sc^3\alpha_s\sigma_x + s^3c\alpha_s\sigma_y + 2s^2c^2\alpha_s\sigma_s\end{aligned} \tag{3.10}$$

By multiplying the second column and second row it can be shown that:

$$\begin{aligned}(s^2\alpha_x + c^2\alpha_y + sc\alpha_s)(s^2\sigma_x + c^2\sigma_y - 2sc\sigma_s) = s^4\alpha_x\sigma_x + s^2c^2\alpha_x\sigma_y - \\ 2s^3c\alpha_x\sigma_s + c^2s^2\alpha_y\sigma_x + c^4\alpha_y\sigma_y - 2sc^3\alpha_y\sigma_s - s^3c\alpha_s\sigma_x - sc^3\alpha_s\sigma_y + 2s^2c^2\alpha_s\sigma_s\end{aligned} \tag{3.11}$$

Multiplying the third column and third row it can be shown that:

$$\begin{aligned}(-2sc\alpha_x + 2sc\alpha_y + (c^2 - s^2)\alpha_s)(-sc\sigma_x + sc\sigma_y + (c^2 - s^2)\sigma_s) = 2s^2c^2\alpha_x\sigma_x - \\ 2s^2c^2\alpha_x\sigma_y - 2sc^3\alpha_x\sigma_s + 2s^3c\alpha_x\sigma_s - 2s^2c^2\alpha_y\sigma_x + 2s^2c^2\alpha_y\sigma_y + 2sc^3\alpha_y\sigma_s - 2s^3c\alpha_y\sigma_s \\ -sc^3\alpha_s\sigma_x + c^3s\alpha_s\sigma_y + c^4\alpha_s\sigma_s - s^2c^2\alpha_s\sigma_s + s^3c\alpha_s\sigma_x - s^3c\alpha_s\sigma_y - s^2c^2\alpha_s\sigma_s + s^4\alpha_s\sigma_s\end{aligned} \tag{3.12}$$

By adding Equations 3.10, 3.11 and 3.12 and factorising the combined equation gives:

$$\alpha_x\sigma_x(c^4+s^4+2s^2c^2)+\alpha_y\sigma_y(c^4+s^4+2s^2c^2)+\alpha_s\sigma_s(c^4+s^4+2s^2c^2+2s^2c^2-c^2s^2-c^2s^2)+$$
$$s^2c^2(\alpha_x\sigma_y+\alpha_y\sigma_x+\alpha_x\sigma_y+\alpha_y\sigma_x-2\alpha_x\sigma_y-2\alpha_y\sigma_x)+$$
$$s^3c(2\alpha_y\sigma_s+\alpha_s\sigma_y-2\alpha_x\sigma_s-\alpha_s\sigma_x+2\alpha_x\sigma_s-2\alpha_y\sigma_s+\alpha_s\sigma_x-\alpha_s\sigma_y)+$$
$$sc^3(2\alpha_x\sigma_s+\alpha_s\sigma_x-2\alpha_y\sigma_s-\alpha_s\sigma_y-2\alpha_x\sigma_s+2\alpha_y\sigma_x-\alpha_s\sigma_x+\alpha_s\sigma_y) \tag{3.13}$$

By solving the linear algebra and using the trigonometric identity ($s^2+c^2=1$), so $(s^2+c^2)^2=(s^4+c^4+2s^2c^2)=1$ it can be shown that:

$$[\alpha]^T_{i,j}[\sigma]_{i,j}=\alpha_x\sigma_x+\alpha_y\sigma_y+\alpha_s\sigma_s \tag{3.14}$$

If a similar treatment is applied in the 1,2 axes then it can also be shown that:

$$[\alpha]^T_{i,j}[\sigma]_{i,j}=\alpha_1\sigma_1+\alpha_2\sigma_2+\alpha_6\sigma_6 \tag{3.15}$$

Therefore the general term $[\alpha]^T_{i,j}[\sigma]_{i,j}$ can be concluded to be an invariant. Furthermore, in the lamina principal material directions $\alpha_6=0$, and in the principal stress direction $\sigma_s=0$, so for an orthotropic laminate Equation 3.14 reduces to:

$$[\alpha]^T_{i,j}[\sigma]_{i,j}=\alpha_x\sigma_x+\alpha_y\sigma_y=\alpha_1\sigma_1+\alpha_2\sigma_2 \tag{3.16}$$

This confirms the treatment in Ref. [39] and shows clearly that the shear terms can be neglected from the analysis. The introduction of the stress invariant concept, to formulate the temperature change from the orthotropic substrate clears any confusion relating to the use of reference axes for the system [42] and that a consistent use of any axes system is acceptable. In this section, it has been assumed that mechanically induced volumetric changes produce very small local temperature variations isolated in a surface orthotropic ply, however the effective thermoelastic response should be considered as a function of the entire laminate. The net effect and influence of the whole laminate on the thermoelastic response will be developed in the next section.

3.3 Thermoelastic response from a multi directional laminate

3.3.1 Definition of a multidirectional laminate

A general laminate has layers of different orientation, θ (between -90^o and 90^o). The behaviour of the laminate depends on the material stiffness, layer thickness and layup. Therefore, a laminate is a collection of a lamina stacked in the desired direction to obtain the preferred material stiffness, strength and behaviour. A section through a multidirectional laminate is shown diagrammatically in Figure 3.4. This orthotropic laminate comprises eight plies, labelled A to H. Each ply has its own principal material direction 1,2. The construction is known as 'stack'. At the top and bottom of the stack there is a resin rich layer that exists due to the manufacturing process and for TSA this needs to be included in the analysis. The plies A to H can be oriented at different angles with reference to the principal laminate axes and relative to each other. The ply by ply orientation is called the stacking sequence and is of paramount importance in laminate analysis. If all the plies are orientated in the same direction, this is known as a unidirectional (UD) material. If the plies either side of the mid plane (i.e. A & H, B & G, C & F and D & E) are orientated in the same direction, this is known as a symmetric lay-up. A laminate is said to be 'balanced' if for every layer in the laminate, another layer with identical thickness and opposite fibre orientation exist (i.e. +45, -45). For example, if the orientation of A is 0^o, B is +45^o, C is -45^o, D is 90^o, E is 90^o, F is -45^o, G is +45^o and H is 0^o this is notated as follows:

$$[0, \pm 45, 90]_s$$

In the following analysis, it is essential to denote the layers in the stack appropriately. The layer immediately beneath the surface resin layer is known as the 'orthotropic surface ply' and the rest of the layers below that are known as the 'orthotropic substrate'.

The elastic material properties are given in terms of reduced stiffness constants in the principal material directions in each ply as:

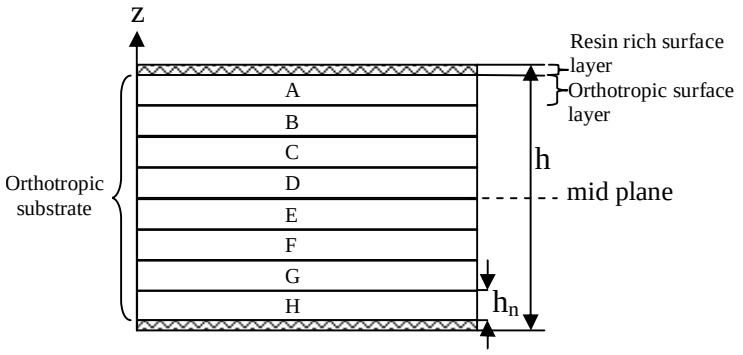

Figure 3.4: Typical stacking sequence of a symmetric laminate

$$\begin{aligned} Q_{11} &= \frac{E_1}{1-\nu_{12}\nu_{21}} \\ Q_{12} &= \frac{\nu_{12}E_2}{1-\nu_{12}\nu_{21}} \\ Q_{22} &= \frac{E_2}{1-\nu_{12}\nu_{21}} \\ Q_{66} &= G_{12} \end{aligned} \tag{3.17}$$

where E_1 is the elastic modulus in the fibre direction and E_2 in the transverse direction. The major Poisson's ratio is denoted by ν_{12} and the shear modulus is denoted by G_{12}.

In the following analysis a plane stress state is considered, so the reduced stiffness constants are sufficient to describe the stress-strain relationship as:

$$\begin{bmatrix} \sigma_1 \\ \sigma_2 \\ \sigma_6 \end{bmatrix} = \begin{bmatrix} Q_{11} & Q_{12} & 0 \\ Q_{12} & Q_{22} & 0 \\ 0 & 0 & Q_{66} \end{bmatrix} \begin{bmatrix} \epsilon_1 \\ \epsilon_2 \\ \epsilon_6 \end{bmatrix} \tag{3.18}$$

To find the specific stiffness in any coordinate system (x,y) relative to the principal material axes a rotational transformation is required to obtain the off-axis stiffness in each lamina:

$$\left[\bar{Q}_{i,j}\right] = [T]^{-1}\left[Q_{i,j}\right][T]^{-T} \tag{3.19}$$

Since the stiffness varies ply by ply, in practice an average stress for the laminate is established using classical laminated plate theory (CLPT) than the actual stress across the laminate. This average stress is used to define the stress-strain relationship of the laminate. For a balanced and symmetric laminate under in-plane loading the in-plane

strains (i.e. plane strain conditions, $\epsilon_{lamina} = \epsilon_{Laminate}$, or $\epsilon_x = \epsilon_{xL}$) remain practically constant through the laminate thickness and this assumption is reasonable when the thickness of the laminate is small. Therefore, the in-plane stress-strain relation for a laminate based on the average stress is given by:

$$\begin{aligned} \sigma_x &= A_{11}\epsilon_x + A_{12}\epsilon_y + A_{16}\epsilon_s \\ \sigma_y &= A_{21}\epsilon_x + A_{22}\epsilon_y + A_{26}\epsilon_s \\ \sigma_s &= A_{16}\epsilon_x + A_{26}\epsilon_y + A_{66}\epsilon_s \end{aligned} \tag{3.20}$$

where A is called the extensional stiffness and the components of this stiffness matrix are defined as follows:

$$A_{ij} = \sum_{n=1}^{N} (\bar{Q}_{ij})_n h_n \tag{3.21}$$

where h_n is the thickness of the n^{th} layer.

Equation 3.20 can be inverted to yield the in-plane strains in terms of the stresses as follows (stress-strain relationship in terms of compliance):

$$\begin{aligned} \epsilon_x &= a_{11}\sigma_x + a_{12}\sigma_y + a_{16}\sigma_s \\ \epsilon_y &= a_{21}\sigma_x + a_{22}\sigma_y + a_{26}\sigma_s \\ \gamma_s &= a_{16}\sigma_x + a_{26}\sigma_y + a_{66}\sigma_s \end{aligned} \tag{3.22}$$

where a is the compliance of the laminate.

3.4 Lamina and laminate strains

The in-plane stresses within a particular ply depend upon the fibre orientation for a multi-directional laminate. Therefore, it is more convenient to work in terms of strain by assuming that the strain field in the surface layer is constant through the laminate thickness under uniaxial tensile loading (i.e. $\epsilon_x = \epsilon_{xL}$). Also, to compare the measured ΔT value with a measured strain value for validation purposes, it is convenient to reformulate the stress based equation in terms of applied strain in the laminate. So in this

section a strain based approach is devised for investigating the thermoelastic response from an orthotropic material.

In classical laminate plate theory, all three through thickness strain components (i.e. in standar tensor notation, ϵ_{zz}, ϵ_{xz} and ϵ_{yz}) are assumed to be zero. Therefore, if the types of laminate to be examined confirm this assumption, Equation 3.16 can be written in terms of the in-plane strains in the laminate:

$$\Delta T = -\frac{T}{\rho C_p} [\alpha]_{1,2}^T [Q]_{1,2} [T] [\Delta\epsilon]_{x,y} \tag{3.23}$$

Equation 3.23 can be expanded as:

$$\Delta T = \begin{bmatrix} \alpha_1 & \alpha_2 & 0 \end{bmatrix} \begin{bmatrix} Q_{11} & Q_{12} & 0 \\ Q_{12} & Q_{22} & 0 \\ 0 & 0 & Q_{66} \end{bmatrix} \begin{bmatrix} c^2 & s^2 & 2cs \\ s^2 & c^2 & -2sc \\ -sc & sc & c^2 - s^2 \end{bmatrix} \begin{bmatrix} \epsilon_x \\ \epsilon_y \\ \gamma_s/2 \end{bmatrix} \tag{3.24}$$

This equation can be simplified as:

$$\Delta T = \begin{bmatrix} \alpha_1 & \alpha_2 & 0 \end{bmatrix} \begin{bmatrix} Q_{11}(c^2\epsilon_x + s^2\epsilon_y + cs\gamma_s) + Q_{12}(s^2\epsilon_x + c^2\epsilon_y - cs\gamma_s) \\ Q_{12}(c^2\epsilon_x + s^2\epsilon_y + cs\gamma_s) + Q_{22}(s^2\epsilon_x + c^2\epsilon_y - cs\gamma_s) \\ Q_{66}(-sc\epsilon_x + sc\epsilon_y + (c^2 - s^2)\gamma_s/2) \end{bmatrix} \tag{3.25}$$

Equation 3.25 can factored in terms of material constants and strain terms as:

$$\begin{aligned} \Delta T = -\frac{T}{\rho C_p} [&(\alpha_1 Q_{11} + \alpha_2 Q_{12}) \left(\epsilon_x \cos^2\theta + \epsilon_y \sin^2\theta + \gamma_s \cos\theta \sin\theta\right) \\ &+ (\alpha_1 Q_{12} + \alpha_2 Q_{22}) \left(\epsilon_x \sin^2\theta + \epsilon_y \cos^2\theta - \gamma_s \cos\theta \sin\theta\right)] \end{aligned} \tag{3.26}$$

This strain based thermoelastic equation will be used in the experimental work to make the comparison between the proposed models and measured thermoelastic data, by incorporating the measured in-plane strains experienced by the laminate.

3.5 Four approaches for defining the thermoelastic response

3.5.1 Influence of the surface resin rich layer on thermoelastic response

In general analysis of the thermoelastic response from composite laminate the stresses in the orthotropic material are coupled with CTEs in the direction of interest. It would therefore be very convenient to be able to apply the strain witness assumption to composite components (by treating it as an isotropic surface medium), so that the coupling between the stresses and the CTE can be neglected in the analysis. In previous studies [11, 12] it has been assumed that the thermoelastic response is from the surface resin layer and it is said to act as a 'strain witness'. Therefore the resin must be such that it prevents the temperature change that occurs in the surface ply from conducting through the resin to the material surface. To act as a strain witness the surface layer must be thin compared to the thickness of the specimen so that the laminate strains are fully transmitted from the surface ply to the surface of the resin. If the resin is acting as a strain witness then the strain in a given direction in the resin layer is equal to the strain in that same direction in the laminate:

$$\begin{aligned} \epsilon_{xr} &= \epsilon_{xc} \\ \epsilon_{yr} &= \epsilon_{yc} \end{aligned} \tag{3.27}$$

The sum of the principal strains in a composite laminate can be related to the stresses in the resin layer as follows:

$$\epsilon_{xc} + \epsilon_{yc} = \frac{1-\nu_r}{E_r}\left(\sigma_{xr} + \sigma_{yr}\right) \tag{3.28}$$

where E is Young's modulus and ν is Poisson's ratio, σ_x and σ_y are the change in the principal stresses and the subscript c and r represent composite material and resin respectively.

$$\Delta T = -\frac{T\alpha}{\rho C_p}\left(\sigma_x + \sigma_y\right) = -\frac{T\alpha_r}{\rho_r C_{pr}}\left[\frac{E_r}{1-\nu_r}\left(\epsilon_{xc} + \epsilon_{yc}\right)\right] \tag{3.29}$$

3.5.2 Orthotropic surface ply

For this approach a strain based approach is devised for investigating the thermoelastic response from the orthotropic surface ply. When a uniaxial tensile stress is applied to a

balanced, symmetric orthotropic laminate the shear strain in the laminate (γ_s) is zero, so Equation 3.26 can be simplified as:

$$\begin{aligned}\Delta T = -\frac{T}{\rho C_p}[&(\alpha_1 Q_{11} + \alpha_2 Q_{12})\left(\epsilon_x \cos^2\theta + \epsilon_y \sin^2\theta\right) \\ &+ (\alpha_1 Q_{12} + \alpha_2 Q_{22})\left(\epsilon_x \sin^2\theta + \epsilon_y \cos^2\theta\right)]\end{aligned} \tag{3.30}$$

In this work, the theoretical temperature change is computed as a function of in-plane strain given by Equation 3.30 instead of Equation 3.16 which requires the in-plane stresses to be calculate using CLPT based on the applied load.

For a balanced orthotropic laminate constructed from $\pm 45^o$ angle ply Equation 3.30 can be further simplified to ($\sin 45^o = \cos 45^o$):

$$\Delta T = -\frac{T}{\rho C_p}\left[\frac{\epsilon_x + \epsilon_y}{2}\right][(\alpha_1 Q_{11} + \alpha_2 Q_{12}) + (\alpha_1 Q_{12} + \alpha_2 Q_{22})] \tag{3.31}$$

This provides a unique equation for angle plies with 45^o plies where the applied strain and material constants are uncoupled (can be separated), unlike Equation 3.30.

3.5.3 Homogeneous orthotropic material

When assessing the behaviour of a general multidirectional composite laminate (consisting of lamina with arbitrary orientations) classical laminate plate theory (CLPT) is generally used so that the material can be treated as a homogeneous orthotropic plate. Here the mechanical and thermoelastic properties are considered ply by ply and then brought together relative to (say) the laminate axis to provide a 'global' stiffness and CTE. This might also be relevant for analysing the thermoelastic effect, where the small temperature change is influenced by the global material behaviour. For quasi-isotropic laminates, it is evident that the global CTE is equal in the longitudinal and transverse directions (i.e. $\alpha = \alpha_{xL} = \alpha_{yL}$) because of the net effect of the stacking sequence. By substituting Equation 3.20 into Equation 3.16, it may be pertinent to express the thermoelastic temperature change in the following manner:

$$\Delta T = -\frac{T}{\rho C_p}\left[\alpha_{xL}\left(A_{11} + A_{12}\right)\Delta\epsilon_{xL} + \alpha_{yL}\left(A_{12} + A_{22}\right)\Delta\epsilon_{yL}\right] \tag{3.32}$$

3.5.4 CTE coupled in the stack

Equation 3.32 simply assumes that the material response is that of a homogeneous orthotropic material. A further and as yet unexplored idea is that the CTE is coupled in the stack. This is because, like the mechanical strain, the thermal strain maybe considered to be constant in the through thickness direction. Therefore the surrounding layers may have an effect on the response from the orthotropic substrate. To explore this, the orthotropic nature of the surface ply is retained in the treatment but the CTE is treated as a global property as the plies are bonded together and are not free to deform independently, which gives the following equation:

$$\Delta T = -\frac{T}{\rho C_p}\left[\alpha_{xL}\left(Q_{11}+Q_{12}\right)\Delta\epsilon_{xL} + \alpha_{yL}\left(Q_{12}+Q_{22}\right)\Delta\epsilon_{yL}\right] \tag{3.33}$$

3.6 Definition of laminate configurations for experimental work

In this section, definition of laminate selections and their characteristics are discussed in detail. The material chosen for the experimental work can be categorised into three main groups such as having same surface ply (0^o or 90^o in this case), exhibit similar global properties (i.e. CTE and stiffness) and laminates without a temperature gradient through the thickness (such as balanced laminates). Some laminates exhibit one or more of these general characteristics. Based on this, eleven different sets of composite samples and a pure epoxy specimen were studied in this work. All the laminates considered in this work are summarised in Table 3.1 and the reason for choosing each type of laminate is explained in the following sections. The composite specimens were chosen to provide variation in the thermoelastic response, so that a systematic assessment of the influence of different inherent properties on the thermoelastic signal is possible.

3.6.1 Unidirectional laminates (UD)

Unidirectional fibre reinforced laminate consist of multiple layers of lamina stacked only in one direction (i.e.$(0)_6$ or $(90)_8$) and exhibit the highest stiffness in the fibre direction but exhibit low strength and modulus in transverse to the fibre direction. The UD(0) and UD(90) laminates with fibres orientated parallel and perpendicular to the applied load provide fundamental data for evaluation of the thermoelastic response. This set of test specimens exhibits the same mechanical and thermoelastic response locally (on the surface) and globally as well as discounting heat transfer between the layers. If the

Table 3.1: Stacking sequence of the test specimens

Specimen	**Stacking sequence**
Epoxy	n/a
UD(0)	$(0)_6$
UD(90)	$(90)_8$
CP(0)	$(0,90)_s$
CP(90)	$(90,0)_s$
CP(0)3	$(0_3,90_3)_s$
CP(90)3	$(90_3,0_3)_s$
AP	$(\pm 45)_s$
AP3	$(+45_3,-45_3)_s$
OA(45)	$(45)_8$
QI(0/45)	$(0,\pm 45,90)_s$
QI(0/90)	$(0,90,\pm 45)_s$

thermoelastic response is a function of surface ply only, then one would expect all the laminates with a 0^o or 90^o surface ply to behaving in the same way as the UD laminate for the same applied strain sum.

3.6.2 Cross-ply laminates (CP)

Cross-ply laminates are those which have a ply orientation of 0^o or 90^o. Since for layers with 0^o and 90^o plies $\bar{Q}_{16}$ and $\bar{Q}_{26}$ are zero, A_{16} and A_{26} are thus also equal to zero (see equation Equation 3.20). The two CP laminates; one with a 0^o surface ply and another with a 90^o surface ply will allow the effect of the surface ply on the thermoelastic signal to be assessed (obtained from the same panel). This would provide indication if the thermoelastic response is from the surface ply or a global response, as both laminates have identical global mechanical (i.e $A_{11} = A_{22}$) and physical properties. The large variation in each ply stiffness will lead to large temperature gradients ply by ply and therefore will show if heat transfer is occuring between the layers.

The CP laminates with 3 surface plies of the same orientation were selected to aid assessment of the influence of the sub-surface ply, as it has 3 layers of similar surface laminae before the next sequence. This again would indicate if the introduction of the three surface plies in the same direction effectively change the heat transfer properties through the thickness of the laminate.

3.6.3 Angle-ply laminates (AP)

Angle ply laminates have ply orientations of θ and -θ with layers having an orientation other than 0^o and 90^o (i.e. $(45,\text{-}45)_s$). For this type of laminate the $\bar{Q}_{16}$ and $\bar{Q}_{26}$ terms of the $+\theta$ and $-\theta$ have equal values with different signs such as:

$$\left(\bar{Q}_{16}\right)_{\theta} = -\left(\bar{Q}_{16}\right)_{-\theta}$$

Therefore, for balanced angle-ply laminates, the sums of the values for each set of angle ply, $\bar{Q}_{16}$ will cancel each other and A_{16} will be zero (similarly for $\bar{Q}_{26}$ and A_{26}). Therefore, the choice of AP laminate would indicate the possible existence of small amount of shear strain in the surface ply and the its influence on the thermoelastic signal. Similar to CP, the AP laminate with 3 surface plies stacked in the same direction was selected to understand how the increase in the number of surface plies affect the thermoelastic response.

The OA(45) laminate would allow the thermoelastic assessment of a non-orthotropic laminate. In this laminate all the lamina are orientated at 45^o (not symmetric, also known as the off-axis laminate). Therefore, the presence of extension shear coupling terms, A_{16} and A_{26} (because of the existence of $\bar{Q}_{16}$ and $\bar{Q}_{26}$), leads to the existence of shear strain under uniaxial loading. This test specimen should aid the assessment of the influence of shear strain on the thermoelastic response and demonstrate the validity of Equation 3.26.

3.6.4 Quasi-isotropic laminates (QI)

Laminates that demonstrate isotropic extensional stiffness in the plane of the laminate, such as $A_{11} = A_{22}$ are called quasi-isotropic laminates. Examples of quasi-isotropic laminates are $(0, 45, \text{-}45, 90)_s$ and $(60, 0, \text{-}60)_s$. The QI laminates represent stacking sequences commonly used in industrial composite structures. QI(0/45) and QI(0/90) laminates were chosen for this work, because they have identical surface ply orientations as well as identical global mechanical and physical properties. This is expected to provide information on the influence of the sub-surface ply, and again indicate if the themoelastic response is a global effect.

In general, a laminate composed of multiple orthotropic layers that are symmetrical about the mid- plane of the laminate does not exhibit shear extension coupling. Symmetric laminates are much easier to analyse and they do not twist due to thermal contraction during the cooling process of the manufacture.

3.7 Summary

The work in this chapter has shown the quantities $\alpha_x\sigma_x + \alpha_y\sigma_y$ and $\alpha_1\sigma_1 + \alpha_2\sigma_2$ are invariants. The theory presented in this chapter has categorically defined the thermoelastic response from an orthotropic lamina. This has been used as a basis to define four possible treatments for assessing the thermoelastic response from a multi-directional laminate. Four theoretical treatments will be used to identify the source and the prominent factors that influence the thermoelastic response from laminated composites; these are crucial in implementing a routine that can be followed to extract reliable and quantitative full-field data from the infrared measurements. It is shown that careful selection of ply orientation within the laminate are necessary. A set of stacking sequences that will demonstrate different possible effects on the thermoelastic response have been defined.

In Chapter 4 a suitable material and manufacturing process is determined and panels with different stacking sequences are produced. In developing the four different equations, it can be seen that for any quantitative interpretation of thermoelastic data to be made between the theory and measurements, a full set of material properties are required. To provide a more detailed assessment of the origin of the thermoelastic response, in Chapter 5 the thermoelastic temperature change based on each treatment is compared with the measured temperature change from an orthotropic laminate. Further to this, the definitive proof that $\alpha_x\sigma_x + \alpha_y\sigma_y$ and $\alpha_1\sigma_1 + \alpha_2\sigma_2$ are invariants, which has been provided for the first time, is an important part of this work. This is demonstrated in Chapter 6, where thermoelastic data from two different coordinate systems are compared.

Chapter 4

Test materials and properties

4.1 Manufacture of test specimens

The overall aim of this work is to ascertain the fundamental quantities that influence the thermoelastic behaviour of laminated composite materials. Therefore, secondary effects such as the large material and manufacturing variability, high void content and high thermal conductivity were set aside. Hence, standard off the shelf material was chosen for all the work described in this thesis. Therefore, unidirectional glass/epoxy pre-impregnated (pre-preg) material consisting of E-glass and Novalac epoxy that requires controlled vacuum assisted autoclave manufacturing process, which minimises the void content in the laminate was selected. It is well known that this process will produce laminates with the most practical repeatable material properties.

Composite panels (0.3 m x 0.3 m) were manufactured from the unidirectional glass/epoxy pre-preg to form the laminates with the stacking sequences given in Section 3.6 from which the test coupons were obtained. The fibre volume fraction was approximately 57%, which was determined from a burn-off test, following the procedures given in ASTM D2584-08 [61]. The specimens were manufactured by curing the stacked pre-preg for 1 hour at 125^oC under 3 bar of pressure in an autoclave and post cured at 150^oC for 16 hours (as shown in Figure 4.1). Finished laminates were cooled and trimmed to size (as shown in Figure 4.2) and bonded with composite end tabs. The dimensions of the test specimens are given in Table 4.1. The epoxy resin used in the prepreg was supplied in solid form by the manufacturer as they receive it, before it is combined with the glass reinforcement to form the prepreg sheets. To simulate the vacuum consolidation process, a bar of epoxy was produced by applying pressure in a hot press at a temperature of 70^oC to melt the epoxy in a mould. Once the material had formed the shape of the mould it was removed from the press and cured and post cured in an oven using the

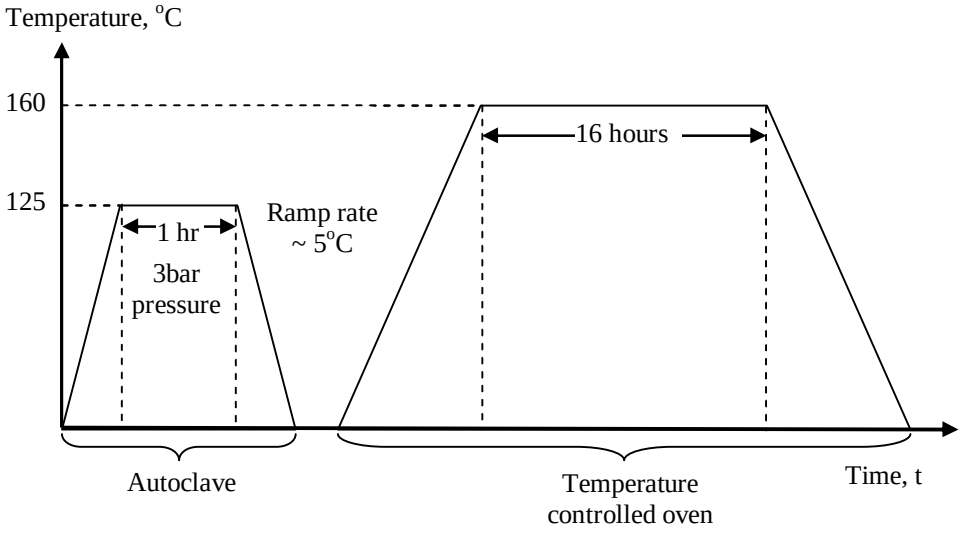

Figure 4.1: Cure cycle for Glass/ Epoxy pre-preg material

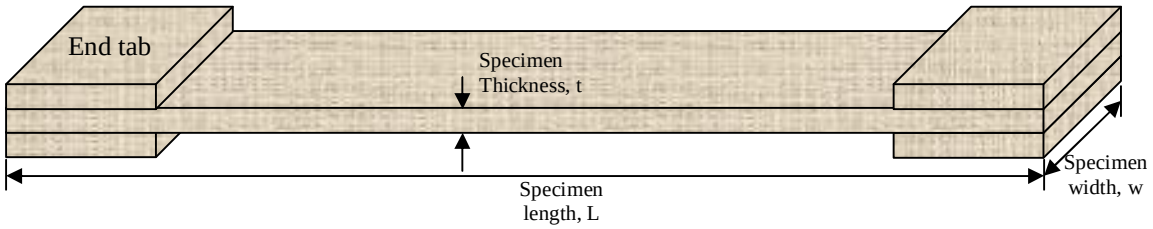

Figure 4.2: Test specimens

same temperatures as the prepreg material. A typical micrograph of the surface layer of a cured UD laminate showed that the thickness of the resin rich layer is about $30\mu \pm 9\mu$m (see Figure 4.3).

Since composite materials generally exhibit substantial variation from one material type to another, the mechanical and physical properties need to be determined experimentally for the specific material considered in this work. Therefore, the mechanical and physical properties described in Chapter 3 such as the CTE, specific heat capacity and density for both the resin and composite material need to be measured experimentally. The procedures for measuring these properties are detailed in the following sections.

4.2 Elastic properties

An orthotropic material possesses nine elastic parameters, namely three Young's moduli, three shear moduli and three Poisson's ratios. Most investigations have discussed in-plane material constants, reducing the nine independent material constants to four.

Table 4.1: Lay-ups and dimensions of test specimens

Specimen	**Stacking sequence**	**Dimensions (mm)**		
		Length, l	Width, w	Thickness, t
Epoxy	n/a	250	40.1	8.2
UD(0)	$(0)_6$	220	20.2	1.5
UD(90)	$(90)_8$	166	39.7	1.9
CP(0)	$(0,90)_s$	220	23.2	1.0
CP(90)	$(90,0)_s$	230	23.3	1.0
CP(0)3	$(0_3,90_3)_s$	220	25.2	3.0
CP(90)3	$(90_3,0_3)_s$	224	26.6	3.0
AP	$(\pm 45)_s$	230	24.1	1.0
AP3	$(+45_3,\text{-}45_3)_s$	217	25.7	2.9
OA(45)	$(45)_8$	230	33.9	1.9
QI(0/45)	$(0,\pm 45,90)_s$	230	24.2	1.9
QI(0/90)	$(0,90,\pm 45)_s$	222	23.7	1.8

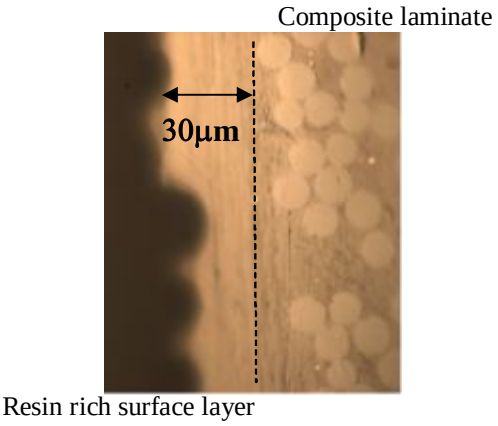

Figure 4.3: Micrograph showing the cross-section of a UD laminate

However, for studies involving 3-D modeling (for the work presented in Chapter 6), material constants in the through-thickness direction (3rd direction) are important. The three mutually perpendicular plane of symmetry for an orthotropic material is shown in Figure 4.4. The elastic properties, $E_1, E_2, E_3, G_{12}, G_{13}, G_{23}, \nu_{12}, \nu_{13}$ and ν_{23} of an orthotropic material can be determined experimentally using appropriate test specimens. The mechanical properties of the epoxy and composite were measured according to ASTM D638-03 [62] for the in-plane properties and ASTM D7291 [63] for the through-thickness properties. In this work, the mechanical properties of the lamina were measured from UD laminates (UD(0) and UD(90)) and the global properties were obtained from each different stacked configuration. The solid epoxy bar was used to obtain the mechanical properties of the resin. The tensile tests were performed using an electro mechanical Instron universal testing machine with a 50 kN capacity. The longitudinal

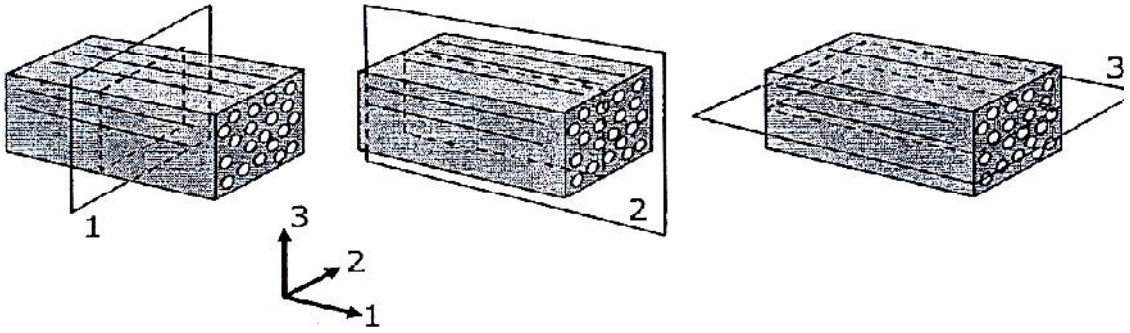

Figure 4.4: Three mutually perpendicular plane of symmetry for an orthotropic composite laminate

and transverse strains were measured using clip extensometers. By applying uniaxial tensile load to the UD(0) specimens (3 different specimens were tested in this work) along the fibre direction and measuring the applied load, P, the cross-sectional area, A, and the longitudinal and transverse strains, E_1 can be calculated as:

$$E_1 = \frac{P/A}{\epsilon_1} \tag{4.1}$$

and ν_{12}, as:

$$\nu_{12} = -\frac{\epsilon_2}{\epsilon_1} \tag{4.2}$$

A typical in-plane stress-strain curve for an unidirectional laminate is shown in Figure 4.5.

Similarly, E_2 and ν_{21} can be determined from the UD(90) specimen (5 different specimens were tested in this work). The G_{12} can be obtained from a tension test of a $\pm$ 45 symmetric laminate. This allows the in-plane 0 degree shear stress strain curve to be generated. This technique has the advantage of using relatively inexpensive straight forward specimens and test equipment. Using the relation derived from CLPT [64], the shear stress (τ_{12}) and shear strain are given as:

$$\tau_{12} = \frac{P}{2A} \tag{4.3}$$

$$\gamma_{12} = \epsilon_x - \epsilon_y \tag{4.4}$$

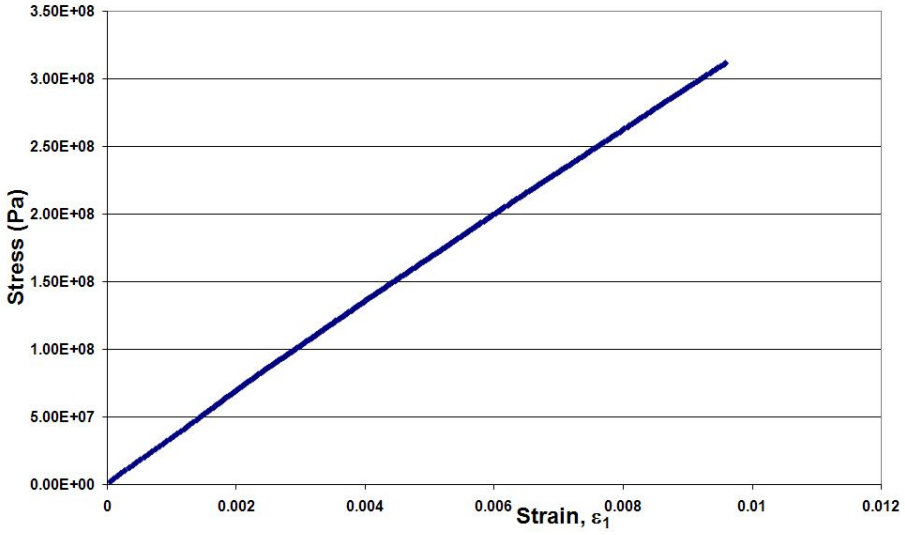

Figure 4.5: Typical stress-strain curve for a UD laminate

The unidirectional shear modulus can be calculated as following:

$$G_{12} = \frac{\tau_{12}}{\gamma_{12}} \tag{4.5}$$

The through thickness test specimens were manufactured from 60 identical plies of glass/epoxy lamina (as shown in Figure 4.6) with dimensions: 20 x 20 x 50mm, to obtain the material properties in the third direction. A fixture with cylindrical ends was built to apply the load to the specimen (as shown in Figure 4.6), which was bonded to the specimen on both sides. The applied load and horizontal and vertical strains in the specimens were measured using strain gauges. This enabled the values of E_3 and ν_{13} to be computed as follows:

$$E_3 = \frac{P/A}{\epsilon_3} \tag{4.6}$$

$$\nu_{13} = -\frac{\epsilon_3}{\epsilon_1} \tag{4.7}$$

The measured average mechanical properties for the epoxy resin and the composite specimens are reported in Table 4.2. If transverse isotropy exists (which is a valid assumption for the UD laminate), only five independent elastic constants, such as E_1, E_2, ν_{12} and the shear moduli in two orthogonal planes (i.e. G_{12} and G_{13}) are sufficient to define the orthotropic material. In this work, the value of G_{13} is assumed to be equal to G_{12} and the value of ν_{23} and G_{23} is obtained from the following equations [65]:

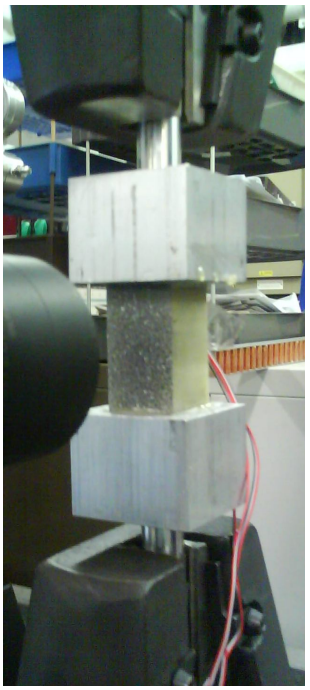

Figure 4.6: Experimental setup for through thickness measurement

$$\nu_{23} = \nu_{12} * \frac{\nu_m(1 + \nu_m - \nu_{12}\frac{E_m}{E_{11}})}{(1 - {\nu_m}^3) + (\nu_m \nu_{12}\frac{E_m}{E_{11}})} \tag{4.8}$$

$$G_{23} = \frac{E_{22}}{2(1 + \nu_{23})} \tag{4.9}$$

where the subscript m denotes the matrix/resin property.

Table 4.2: Elastic properties of E-glass/epoxy pre-preg composite and epoxy resin

Specimen	**Young's Modulus (GPa)**			**Poisson's ratio**			**Shear Modulus (GPa)**	
	E_1	E_2	E_3	ν_{12}	ν_{13}	ν_{23}	G_{12}	G_{23}
UD(0)	34.2±0.5	10.0±1.2	7.8	0.25±0.12	0.27	0.40	3.00	3.57
Epoxy	4.0	n/a	n/a	0.27	n/a	n/a	n/a	n/a

4.3 Coefficient of thermal expansion

The determination of the coefficients of thermal expansion (CTEs), α, requires precise measurement of the change in length of a specimen with temperature. There are various test methods and techniques available for determining a temperature induced displacement ranging from electrical transducers (e.g. resistance strain gauges, dilatometer) to

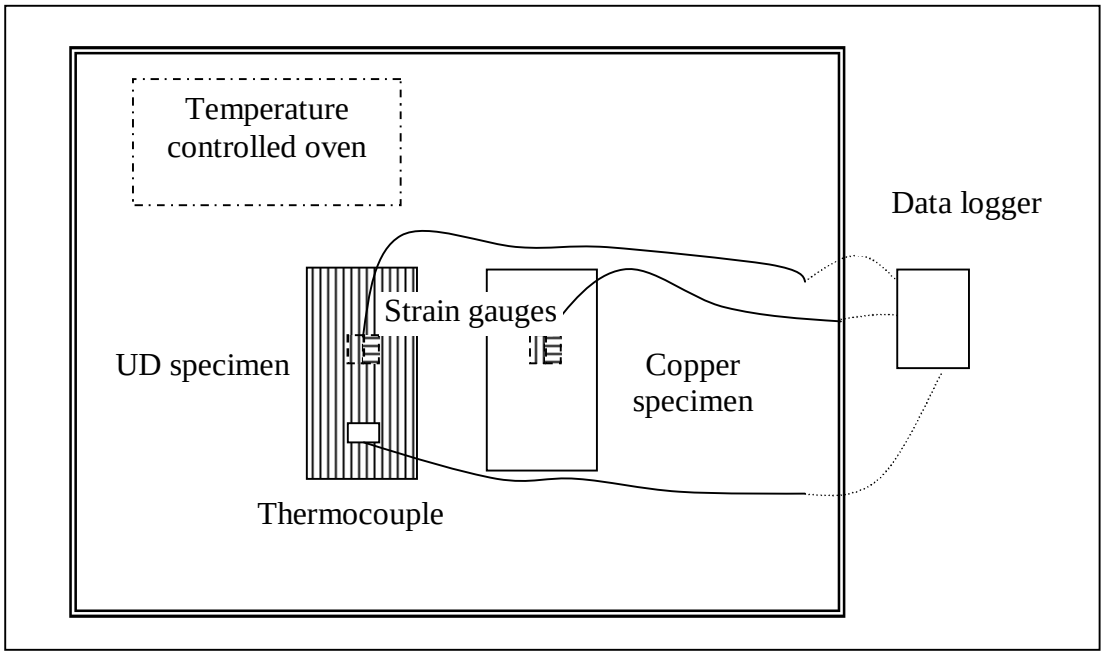

Figure 4.7: Experimental setup for CTE measurement

electrical-optical transducers (e.g. fibre optics, scanning beams). The CTEs of the composite material used in the work were measured using two element rectangular rosette (electrical resistance strain gauges) following the procedure of Ref. [66]. The experimental set-up for the 20 mm x 25 mm x 1.5 mm specimen is shown in Figure 4.7. The technique determines the thermal expansion behaviour of a glass fibre-reinforced epoxy unidirectional lamina using a pure copper specimen (with known CTE) as a reference material. In this case the CTE of copper (α_{ref}) was taken to be 17.00 x $10^{-6}/^{o}$C. The strain gauges were attached to the specimens by adhesive bonding. The two specimens were exposed to the same variation of temperature (heating rate was 1^{o}C/min). The CTE of the test material relative to the CTE of the reference specimens can be obtained from the difference of the output of the two strain gauges as:

$$\alpha = \alpha_{ref} + \frac{\epsilon_i - \epsilon_{ref}}{\Delta T} \tag{4.10}$$

where α_{ref} is the CTE of the reference specimen and α_i is the CTE in the principal material direction, i = 1, 2. The CTE in the 1 and 2 direction for UD laminate is shown in Figure 4.8. The measured values for the UD laminate are reported in Table 4.3 and the global CTEs are given in Table 4.4.

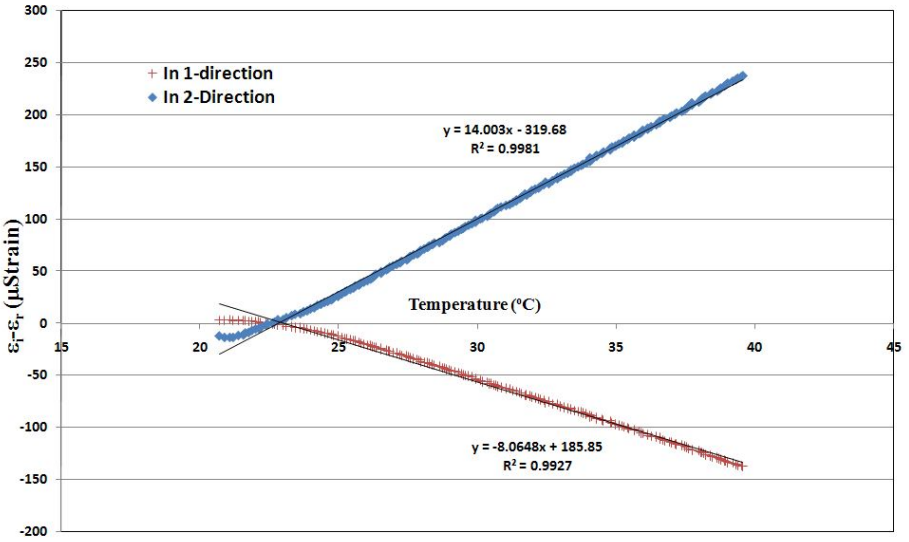

Figure 4.8: Typical output from CTE measurements on a UD laminate

4.4 Specific heat capacity

The physical properties of the composite laminate such as the specific heat capacity and density are independent of the directionality of the material. The test method used to determine the specific heat capacity is a standard method based on Differential Scanning Calorimetry (DSC) [67]. Four UD composite and two epoxy specimens with an approximate mass of 10 mg, were tested to account for material variability. The specific heat capacity was determined for temperatures ranging from 10 to 50^{o}C. This is the range of practical application of TSA for composite material. The DSC system was nitrogen cooled to achieve temperatures below ambient. The heating program for the heat capacity measurements started with an equilibration at 10^{o}C for 15 min and then progressed to 40^{o}C by applying a ramp of 5^{o}C per minute (the heating rate) and continuous measurements were taken by the DSC system. The quantity of heat, q, necessary to raise the temperature of the material of mass, M by ΔT at constant pressure is obtained by:

$$C_p = \frac{q}{M\Delta T} \tag{4.11}$$

The average value of the heat capacity measurements for the composite material is calculated for each temperature and plotted as shown in Figure 4.9. Clearly, variation of the C_p value between the four composite specimens can be seen. It is important to note that the fibre/epoxy weight fraction of the material is ignored in the process of deriving the C_p values for the composite specimens. The results for all the specimens

are found to be closer to values given in Ref. [68]. The average values of C_p for the composite material and epoxy resin are given in Table 4.3.

4.5 Density

The density of the epoxy and the composite specimens were measured based on the method of measuring the volume of small objects using a version of the hydrostatic weighing method. This involves submerging the object in a container of water placed on an electronic balance. A retort stand is used to suspend the object in the container of water. The volume of the immersed object, v_o, is simply the increase in mass divided by the density of the fluid:

$$V_o = \frac{\Delta M}{\rho_{water}} \tag{4.12}$$

where ρ_{water} is the density of the fluid (water), ΔM is the change in the mass recorded by the balance with and without the object. The precision of the technique depends on the precision of the scales, which was $\pm$ 0.01 mg. The density of the composite material with known mass can be determined using this technique. The average density of the composite and epoxy specimens is given in Table 4.3.

4.6 Global laminate properties

The properties of the laminates were determined in a similar way as for the lamina and are shown in Table 4.4. Also given in Table 4.4 are the theoretical values for the Young's modulus and Poisson's ratio for the laminates considered based on CLT and these show close agreement with the measured data. However, the value of measured Poisson's ratio and predicted using CLT is greater than 0.5.

Table 4.3: Average physical properties of an UD glass/epoxy composite laminate and epoxy specimen

Specimen	**Density(kg/m^3)**	**C$_p$ (at 25^oC) J/(kg^{o}C)**	**CTE, α (x10^{-6}/^oC)**	
			α_1	α_2
UD(0)	1895	843	9	31
Epoxy	1156	1230	52	n/a

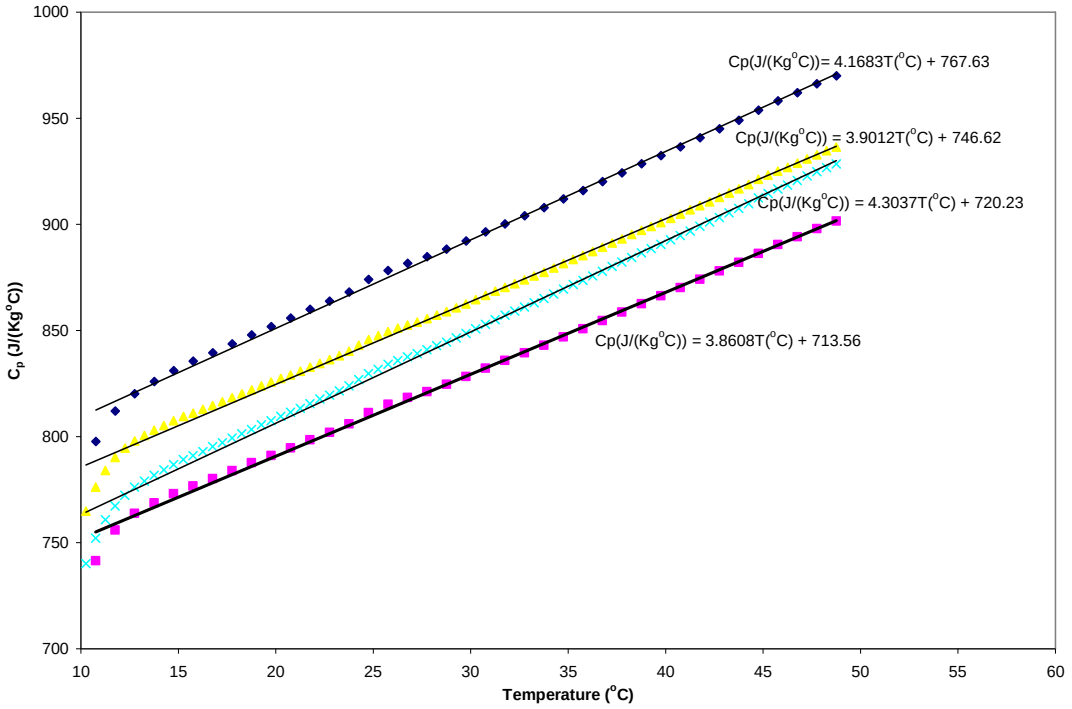

Figure 4.9: The specific heat capacity of an UD glass/epoxy composite in the temperature 10-50 ^{o}C

Table 4.4: Global mechanical and physical properties of cross-ply, angle-ply and quasi-isotropic laminate

Specimen	**CTE,α** (x$10^{-6}/^{o}$C)	**Young's Modulus, E(GPa)**		**Poisson's ratio, ν_{xy}**	
		Measured	CLT	Measured	CLT
CP(0)	10.59	20.0	22.4	0.15	0.11
AP	16.20	9.5	9.5	0.55	0.62
QI(45)	9.25	20.0	17.2	0.29	0.32

4.7 Uncertainty in the calculation of the material properties

Often two or more quantities need to be measured separately and combined arithmetically to obtain the resultant quantity. Examples include dividing a mass by volume to obtain density, or adding two lengths to get a total length. The general rule for the error in the case of sums and differences is that the absolute error of the result is the sum of the absolute errors of the original quantities.

It is important to determine the error in each measured quantity and analyse how these errors propagate to form a combined error in the final result. Based on the explanation

given in the previous sections on different characterisation techniques and the instruments involved, the estimated reading error in each instrument utilised is summarised in Table 4.5.

Table 4.5: Estimate of reading error for error analysis

Instrument	**Estimate of reading error**
Strain gauge	0.1% [69]
Extensometer	0.5%
Thermocouple (Type K)	$\pm 2^oC$[70]
Instron load cell (50kN)	±0.25%[71]
Laboratory balance	±0.01 mg
Oxford Precision Digital Caliper	±0.01 mm
DSC	2% [72]

Based on the values given in Table 4.5 the amount of estimated error in each material property determined experimentally can be calculated. The amount of error involved in calculating the different material properties can be shown as:

i Poisson's ratio

$$\nu = \frac{strain[Extensometer]}{strain[Extensometer]} = \frac{[0.5\%]}{[0.5\%]} = \frac{(1+0.005)}{(1-0.005)} = 1 + 0.01003 = 1\% \quad (4.13)$$

The terms in the brackets [], show the type of instrument involved and also the amount of [percentage] of error involved. The identity, $\frac{1}{(1-g)} = (1+g)$ is true for small value of g and is useful to obtain reasonable solution. This shows about 1% of error is expected in obtaining the values of Poisson's ratio.

ii Young's modulus

The largest error in the digital caliper occurs while measuring the thicknesses of the laminate, where t = 1 ± 0.01mm therefore contributing to 1% of error. In a similar way, the smallest width measured using the caliper is 20.2 ± 0.01 mm and contributing 0.05% error while measuring the width.

$$E = \frac{\frac{Load[Loadcell]}{Area[Caliper]}}{strain[Extensometer]} = \frac{\frac{[0.25\%]}{[1\%][0.05\%]}}{[0.5\%]} \quad (4.14)$$

The solution for this equation need to be considered in two parts, by solving the numerator before the denominator. For the numerator, $\frac{Load[Loadcell]}{Area[Caliper]}$ can be simplified as (when multiplying two quantities, their relative errors are added):

$$= \frac{[0.25\%]}{[0.0105\%]} = (1+0.0025)(1+0.0105) = 1+0.0105+0.0025+2.625e^{-5} = 1+0.013026 \tag{4.15}$$

This solution is combined with the denominator to provide:

$$= (1+0.013026)(1+0.005) = 1+0.005+0.013026+1.1275e^{-4} = 1+0.01809 \tag{4.16}$$

In total about 1.8% of error is estimated for Young's modulus measurements.

iii Coefficient of thermal expansion

The α_{ref} value is an estimation of different values of pure copper available in the open literature, the highest value available is 17.6^{o}C/min and lowest is 16.5^{o}C/min and the values used in this work is 17.00/^{o}C. This gives the CTE value to be 17 $\pm$ 0.55/^{o}C or 3% scatter in the value of α_{ref}. By taking the differences between temperature and strain values the possible constant offset from the instruments have been mimimised. Also, noticeble scatter is not present (shows also a very close fit nearing 1) in $\frac{\Delta\epsilon[strain\ gauges]}{\Delta T[Thermocouple]}$ values (slope of the graph shown in Figure 4.8). Therefore, the error from this measurement is assumed to be negligible.

$$\begin{aligned} \alpha_i = \alpha_{ref}[strain\ gauge] + \frac{\Delta\epsilon[strain\ gauges]}{\Delta T[Thermocouple]} \\ = [3\%] \end{aligned} \tag{4.17}$$

Therefore, about 3% of error due to the estimated value of α_{ref} is the main source of error in measuring the CTE.

iv Density

The minimum quantity of weight measured is 0.01313 g $\pm$ 0.01 mg which gives about 0.076% of error. The smallest value of volume measured in this work is 1450 mm^3 or 1450 mm^3$\pm$ 0.01mm^3 which contributes about 0.0007% error in total for the measurement of the density.

It is evident from the analysis that the measurement of CTE provides the largest error (about 3%). Combination of all of these estimated error in experimentally determining the actual material properties, will lead to accumulated error in the prediction of the ΔT/T values based on the proposed models in Chapter 3.

4.8 Summary

To assess the validity of each approach proposed in Chapter 3 accurate material properties are required. Therefore each relevant material property has been obtained experimentally for all the material configurations used in this work. Thus the mechanical and thermal behaviour of the composite material is fully defined, enabling theoretical treatment of each assumption in Chapter 3. By using the measured material properties and the associated error, the comparison between the experimental ΔT values and ΔT based on the proposed models is presented in the next chapter.

Chapter 5

Thermoelastic analysis of composite materials

5.1 Introduction

The purpose of the experimental work reported in this chapter is to assess the prominent factors that influence the thermoelastic response from laminated composites. Thereby providing the essential base for implementing a routine that can extract quantitative full-field stress/ strain data from TSA data obtained from laminated composite structures. The average thermoelastic response (ΔT) is recorded from the infrared detector from each specimen. To provide the detailed assessment of the nature of the thermoelastic response it has been decided to focus on glass fibre/epoxy system composites and examine the experimental results from the variety of laminates with different stacking sequences in comparison with theoretical values given by the four treatments listed in Chapter 3. Although there have been a number of quantitative studies (as detailed in section 2.4) on the application of TSA to composite materials, they have always considered a specific material or a particular structure and there is no general methodology of applying TSA to composite materials. The goal of the work described in this chapter is to assess and demonstrate if this is possible. In doing this, fundamental parameters such as non-adiabatic effects, the source of the thermoelastic signal and the influence of the applied loading conditions (e.g. mean load and frequency) on the thermoelastic response are considered in detail.

5.2 Experimental data

The starting point of the experimental work is in evaluating the response from the different laminates for the same applied strain sum. To do this a strain gauge rosette was attached to each of the test specimens. The test specimens were mounted in an Instron servo-hydraulic test machine and a cyclic load applied at 10 Hz so that the strain sums ($\epsilon_x + \epsilon_y$) were almost the same. It was decided to use a practical loading frequency of 10 Hz to obtain the thermoelastic response as previous work, e.g. [10, 11], has indicated that this is sufficient to achieve adiabatic conditions in glass/epoxy specimens. The thermoelastic readings were taken directly from the specimens, as the material provided a high and uniform surface emissivity of 0.92 [34, 36]. To aid comparison of the response it was decided to apply approximately the same strain sum to each specimen. A target of 1600 $\mu\epsilon$ was set for the strain sum but because of differences in the Poisson's ratios of the specimens this was difficult to achieve exactly; a summary of the applied load conditions and the strains is given in Table 5.1. TSA data was collected from all twelve specimens; the thermoelastic response from each specimen is shown in Figure 5.1. The average thermoelastic response, ΔT, recorded from the infrared detector from each specimen is provided in Table 5.1, these values were taken from a box of data indicated in Figure 5.1(a). Since it is difficult to obtain the strain sum and practically impossible to control the surface temperature of the specimen the temperature data have been normalised to discount for the variations. The scatter in the measured ΔT data (as mean value $\pm$ standard deviation) is also given in Table 5.1 to indicate the point wise variation in the data.

In all the images from the composite materials the indentation of the peel ply can be seen, although this does not cause a large detraction. It is also apparent that the surface ply orientation is indicated in the data; this suggests that the response is coming from the orthotropic material and not the resin rich layer or possibly a combination of both. It is also clear that the response in each composite specimen is not uniform, with large point wise variations. This is particularly evident for the CP(90), UD(90) AP(45) and OA specimens. It is noteworthy that the epoxy specimen shown in Figure 5.1 (a) provides the most uniform response. Finally, it is also clear that although the strain sums are similar, the response from each specimen is different. The scatter in the data is large, as reflected in the images and it is evident that the response is affected by the orthotropic subsurface ply.

There is no question that the epoxy resin is homogeneous and this as provides the most uniform response of all specimens and Equation 3.29 is valid in this situation. If the strain witness assumption is correct and the strain sums are similar, the epoxy resin should give the same response as the other composite specimens. To aid comparison

Table 5.1: Details of applied load, strains and thermoelastic data from the test

Specimen	**Load(kN)**		**Applied strain**		**Strain sum** $\Delta(\epsilon_x + \epsilon_y)$	**Surface temperature** T(K)	**ΔT(K)±(std.)**	$\frac{\Delta T}{T\Delta(\epsilon_x+\epsilon_y)}$
	Mean	**Amplitude**	$\Delta\epsilon_x$	$\Delta\epsilon_y$				
Epoxy	1.4	1.30	0.002690	-0.001090	0.001600	291.35	0.120±0.00510	0.257
UD(0)	1.5	1.20	0.002264	-0.000581	0.001683	292.25	0.147±0.0090	0.299*
UD(90)	0.7	0.60	0.001738	-0.000114	0.001624	290.11	0.104±0.0135	0.221**
CP(0)	0.7	0.55	0.001949	-0.000296	0.001653	291.55	0.147±0.0089	0.305*
CP(90)	0.7	0.55	0.001993	-0.000312	0.001681	290.57	0.139±0.0214	0.285
CP(0)3	1.7	1.55	0.001750	-0.000209	0.001541	294.90	0.119±0.0069	0.309*
CP(90)3	1.7	1.55	0.001780	-0.000216	0.001564	295.46	0.101±0.0107	0.219**
AP	0.5	0.41	0.003371	-0.001640	0.001731	294.91	0.121±0.0152	0.237
AP3	1.7	1.60	0.004425	-0.002725	0.001700	295.20	0.127±0.0111	0.253***
OA	0.7	0.60	0.002119	-0.000803	0.001316	293.45	0.095±0.0012	0.246***
QI(0/45)	0.9	0.88	0.002281	-0.000694	0.001587	292.03	0.138±0.0012	0.298*
QI(0/90)	0.9	0.85	0.003210	-0.001021	0.002189	296.09	0.112±0.0090	0.173

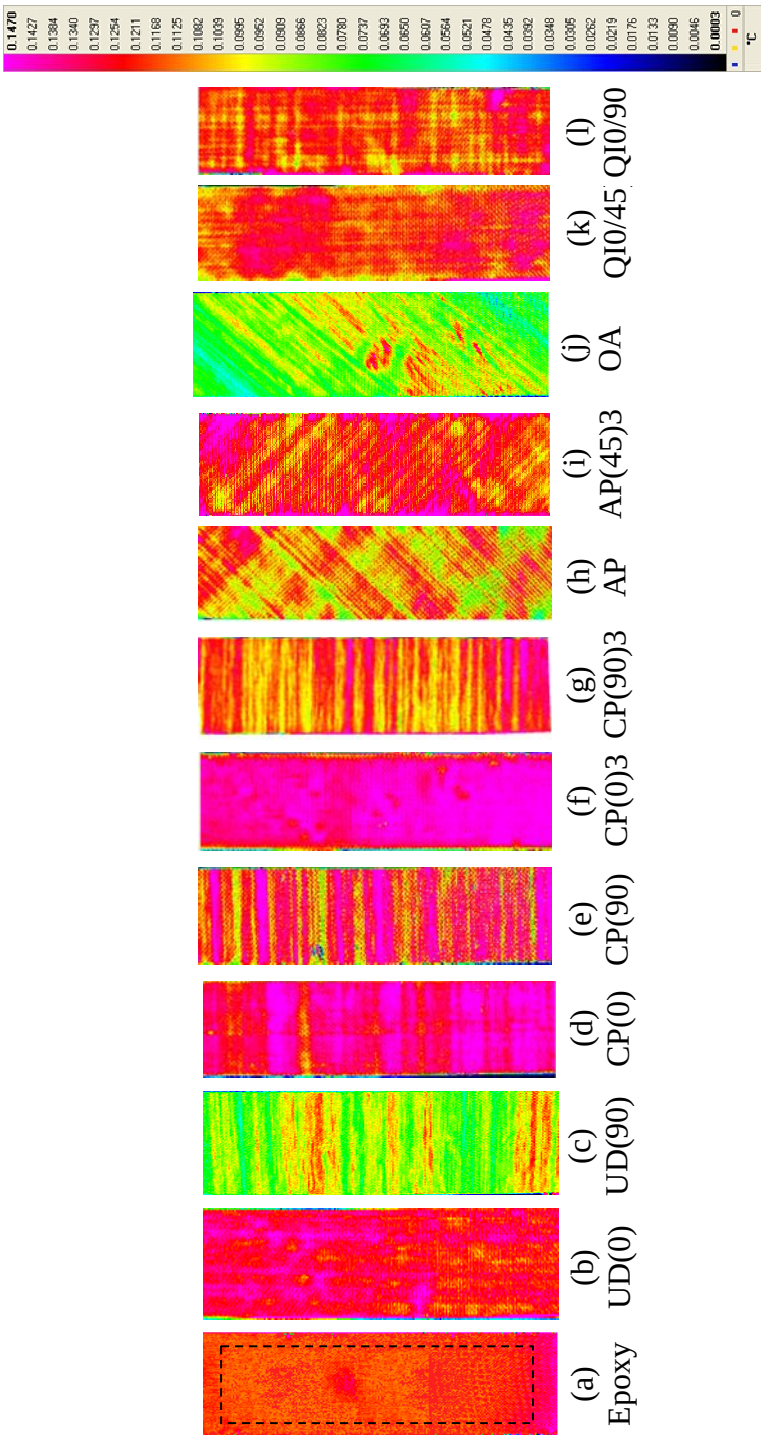

Figure 5.1: Temperature profiles obtained from specimens at loading frequncy of 10Hz; a)Epoxy, b)UD(0), c)UD(90), d)CP(0), e)CP(90), f)CP(0)3, g)CP(90)3, h)AP, i)AP(3), j)OA, k)QI(0/45), l)QI(0/90)

the ΔT data in Table 5.1 has been normalised for strain sum and surface temperature. Whilst the specimens provide a similar normalised response to each other it is clear that the thermoelastic response is not in general equal to that of the epoxy resin. However, there are groups of specimens, in the normalised data in Table 5.1 that show close correspondence with each other. The first group, indicated with *, UD(0), CP(0), CP(0)3 and QI(0/45), all show values within a few percent of each other and greater than the value for the pure resin, strongly indicating that the 0 degree surface ply is giving a uniform response for the same ply orientation. The only laminate with a 0 surface ply is the QI(0/90) that does not fit this pattern. The second group, indicated with **, UD(90), CP(90)3 have values within a few percent of each other and less than the pure resin. The CP(90) value does not correspond and in fact is closer to that of the 0 degree surface plies. In a similar fashion the AP3 and the OA (denoted ***) laminates show similar values (very close to the pure resin) but the AP shows a value that is less. This initial scrutiny of the data indicates that the strain witness assumption is not valid, but does not clarify the source of the response as the surface ply.

The scatter in the data is the highest for laminates with 90 surface plies (fibre directions are perpendicular to the loading direction). This is because the resin has a different response to the fibre. The mismatch between the response of the resin and the fibres indicates the clear influence of the surface ply. However this can only be determined by knowing the local variation and fibre distribution in the laminate. A further observation from the images is that there are significant differences in the thermoelastic temperature change obtained from the CP(0) and CP(90) specimens due to the differences in the surface ply orientations and the data becomes much more uniform when there are more plies at the surface introduced in the same way. A similar trend is also observed for the AP and AP3 plies indicating the possible influence from sub-surface plies. This statement is further supported by the observed difference between the two different QI laminates, which have the same surface plies and global mechanical and physical properties, yet there are clear differences in the thermoelastic data.

The conclusion from this part of the work might go some way to indicate the response from the composite specimens is from the orthotropic substrate; however, there are other influencing factors such as mean stress levels, possible heating and non-adiabatic behaviour, which are considered in subsequent sections of this Chapter. To resolve the issues of scatter a detailed analysis will be conducted in the next section that quantifies the scatter in the data.

5.3 Analysis of the thermoelastic response

Based on the experimental data presented earlier, comparison between each model (see Equations 3.30, 3.32, 3.33 and 3.29) and the measured data is expected to provide further insight into the thermoelastic behaviour of composite material. This is achieved by computing the thermoelastic temperature change based on each treatment using the material properties given in Chapter 4 and comparing it with measured temperature change for all the cases. The measured (with standard deviation) and calculated thermoelastic temperature changes are summarised in Table 5.2 and illustrated in Figure 5.2 with error bars inclused for the measured data. The values that provide the closest match with the measured data are highlighted in Table 5.2.

For the UD(0) and UD(90) specimens each theoretical treatment predicts an identical response with the exception of the resin. For the UD(0) laminate the measured ΔT value is 12% greater than the calculated resin value and 4% greater than the other three techniques. Likewise for the UD(90), the calculated resin value gives a slightly different response and the measured values are identical for the surface, global and mixed values. For CP(0) the calculated value based on the global approach gives the largest difference and closest to mixed approach. Similarly the global approach gives the largest deviation from measurements taken from CP(90), CP(0)3, CP(90)3, AP3 and QI(0/90) specimens. The measured values from the CP(90) and CP(0)3 specimens are closest to the resin approach. The measured ΔT values from the CP(90)3, AP, AP3 and QI(0/45) specimens shows close match (with a maximum difference of 4%) with ΔT values obtained from surface ply approach. The measurement from QI(90) and OA laminate shows close prediction with the resin approach.

Table 5.2: Thermoelastic response (measured and calculated) with experimental error from composite specimens

Specimen	**ΔT, Measured (K)**	**ΔT, Resin(K)** (Eq. 3.29)	**ΔT, Surface ply (K)** (Eq.3.30)	**ΔT, Global(K)** (Eq. 3.32)	**ΔT, Mix (K)** (Eq. 3.33)
UD(0)	0.147(±0.0090)	0.129	0.141	0.141	0.141
UD(90)	0.104(±0.0135)	0.124	0.104	0.104	0.104
CP(0)	0.147(±0.0089)	0.127	0.135	0.175	0.141
CP(90)	0.129(±0.0214)	0.130	0.106	0.171	0.104
CP(0)3	0.119(±0.0069)	0.118	0.125	0.174	0.143
CP(90)3	0.101(±0.0107)	0.118	0.097	0.173	0.106
AP	0.121(±0.0152)	0.133	0.125	0.132	0.127
AP3	0.127(±0.0111)	0.130	0.125	0.135	0.131
QI(45)	0.138(±0.0102)	0.123	0.136	0.144	0.136
QI(90)	0.112(±0.0090)	0.120	0.133	0.143	0.129
OA	0.095(±0.0134)	0.094	0.100	0.100	0.100

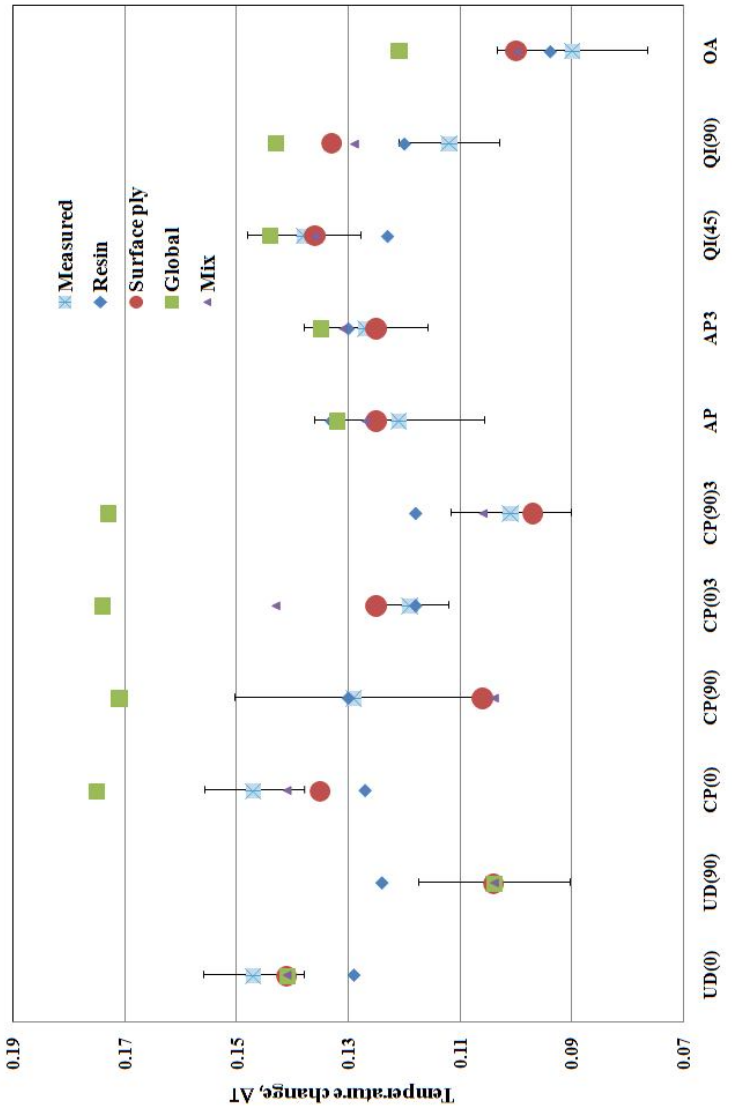

Figure 5.2: Predicted and measured thermoelastic response of the laminated composite

Figure 5.2 provides a visual representation of the data. Here it is clear that the experimental data straddles the resin values. The global values are clearly not providing a good model in many instances, they are far outside the experimental error. The mixed approach provides close agreement in many cases. The surface ply assumption also predicts well for many cases.

The differences in the thermoelastic temperature change obtained from the specimens, can only be due to the difference in the ply orientations as some of the specimens were obtained from the same panel and in some cases the specimens (i.e. CP(0), CP(90) and CP(0)3, CP(90)3) were subjected to same loading conditions. This clearly violates the 'strain witness' assumption, since local variability in the constituent material is discounted. By accounting for the scatter in the data, the predictions based on both surface ply and mixed seem to be valid. The approach in which the CTE is coupled in the stack, gives a better agreement to the measured data than the 'strain witness' and 'Global' assumptions, as does the surface ply assumption. However, by accounting for the large scatter in the data, it is difficult to establish if one prediction is providing better results than another. For laminates with stacked ply group of surface layers there is a good agreement between the measured data and the surface ply approach. It should be noted that the stresses in the orthotropic layers of a composite laminate vary with fibre orientation and moreover it is certain that the stress carried by the resin surface layer will be small compared to that of laminate. This means that the stress induced temperature change in the resin surface layer will be different to that in the surface ply of the laminate and depending on the ply orientation may cause large temperature gradients between the surface layer and the orthotropic substrate. Heat transfer between the resin and the laminate and vice versa is therefore a distinct possibility. The measured surface temperature changes could therefore be a result of the 'strain witness' effect, a result of heat transfer through the resin giving a response from the surface ply, or a combination of both. The response is clearly dependent on the thickness of the surface resin and the orientation of the subsurface ply.

To illustrate the difference in the stress induced temperature change in the resin and the orthotropic substrate for each specimen in each loading case, the calculated ΔT values for the resin are subtracted from ΔT for the orthotropic substrate (as shown in Figure 5.3). In instances where the difference is greatest non-adiabatic behaviour (i.e. heat transfer between the resin layer and the orthotropic surface layer) can be expected. The negative region shows the heat transfer is from resin layer to substrate (i.e. UD(90), CP(90) and CP(90)3). Accordingly, the measured values also show similar trends, such that when the heat transfer is from the resin to substrate the measured value is lower than the calculated resin value see Figure 5.2. When the heat transfer is from the surface ply to the resin the measured value is higher than the calculated resin value. This is

a clear indication of possible heat transfer between layers, in which the thermoelastic response can be a combination of the temperature change in the resin layer and in the orthotropic surface layer. To provide further insight into this, the effect of heat diffusion with respect to loading frequency is investigated in detail in the following section.

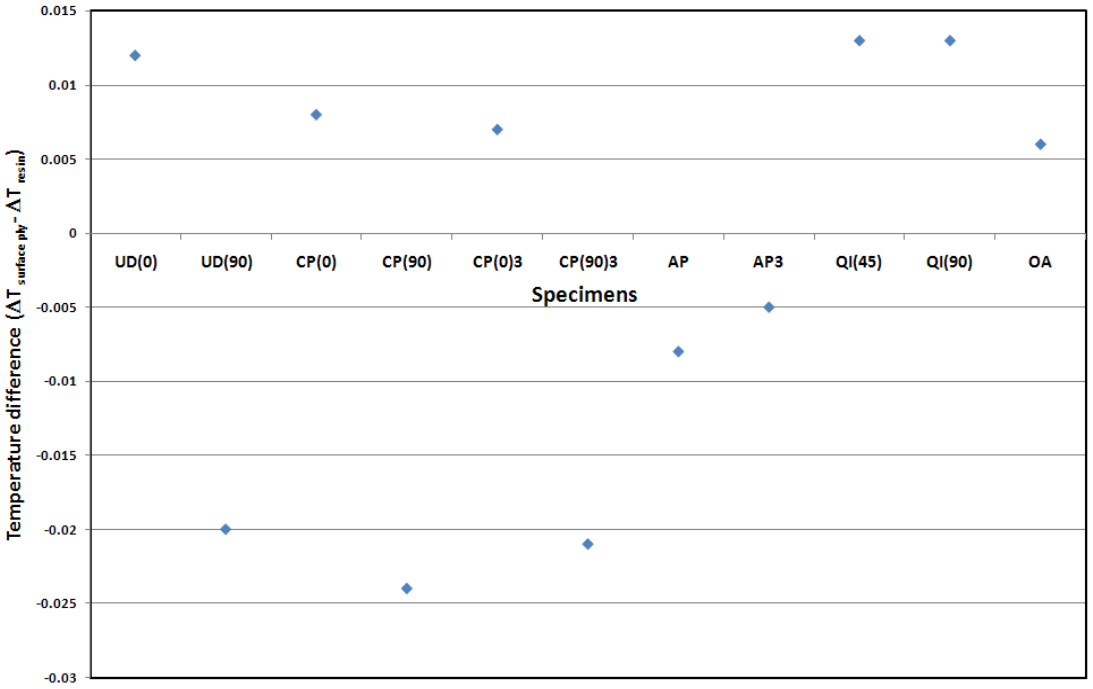

Figure 5.3: Temperature difference between the orthotropic surface layer and the isotropic resin layer

5.4 Non-adiabatic behaviour

5.4.1 Background to surface coatings

The stresses in the different plies in a composite laminate vary with fibre orientation. This could lead to high stress induced temperature gradients between the plies and affect the observed surface temperature changes. A non-adiabatic thermoelastic theory was developed by Dunn [73] for laminated carbon fibre composite by modelling interlaminar heat transfer, which showed a good agreement with the surface temperature measurements using the SPATE 8000 system. The normalised signal change (amplitude) for aluminium, CFRP laminates with $(\pm 45)_6$ and $(0,\pm 45)_4$ configurations at different loading frequencies were measured. Carbon has a very high thermal conductivity compared to the GFRP composite used in the current work. However, it is not just the thermal

conductivity that is important but the stress gradient between the layers. It was observed that for $(\pm 45)_6$ laminates in a similar manner to aluminium, a change of signal was not observed with an increase in the frequency. However, $(0,\pm 45)_4$ laminates responded differently at different loading frequencies, and it was concluded that adiabatic conditions were not achieved in the specimen. So far, in the current work, it has been assumed that heat transfer between layers in the glass/fibre epoxy specimens is small. This is because of the low thermal conductivity of the constituent materials. The cyclic loading frequency has to be high enough to avoid internal heat conduction between regions of different stress levels. In this work, the surface resin layer is of the order of 30 μm thick. This is more than a standard paint coating, but it should be considered that the surface resin layer has very similar thermal conduction properties to that of a paint coating. Mackenzie [74] reported progressive attenuation in the thermoelastic signal with increasing frequency and thickness of the paint coating and then a recovery of the signal beyond 50 Hz and at thicknesses above 70 μm. It is likely that at higher frequencies the paint coating was actually acting as a 'strain witness'. In the case of the resin layer, the question is if the mismatch in results shown in Figure 5.2 is as a result of non-adiabatic behaviour in the surface resin layer (the specimens in this work were unpainted) as observed by Mackenzie in the paint coating. Experiments on composites have shown that if the strain amplitude is large, a loading frequency in excess of 5 Hz can cause significant heating of the specimen and it is desirable to keep the loading frequency low [42]. In this work, where experiments are conducted at 10 Hz, thermoelastic data was corrected for changes in surface temperature. During each test the temperature of the specimen was monitored and it was shown that the greatest temperature change occurred in the AP specimen and this was only 0.2 ^{o}C. Therefore, it can be concluded that the heating of the specimen is not significant. In the following sections, numerical models have been developed in comparison with experimental model to study heat transfer effect in the composite laminate.

5.5 Experimental model

In TSA, a cyclic load is applied to achieve pseudo adiabatic conditions. The question is at what frequency is heat diffusion through the resin rich surface layer prevented so that it can act as a strain witness. It is impossible to remove the epoxy layer effectively from the surface of a composite laminate. Furthermore, it is extremely difficult to manufacture a fibre reinforced polymer composite without a surface resin layer, particularly if a vacuum consolidation is used. Therefore it was decided to add a resin layer to a simple specimen. A simple way of addressing this would be to produce two specimens one with and one without a surface resin layer. An aluminium strip specimen of dimensions 105 x 13 x

1.2 mm was prepared with part of the surface coated with epoxy resin (about 60 μm thick) and the other part coated with two passes of RS matt black paint (as shown in Figure 5.4).

To examine if at practical laboratory loading frequencies adiabatic conditions could be achieved the specimen was subjected to a constant uniaxial stress range of 52.2 MPa whilst the loading frequencies was varied from 10 to 60 Hz. Under pure tension loading, the stress in the specimen is uniform and therefore no heat transfer can occur in the specimen, enabling the diffusion characteristics of the coatings to be examined in isolation. If the response is constant over the frequency range this is a good indication of adiabatic behaviour.

The temperature changes measured from the painted and epoxy coated parts of the specimen are shown in Figure 5.5. Using the material properties for the aluminium given in Table 5.3 it is possible to derive a theoretical temperature change for the aluminium; this is shown in Figure 5.5. It is also possible to derive the temperature change for the epoxy acting as a strain witness using the values given in Table 4.3. It is assumed that the emissivity of the paint and the epoxy is 0.92 [34, 36]. The response from the painted surface is constant over the frequency range and virtually identical to the calculated ΔT value. This is a clear indication that the response is adiabatic and the paint coating is sufficiently thin to allow complete heat transfer from the surface of the aluminium to its painted surface. The measurements from the resin do not correspond with the calculated value for the strain witness response and show a monotonic decrease over the frequency range. As the frequency increases the values approach the strain witness value. These results indicate that there is heat transfer from the interface between the epoxy and the aluminium to the surface of the resin. As the resin layer is usually much thinner than 60 μm in a polymer composite this clearly indicates that the orthotropic surface layer plays a significant role in the thermoelastic measurements.

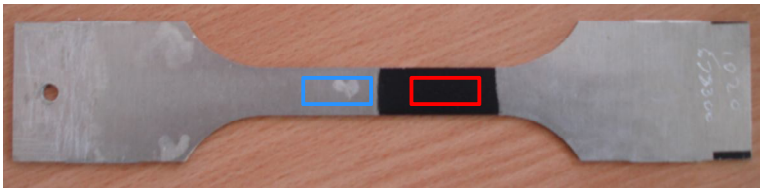

Figure 5.4: Aluminium strip specimen: with part of the surface coated with epoxy resin and the other part coated matt black paint

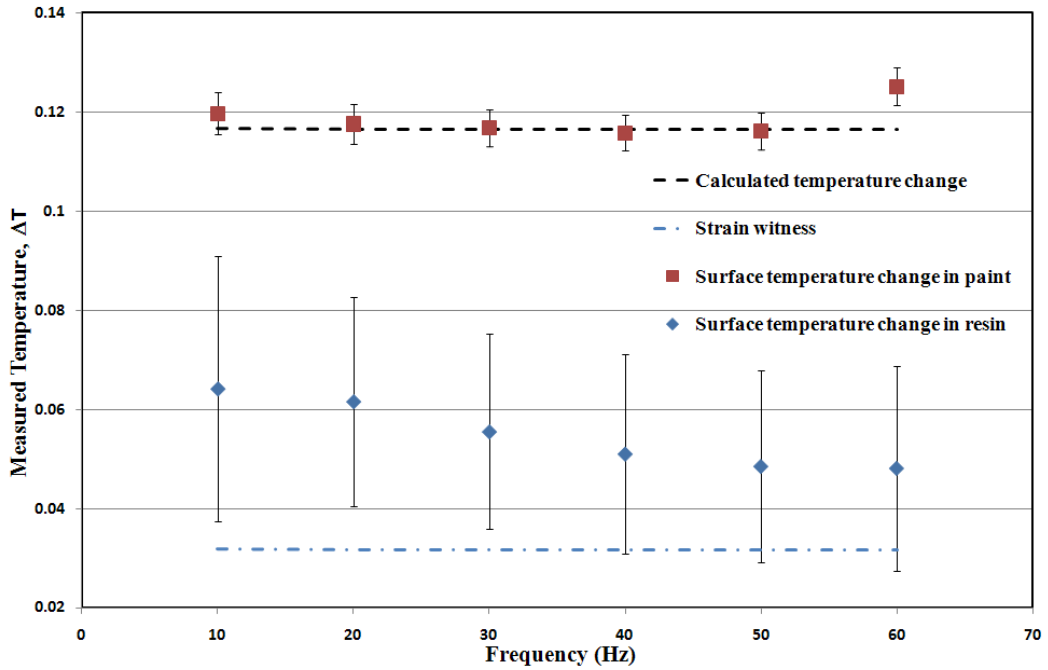

Figure 5.5: Change in the surface temperature of aluminium coated with an epoxy layer and paint coating

Table 5.3: Mechanical and physical properties of aluminium

Specimen	**Young's Modulus,** (GPa)	**Poisson's ratio**	**Density** (kg/m^3)	**CTE** (x10$^-$6/^{o}C)	**Specific heat capacity, C$_p$** (J/(kg^{o}C)
Aluminium	68	0.33	2700	21	900

5.6 FE model

In order to understand the effect of the resin layer on the thermoelastic response, a simple 2D heat transfer model was constructed to determine the thickness of the surface resin required to prevent heat conduction in order for the 'strain witness' assumption to be applicable. The model was constructed using ANSYS with PLANE55 thermal elements and the experiment was replicated numerically. The model was constructed assuming that the coating has a initial uniform temperature (initial boundary conditions) and a fixed temperature was applied to one end to replicate the temperature change in the substrate (which is equal to the measured value in the paint coating). Then transient heat transfer analysis was performed to obtain the time (i.e. $f = 1/t$) required to achieve equilibrium between the interface and the surface.

The model showed that a loading frequency above 33 Hz is required for the 'strain witness' treatment to be applicable. This finding is somewhat supported by the data in Figure 5.5 as at around 30Hz the response seems to become uniform. The difference between the experimental and calculated values at higher frequencies could be attributed to the differences in material properties and the assumed emissivity. It was considered that the same model could be implemented for a unidirectional laminate (to consider the resin layer and composite material interface) and was expected to give a reasonable approximation of the heat transfer characteristics. The initial uniform temperature in the surface layer was calculated using Equation 3.29 and at the interface, using Equation 3.30, for a given loading condition. The FE results showing the relationship between the resin thickness and the loading frequency for thermal equilibrium to be achieved in the surface resin layer for UD(0) and UD(90) are shown in Figure 5.6. This clearly shows that for a loading frequency of 10 Hz, for the given temperature gradient the resin layer thickness should be a minimum of 80 μm for UD(0) and 110 μm for UD(90) so that the surface measurements are not affected by the heat transfer. The thickness of the resin layer for the specimens used in this work is 30 μm according to Figure 5.6 and thus a loading frequency of approximately 67 Hz for UD(0) and 112 Hz for UD(90) are required to achieve adiabatic conditions for the 'strain witness' treatment to be valid. This shows that for the material considered in this work (considering the temperature gradient between the interface and surface layer) result of heat transfer through the resin a response from the surface ply.

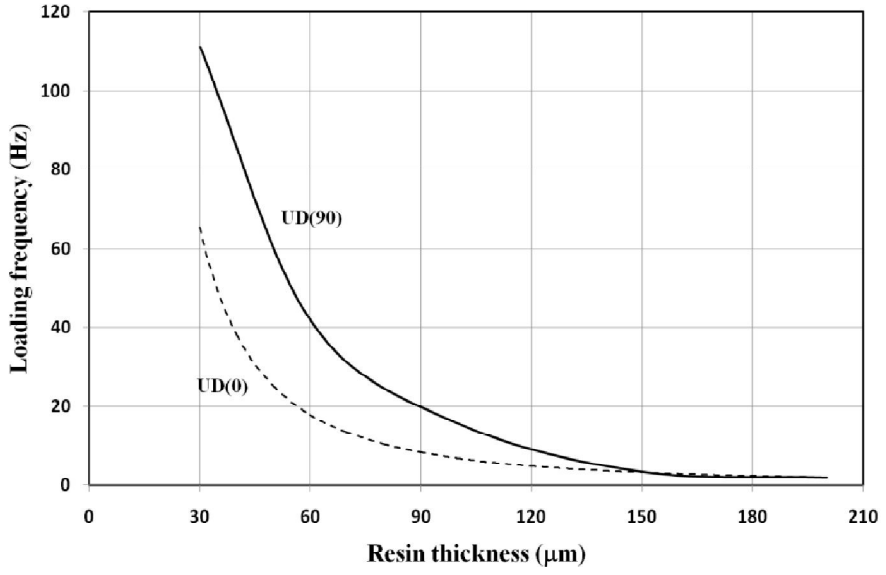

Figure 5.6: The relation between the thickness of the resin rich surface layer and the required loading frequency to achieve adiabatic conditions (from 2D FE analysis)

To further support the analysis, the tests results reported in Table 5.1 were repeated at loading frequencies of 15 and 20 Hz; Figure 5.7 shows a plot of thermoelastic temperature change against frequency. The values vary somewhat for the CP(90) specimen where the stress induced temperature change ply by ply is different, but also indicate that the same attenuation reported previously as the frequency increases.

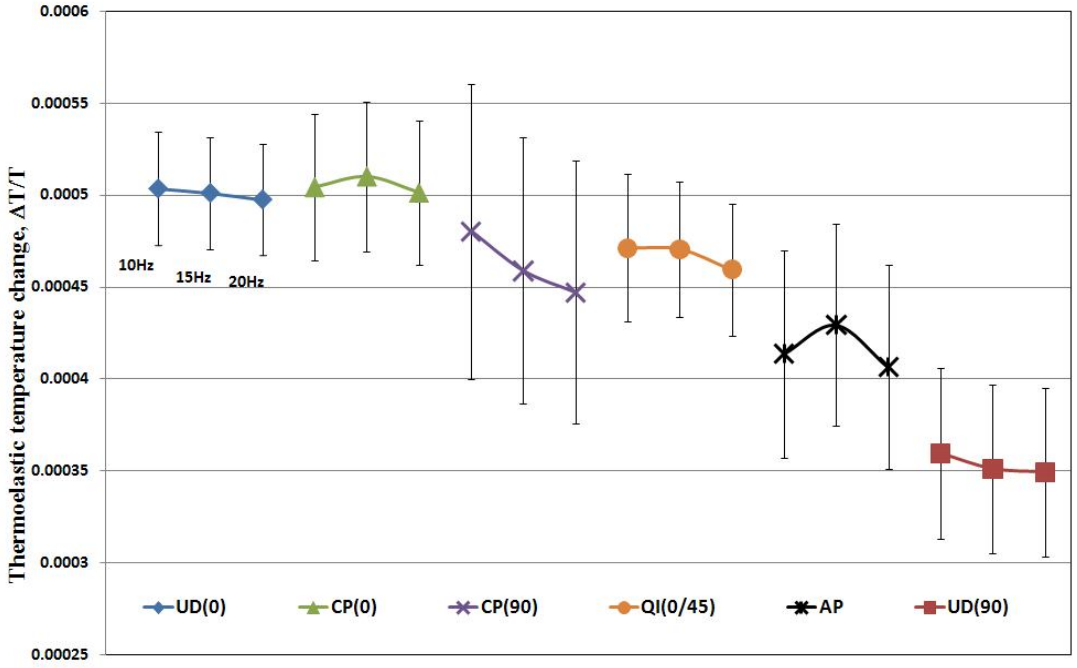

Figure 5.7: The variation of thermoelastic temperature change for different loading frequencies (10,15 and 20Hz)

The effect of mean load was also investigated in this work; it is show in Figure 5.8 that the thermoelastic signal is influenced to some degree by the applied mean load. However, the effect was not systematic and no clear trend was observed. The changes in the thermoelastic response are small and thus the effect of mean load can be neglected.

The FE analysis explained in this section was performed considering only the temperature gradient and performing the transient heat transfer analysis to obtain the time (i.e. $t = 1/f$) required to achieve the adiabatic condition (i.e. to reach temperature equilibrium). Therefore, this analysis does not reveal how the thermoelastic effect is coupled with the heat diffusion to account for the sinusoidal temperature change occuring in the surface layer. Therefore, the next section explores fully the coupling of the sinusoidal thermoelastic temperature change and heat diffusion from the substrate.

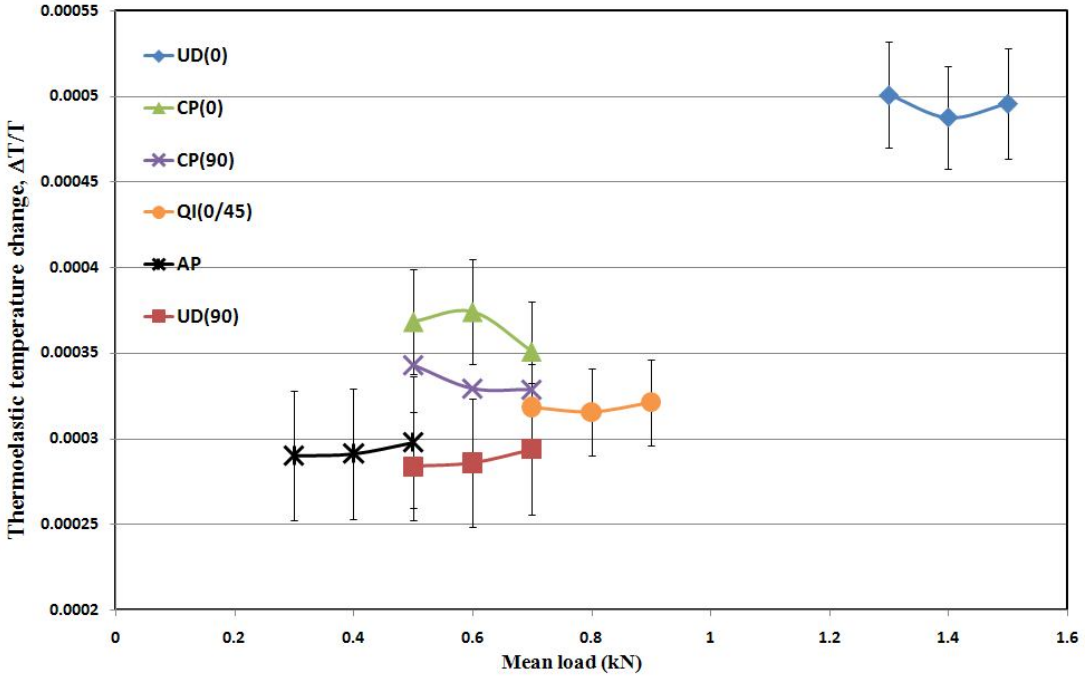

Figure 5.8: The variation of thermoelastic temperature change for different mean load

5.7 Periodic heat transfer model

To study the coupling of the thermoelastic effect and heat diffusion, a 1D heat transfer model was constructed to determine the thickness of the surface resin required to prevent heat conduction in order for the 'strain witness' assumption to be applicable. The model was developed using the the finite difference method to study the periodic heat diffusion through the surface resin layer. As the sub-surface temperature changes in a sinusoidal manner, the heat will diffuse from the substrate to the surface layer in the same way. Mathematically, diffusion may be represented by:

$$\frac{\partial^2 T(t,z)}{\partial z^2} = \frac{1}{\kappa}\frac{\partial T(t,z)}{\partial t} \tag{5.1}$$

where $T(t,z)$ is the temperature at time t and depth z, and κ is the thermal diffusivity of the resin. The above equation may be solved "analytically", i.e. $T(t,z)$ may be given as a solution for simple cases with temperature variation described by a cosine function (without the internal heat generation term and by ignoring transient perturbation)[75]. In this work MATLAB code has been developed for solving the problem using the Finite Difference Method (FDM). The analysis will allow the effect of sinusoidal temperature variation in the bottom boundary (i.e. resin surface adjacent to the substrate), to be amounted for and the observed surface temperature change can be computed. The heat

diffusion is assumed to occur in the through thickness direction only and changes with the loading frequency.

If the time be 0, Δt, $2\Delta t$,....., NΔt and position be a, a+Δz, ..., a+JΔz = thickness of resin layer, then Equation 5.1 in the form of finite difference equation (FDE) can be written as:

$$\frac{T_{i-1} - 2T_n + T_{i+1}}{\Delta z} = \frac{1}{\kappa}\frac{T_i^{'} - T_i}{\Delta t} \tag{5.2}$$

where T_n is the temperature at the node. Since the surface temperature is unknown (i.e. the value of interest), the bottom boundary is assumed to be a radiative boundary condition.

The result from the analysis is shown in Figure 5.9, which shows 4 different lines indicating: a) the thermoelastic temperature change in the substrate (Aluminium) obtained using Equation 3.30, b) the heat diffusion from the substrate to the surface resin layer, which is the solution based on Equation 5.2 or FDE, c) the thermoelastic temperature change of resin based on Equation 3.29 and d) the point by point addition of (b) and (c) (in the time domain) to obtain the combined effect (i.e. combination of the two sinusoidal plots). To make the comparison between the results of the FDM and the experimental model, the output from the FDM analysis, which is the diffusion from the substrate, is post processed in two different ways. Firstly, the net temperature change in the resin layer is combined with the temperature change due to the diffusion (i.e (b)+(c)) and this is labelled 'FDM' in Figure 5.10. In the second approach the combination of (b) and (c) in the time domain is labelled as 'Combined' in Figure 5.10.

Clearly, the numerical FDM results show similar trend to the experimental data. There is a small difference between the experimental and numerical result at 10 Hz. The surface temperature change and diffusion at 10, 20 and 120 Hz are shown in Figures 5.11, 5.12 and 5.13. The surface temperature change (contribution of diffusion) is not in phase (different shape and frequency) with the source but the thermoelastic temperature change in the resin layer is assumed to be in phase with the source. Although these results fit well with the experimental data, intuitively both the diffusion and thermoelastic temperature change should be added (combination of two sine waves) in the time domain to form a new signal that reflects the measured temperature change in the surface layer (as shown as 'Combined' in Figure 5.9, Figure 5.11, Figure 5.12 and Figure 5.13. The results of this analysis deviate from the experimental data a great deal at lower and higher frequencies but it captures the recovery of the thermoelastic signal at higher frequencies as reported previously by Mackenzie [74]. The build up of signal using the two frequencies would complicate (i.e. contain two spikes) the process

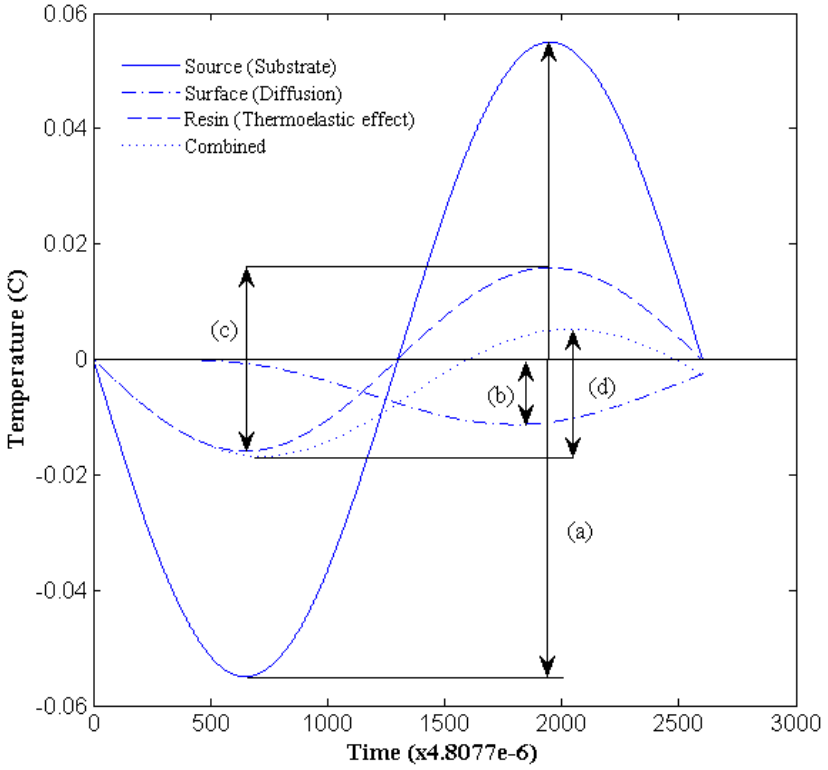

Figure 5.9: Temperature change in the surface and combination of heat diffusion and thermoelastic effect at frequency of 80 Hz

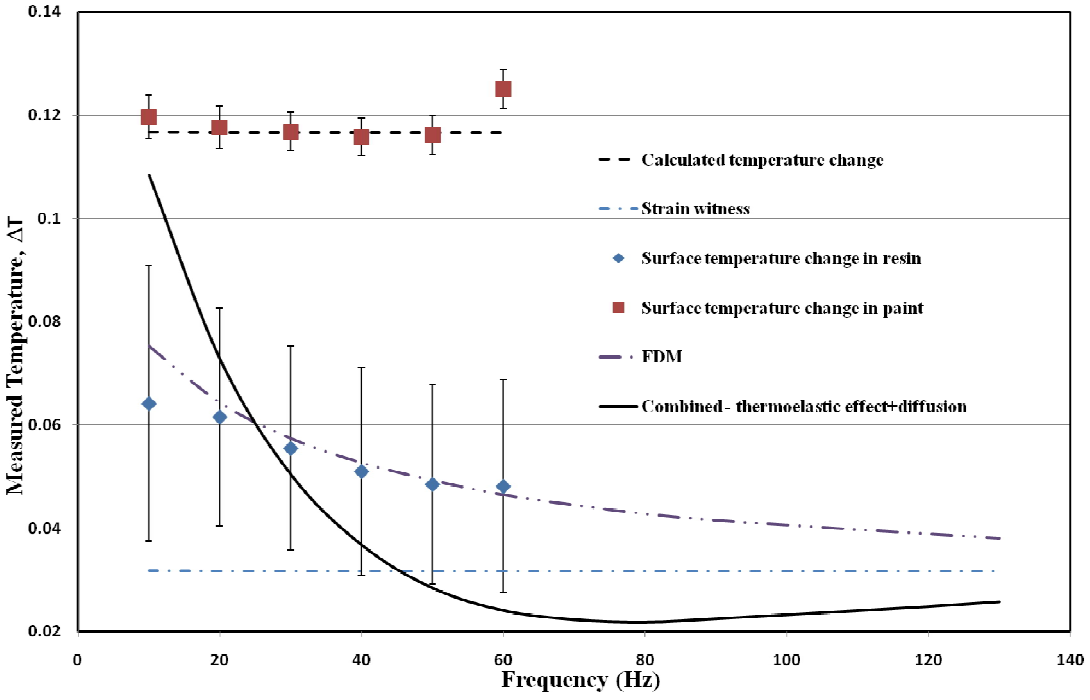

Figure 5.10: Comparison of experimental data and FDM results)

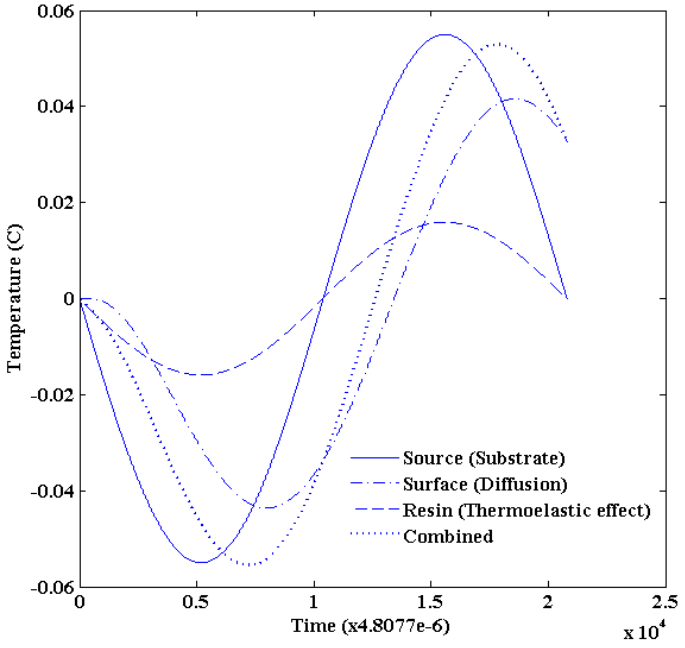

Figure 5.11: Temperature change at the surface and from a combination of heat diffusion and the thermoelastic effect, at a loading frequency of 10 Hz

of converting the signal in the time domain to the frequency domain where the signal breaks back down to the frequencies that it is composed of, and how the Cedip software accounts (i.e. FFT and noise filtering routines) for this is unknown.

5.8 Summary

The thermoelastic temperature change from several laminates subjected to in-plane stresses has been computed and compared with experimental results. The results show that the thermoelastic response is affected by several factors, one of which is orientation of the surface lamina. The pattern of the surface lamina is clearly visible in the TSA images. Detailed analyses show that there are differences in the thermoelastic signal from the surface resin layer from the laminates considered and that there is an influence from the orthotropic layer but that the existence of the resin layer should not be disregarded in the analysis. However, the response is not solely due to the orthotropic layer, below the resin surface either, since both the UD and CP(0) specimens have the same 0^o surface ply and their thermoelastic response is different. The UD(90) and CP(90) laminates show that the unequal thermoelastic properties of the fibre and matrix in a fibre reinforced composite material result in non-uniform deformation and temperature changes in their micro-constituents and not the net effect of such phenomena. This

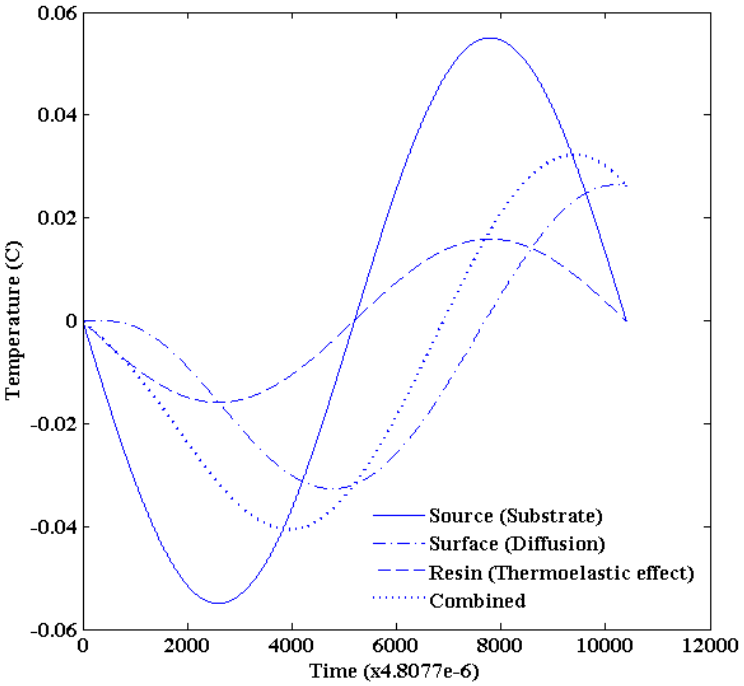

Figure 5.12: Temperature change in the surface and combination of heat diffusion and thermoelastic effect, at a loading frequency of 20 Hz

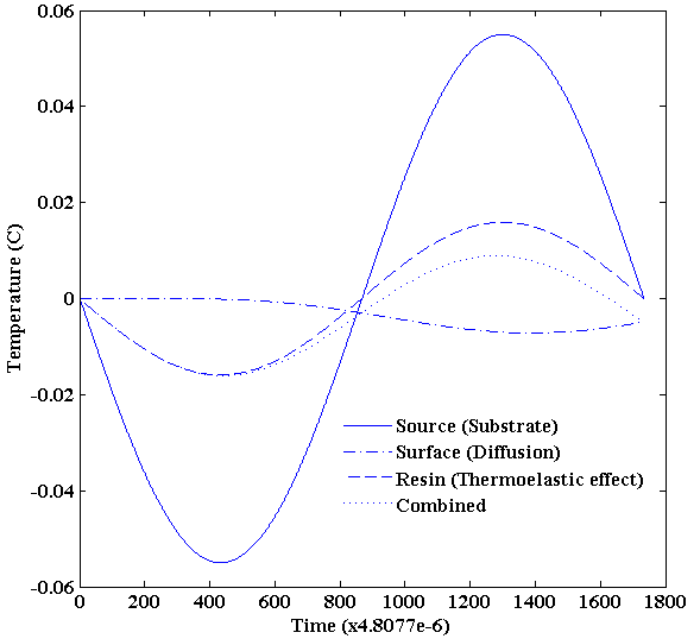

Figure 5.13: Temperature change in the surface and combination of heat diffusion and thermoelastic effect, at a loading frequency of 120 Hz

shows the necessity for a detailed micromechanical model to interpret the thermoelastic effect (coupling of change in the mechanical and thermal properties) precisely and are not averaging over the whole laminate (e.g. averaging over a large number of pixels) which leads to large scatter in the data and disregards precious information. This will support a more accurate interpretation of the thermoelastic response.

This study has shown that for the material considered, E-glass/ epoxy pre-preg laminates, consideration of the surface resin layer does not give the best agreement to the measured thermoelastic data. However, the small difference (within the error/scatter of the measured data) between the predicted thermoelastic temperature change based on the resin (the strain witness assumption) and the orthotropic substrate formulations for this material hinders clear conclusions being drawn. It is clear from the experimental results that the crucial parameters that distinguish each laminate are the differences in the Poisson's ratio and orientation of the orthotropic surface layer. The experimental work carried out using laminates with identical properties to properly identify the source of the thermoelastic response (e.g. $(0, \pm 45, 90)_s$ and $(0,90,\pm 45)_s$), which are identical in terms of global stiffness, CTE and surface ply) provided additional information to judge the depth and detail of the source of the thermoelastic response, and showed that the response is not a function of the global behaviour. A new approach, in which the CTE is coupled in the stack, gives a much better agreement to the measured data than the strain witness assumption, similar to consideration of the surface ply only. This study has shown that for the material considered, E-glass/epoxy pre-preg laminates, of the two standard approaches the orthotropic surface layer interpretation provides the better agreement to the measured data.

The strain witness assumption also needs to be investigated further, although it is apparent that it is not suitable for the current work, as this assumption would simplify the stress analysis of composite laminates using TSA for those materials it was valid for. It is crucial to identify the relative thickness of the resin rich layer to the orthotropic substrate that allows the strain witness assumption to be applicable, bearing in mind that it should be relatively thin compared to the substrate in order for the plane stress assumption to be valid. This adds further complication unless it is possible to identify material or material types that would show such behaviour, where the resin layer would be thin enough so that it experiences the same amount of strain as the substrate but still able to prevent heat transfer from the substrate at practical loading frequencies.

The work in this Chapter has clearly shown that the proposed theoretical models predict the thermoelastic temperature change as a function of applied strain giving values in all cases that are close to the measured data, even for the global model. It is essential to be able to theoretically formulate to quantify accurate the behaviour accurately, so that

a better understanding of the thermoelastic response is provided the strain and stresses experienced in the material. With the shortcomings of the approach described in this Chapter in mind (i.e. non-adiabatic behaviour, scatter) in the next Chapter it is shown how the proposed models can be applied to a specimen with a stress raiser. This will provide further understanding of the thermoelastic behaviour of composite structures.

Chapter 6

Stress concentration at holes in laminated composite material

6.1 Introduction

The heterogeneous and anisotropic properties of composite materials make their application complicated in design and analysis. Structural members with cut outs and holes add additional difficulty due to stress raisers caused by these features. Failure of structures at holes is generally caused by an excess amount of stress/strain around the holes which leads to crack initiation and propagation of delamination (due to interlaminar stresses occurring at the free edge) [76].

When an isotropic plate containing a circular hole is subjected to uniaxial tensile load, the tangential stress at the boundary in the direction perpendicular to the loading axis reaches a value of three times the remote tensile stress, which is independent of the hole size for an infinite plate (assuming plane stress conditions). However, for the case of anisotropic materials such as composites, the value and position of the maximum stress at the edge of a hole shifts depending on the fibre orientation and stacking sequence of the laminate [77].

There are many publications that address failure prediction or failure strength of composite laminates with stress concentration; a detailed review can be found in Ref. [77]. In this book, a procedure for determining the strain and stress concentrations based on an analytical method is given, with some results validated against experimental data. Best laminate configurations are also investigated by considering the failure strength. However, the problems addressed are limited to the behaviour of the laminate under static conditions, which provide the ratio of the ultimate strength of the laminate with

and without a hole. Thus, this provides a means for an adequate safety margin for design purposes. It is well known that stress concentration in components subjected to repeated stresses are potential sites for initiation of fatigue cracks, which may lead to failure. In the context of composite material the stress concentration can cause damage accumulation in the form of delamination, fibre failure and matrix cracking or various combinations of these. The distribution of stress in the vicinity of the hole is one of the parameters that has a large influence on the fatigue behaviour of the material. Therefore, before simple and robust models can be developed for understanding fatigue behaviour, the stress concentration in the structure needs to be understood.

The purpose of this Chapter is to build on the findings from the detailed characterisation of the thermoelastic thermoelastic response from orthotropic materials presented in the previous Chapter. Quantitative thermoelastic studies of stress concentrations in metallic plates is a straightforward matter, all that is required is the ratio of the response from the hole and a far-field reading. For orthotropic materials the situation is more complex as the response is not simply proportional to the sum of the principal stresses. In general the thermoelastic response of an orthotropic laminate is a function of the stresses in the principal material directions and the associated coefficient of thermal expansion (see chapter 3). The approach in this Chapter is to obtain 'stress factors' around the hole and identify the maxima in the plot to give a stress concentration factor. Specimens manufactured from four different laminate lay-ups (unidirectional (UD(0)), cross-ply (CP(0)), angle-ply (AP) and quasi-isotropic (QI(0/45))) are considered in this work. One of the main conclusions in Chapter 5 was that through thickness heat conduction from the orthotropic substrate influences the surface response. This is clearly a major finding for the application of TSA in a quantitative manner to composite structures. The purpose of the work in this Chapter is also to assess the magnitude of the non-adiabatic effect in the contex of more realistic structure and define if TSA can provide meaningful data that is useful in an industrial context. In a specimen with a stress concentration developed by a hole there will be a conduction of the through thickness non-adiabatic response and a possibility of in-plane heat conduction because of the severe stress gradient local to the hole. In an attempt to mitigate the through thickness effect the results are normalised to a 'far-field' reading that will also contain similar through thickness characteristics. To validate this approach the experimental data are compared to analytical models. To better understand the nature of the response the results from finite element models, that mimic the thermoelastic response are considered. The results from the FE and analytical models were modified to provide SCF_{TSA} that gives takes into account different theoretical approaches presented in chapter 3.

6.2 Stress concentration factor

Structural components are strongest when the service loads are evenly distributed over their area, where a reduction in this area, (i.e caused by discontinuities) occurs, this results in a localised increase in stress, which can be expressed as a stress concentration factor (SCF) and must be established for effective engineering analysis and design. SCF's also provide strategy for design and even form a prerequisite for some modelling and analysis approaches in theoretical investigations in damage and fracture mechanics, as the stress raisers are often the location for initial failure and fracture. For orthotropic materials it is not possible to obtain exact and explicit SCF expressions due to variation in the available material selection. Therefore, it is important to seek approximate (e.g. from analytical models) SCF expressions which are accurate and simple.

The SCF can be defined as the ratio of the maximum stress in the structure to a reference stress experienced by the structure. Stress concentration factors can be obtained analytically from elasticity theory [78], computationally using finite element methods and experimentally using a wide variety of techniques such as photoelasticity, strain gauges and TSA. Stress concentration factors related to the reference stress or nominal stress are defined using either the original gross cross-section or the net cross section. In some cases calculations are made with respect to bearing area (for loaded holes). The general representation of a plate with a hole is shown in Figure 6.1.

If a plate is loaded in uniaxial tension, the SCF based on the gross cross-sectional area can be defined as following:

$$k_{tg} = \frac{\sigma_{max}}{\frac{P}{wt}} = \frac{\sigma_{max} wt}{P} \tag{6.1}$$

where σ_{max} is the peak stress in a component and P is the applied load.

In a similar manner, SCF's based on the net cross-section are taken to be the ratio of the average stress on the minimum net section of the plate to the stress at which the specimen failed. The stress concentration factor based on the net cross-sectional area is given by:

$$k_{tn} = \frac{\sigma_{max}}{\frac{P}{(w-d)t}} = \frac{\sigma_{max}\,(w-d)\,t}{P} \tag{6.2}$$

The SCF most easily determined from TSA data by taking the ratio of the maximum tensile stress at the edge of the hole to the average stress at a far-field location of the plate and this is equivalent to k_{tg}. TSA data can be obtained in the form of temperature

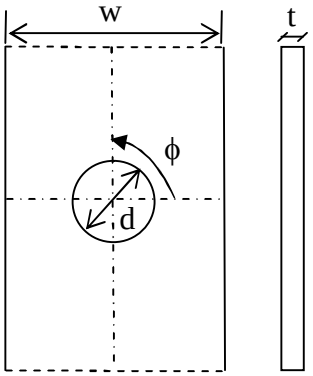

Figure 6.1: Hole in a plate nomenclature

difference, or uncalibrated signal. For isotropic specimens under uniaxial tensile load, the SCF can be extracted from the thermal maps by taking a ratio of the highest temperature signal adjacent to the hole to the average temperature signal measured in the far field:

$$k_{tg} = \frac{\Delta T_{local}}{\Delta T_{farfield}} = \frac{-KT\Delta\sigma_{xlocal}}{-KT\Delta\sigma_{xfarfield}} = \frac{\Delta\sigma_{xlocal}}{\Delta\sigma_{xfarfield}} \tag{6.3}$$

The uncalibrated signal data can also be used in a similar manner to obtain the SCF:

$$k_{tg} = \frac{\Delta S_{local}}{\Delta S_{farfield}} = \frac{\frac{\Delta\sigma_{xlocal}}{A}}{\frac{\Delta\sigma_{xfarfield}}{A}} = \frac{\Delta\sigma_{xlocal}}{\Delta\sigma_{xfarfield}} \tag{6.4}$$

Equations 6.3 and 6.4 are derived based on the assumption that the average stress over some distance away from the hole is equal to the unnotched material stress. Equation 6.4 has been used in previous work [47] to successfully derive SCF's at holes in isotropic materials.

6.3 Stress and strain concentration in composite materials

There are limited analytical models for determining stress concentrations in composite materials. The available models are expressed in terms of complex parameters [79] and in most cases the composite material is assumed to be a homogeneous plate [80]. These models are usually incorporated in the strength analysis of composite loaded holes (e.g. pin-loaded holes) [81]. Such work is essential for the design and optimisation of laminates to withstand repeated loading cycles. In most cases a three-dimensional model

needs to be considered, from the fact that only then the influence of stacking sequence and through-the-thickness loadings (e.g. additional fittings at the hole) on strength can be rigorously addressed. This means that an efficient method is still not available for preliminary design. It is important to note that as most of the available analytical solutions considering holes in composite components address infinite orthotropic plates an additional scaling factor, also known as the finite width correction factor, FWC is required when comparing experimental data available from composite strips (finite plates). In adition to the usual test procedure (i.e. failure test), non-contact measurements such as electronic speckle pattern interferometry (ESPI) and strain mapping techniques (e.g. Digital Image Correlation, DIC) have been used to study stress profiles in composite laminates. A detailed review of the available literature on the analysis of composite laminates with open holes is given in following section in three parts: analytical, numerical methods and experimental investigations.

6.3.1 Analytical methods

An analytical model for expressing the stresses (tangential stresses) around a hole in an anisotropic plate subjected to uniaxial tensile stress) was first developed by Lekhnitskii et al. [82]. The aim was to show that based on the tangential stress (σ_ϕ) acting on the edge of the hole (radial stress, $\sigma_r = 0$) with known applied stress, the SCF around the rim of the hole, k_ϕ can be obtained.

For a plate subjected to uniaxial tension at a distance from the opening, which is acting at an angle, θ in relation to the principal material direction, (see Figure 6.2), k_ϕ is given as:

$$\begin{aligned} k_\phi = \frac{\sigma_\phi}{\bar{\sigma}} = \frac{E_\phi}{E_1}[-\cos^2\theta + (k+n)\sin^2\theta]k\cos^2\phi + [(1+n)\cos^2\theta - \\ k\sin^2\theta]\sin^2\phi - n(1+k+n)\sin\theta\cos\theta\sin\phi\cos\phi \end{aligned} \tag{6.5}$$

where E_ϕ is the modulus of elasticity in the ϕ direction given by:

$$\frac{1}{E_\phi} = \frac{\sin^4\phi}{E_1} + \left(\frac{1}{G_{12}} - \frac{2\nu_{12}}{E_1}\right)\sin^2\phi\cos^2\phi + \frac{\cos^4\phi}{E_2} \tag{6.6}$$

Values of k and n are given as:

$$k = -\mu_1\mu_2 = \sqrt{\frac{E_1}{E_2}} \tag{6.7}$$

$$n = -i(\mu_1 + \mu_2) = \sqrt{2\left(\frac{E_1}{E_2} - \nu_{12}\right) + \frac{E_1}{G_{12}}} \tag{6.8}$$

where i $= \sqrt{-1}$ and μ_1 and μ_2 are the complex roots of the following characteristic equation:

$$\mu^4 + \left(\frac{E_1}{G_{12}} - \nu_{12}\right)\mu^2 + \frac{E_1}{E_2} = 0 \tag{6.9}$$

In this case the largest stress will not be at the horizontal hole diameter normal to the applied load but will be at another location.

For the case where uniaxial tension is in the principal direction Figure 6.2 ($\theta = 0$), k_ϕ can be simplified as:

$$k_\phi = \frac{\sigma_\phi}{\sigma} = \frac{E_\phi}{E_1}\left[-k\cos^2\phi + (1+n)\sin^2\phi\right] \tag{6.10}$$

In this case the stress distribution will be symmetrical with respect to the principal material directions.

The most frequently referred criteria for predicting the strength of composites with circular holes are the point stress criterion (PSC) and the average stress criterion (ASC). Both were derived by Whitney and Nuismer [83, 84] based on:

$$\sigma_x(0,y) = \frac{\bar{\sigma}}{2}\left(2 + \left(\frac{R}{y}\right)^2 + 3\left(\frac{R}{y}\right)^4 - \left[(k_T - 3)\left(5\left(\frac{R}{y}\right)^6 - 7\left(\frac{R}{y}\right)^8\right)\right]\right) \tag{6.11}$$

where y is the distance along the horizontal diameter of the hole (see Figure 6.2) and σ_x is the applied stress. k_T is the orthotropic stress concentration factor for an infinite width plate as determined from the following relationship:

$$k_T = 1 + \sqrt{\frac{2}{A_{22}}\left(\sqrt{A_{11}A_{22}} - A_{12} + \frac{A_{11}A_{22} - A_{12}^2}{2A_{66}}\right)} \tag{6.12}$$

At the hole boundary, where y is equal to R (see Figure 6.3), Equation 6.10 gives the stress concentration factor as follows:

$$\frac{\sigma_x(0,y)}{\bar{\sigma}} = k_T \tag{6.13}$$

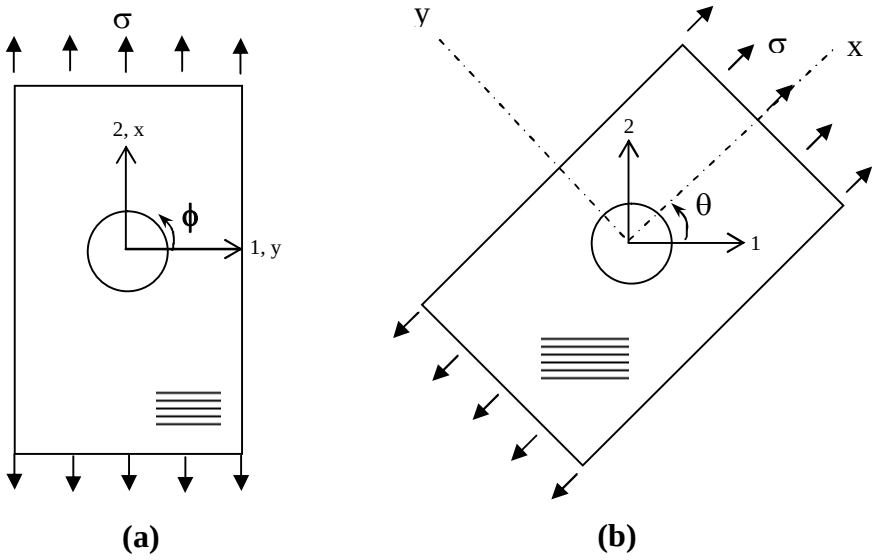

Figure 6.2: Tensile load applied a) in the principal direction of an anisotropic plate with circular hole b) at an angle to the principal material direction

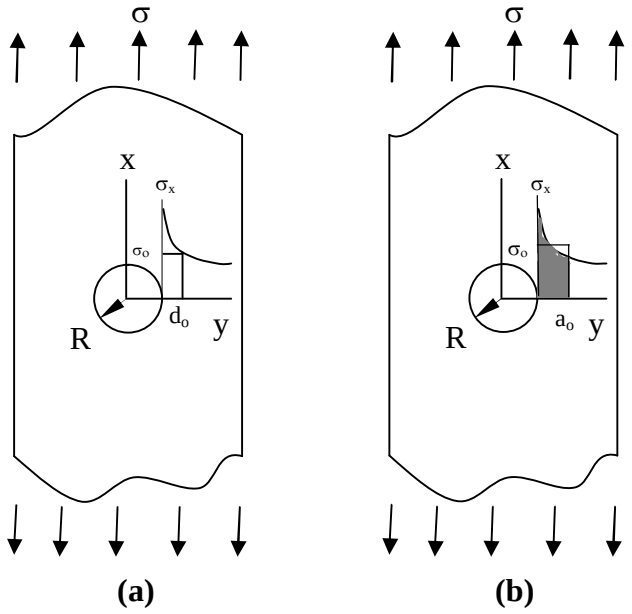

Figure 6.3: Graphical presentation of the a) point stress criterion b) average stress criterion

This indicates that the stress concentration value for a similar material is not dependent on the size of the hole.

The point stress criterion (see Figure 6.3a) for laminated composites containing stress concentrations is based on the assumption that the failure occurs when the stress at some

distance (d_o) away from the notch is equal to or greater than the unnotched laminate strength (σ_o):

$$\sigma(0,y)_{for\, y=R+d_o} = \sigma_o \tag{6.14}$$

Since the stress concentration factors at a point (0, d_o) are dependent on the hole size, this technique takes into account the influence of the size of the hole.

Based on this criterion the stress concentration factor can be written as:

$$\frac{\sigma_x}{\sigma_o} = \frac{2}{2+\xi_1^2+3\xi_1-(k_T-3)(5\xi_1^6-7\xi_1^8)} \tag{6.15}$$

where $\xi_1 = R/(R+d_o)$.

The average stress criterion (see Figure 6.3b) is based on the assumption that failure occurs when the average stress at some distance (a_o) ahead of the notch is equal to the unnotched laminate strength (σ_o):

$$\frac{1}{a_o}\int_{R}^{R+a_0} \sigma_x(0,y)dy = \sigma_o \tag{6.16}$$

It can be observed from Figure 6.4 that a larger volume of material is subjected to high stress in the case of the plate containing the larger hole. Compared to the previous criterion, ASC considers the average stress over a characteristic length, a_o.

In this case the stress concentration factor can be written as:

$$\frac{\sigma_x}{\sigma_o} = \frac{2(1-\xi_2)}{2+\xi_2^2+3\xi_2^4-(K_T-3)(5\xi_2^6-7\xi_2^8)} \tag{6.17}$$

where $\xi_2 = R/(R+a_0)$.

In both cases, the values of d_o and a_o need to be determined experimentally, by obtaining $\frac{\sigma_x}{\sigma_o}$ from failure tests of notched specimens. By substituting $\frac{\sigma_x}{\sigma_o}$ in Equations 6.15 and 6.17 with R value measured from the failed specimen the approximate values of d_o and a_o can be determined.

For an isotropic material, the elastic stress concentration factor is equal to the strain concentration factor ($SCF_\sigma = SCF_\epsilon$). In the case of composite plates, the relationship is less straightforward. The relationship between SCF_σ and SCF_ϵ is given by [77]:

$$SCF_{\epsilon} = \frac{\epsilon_{\phi}(\phi = 0)}{\bar{\epsilon_1}} = \frac{a_{11}\sigma_{\phi}(\phi = 0)}{a_{22}\bar{\sigma_x}} \tag{6.18}$$

where a_{11} and a_{22} are the compliance of the laminate in the 1 and 2 directions.

Equation 6.18 shows that SCF_{ϵ} is dependent on the lay-ups and is only equal to SCF_{σ} when $a_{11} = a_{22}$, which is true for quasi-isotropic laminates including angle ply and cross ply laminates. Therefore, laminates with these configurations are used in the experimental work.

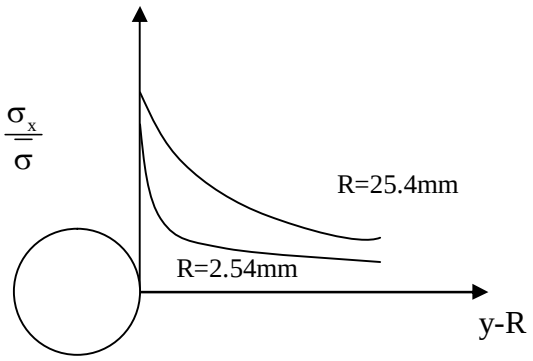

Figure 6.4: Stress distribution for a finite plate containing a hole

The SCF around holes in multilayered laminates can be expressed as the average of the SCFs for all layers [85] given as:

$$k_{\sigma} = \frac{\sum_{i=1}^{m} N_i k_i}{N} \tag{6.19}$$

where N is the number of the layers, m is the number of plies with different fibre lay-up directions, N_i is the repeated layer number of the ith ply, and k_i is the SCF in the ith ply. The ratio between the SCF of a finite plate and the corresponding infinite plate, k_i^{∞}, is given as:

$$\frac{k_i^{\infty}}{k_i} = \frac{3(1 - d/w)}{2 + (1 - d/w)} + \frac{1}{2}\left(\frac{d}{w}B\right)(k_i^{\infty} - 3)\left[1 - \left(\frac{d}{w}B\right)^2\right] \tag{6.20}$$

where B is a magnification factor given as:

$$B^2 = \frac{\sqrt{1 - \left[\frac{3(1-d/w)}{2+(1-d/w)^3} - 1\right]} - 1}{2(d/w)^2} \tag{6.21}$$

It is important to note that k_σ can only be found if all the k_i values in each layer are known. Depending on the stacking sequence the maximum value of the stress concentration is not necessarily at the same position (e.g. perpendicular to the loading direction) and largely depends on the fibre orientation of the lamina. However in many cases, once the strain concentration at the hole edge is measured, the stress concentration at the hole edge can be determined accordingly using Equation 6.18.

The theoretical solution for the SCF in a finite-width composite laminate with a hole does not exist. For a finite width orthotropic plate the SCF can be calculated by using a finite width correction (FWC) factor to assess the SCF of smaller strips (commonly used in laboratory testing) with a similar opening. These factors, which are dependent on material properties, can be obtained by elasticity equations [77] or finite element methods.

6.3.2 Numerical methods

It is clearly shown in the previous section that the analytical treatment of SCFs in laminated composites is tedious and finite element analysis is need to be adopted to fully determine the stress state in a plate, where a three-dimensional analysis is required. There are a number of numerical investigations [85, 86, 87](i.e. finite element method) devoted to analysing the effect of holes and cut outs in laminated composites by considering factors that are too complex to be assessed by analytical methods. A study of the effect of fibre orientation on stress concentration factor under in-plane static load on a rectangular laminated plate with a central hole is given in Ref. [88]. Bakhshandeh and Rajabi [89] studied the effect of orthotrophy ratio and plate length on the SCF of similar problem. They also showed that Tan's [77] finite width orthotropic plate equation has limitations and proposed a transition ratio that depends on the length of the specimen.

A three dimensional stress state occurs at free edges (i.e. at the rim of a hole) caused by the mismatch of Poisson's ratios between plies with different orientations in a laminated plate. This raises the interlaminar shear and normal stresses at the free edge. Therefore a detailed and accurate stress analysis requires all the individual plies and the resin-rich zone between the plies to be incorporated in an FE model for accurate results. In most cases considerable simplification was made by omitting the interlaminar stresses close to the edge of the hole by treating the laminate as a homogeneous anisotropic plate (e.g. similar to classical laminate theory). It is shown, using 3D finite element analysis [89], for a large finite thickness plate containing a hole that the maximum stress and strain concentration factors increase from their plane stress value to their peak values, then

decrease gradually with increasing thickness. Examples of 2D and 3D FE analysis of laminates with different layups are given in Section 6.7.

6.3.3 Experimental investigations

Strain gauges have been widely used to measure strain concentration in laminated composite material. Many experimental studies have used strain gauges to study the effect of hole size on stress concentration [77]. However the accuracy of the technique depends on the size of the strain gauges, which determines how close to the edge of the hole the measurement is taken and the degree of strain averaging (distance from the edge of the opening) over the active area of the strain gauge. It has been generally concluded that laminates with smaller holes have significantly lower stress concentrations and thus higher strength than those with larger holes yet it is important to pay attention to the lay-up of the composite, which has a significant role in determining the SCF. In interpreting the reading from the strain gauges, only the stress concentration at the edge of the hole and the axis normal to the applied loading are the same as the strain concentration. The stress concentration at the top of the hole (90^o) and along the 45^o direction can be calculated by multiplying the measured strain with the laminate modulus parallel to the applied direction of the strain gauge and divided by the applied laminate stress (see Equation 6.18).

Apart from strain gauges, other full field strain measurement techniques such as DIC [90], Electronic Speckle Pattern Interferometry (ESPI) [91] and moiré interferometry [92, 93] have been used to investigate the presence of stress concentrations in composite materials. In using the DIC and ESPI techniques it has been identified that the strain concentrations are influenced by the loading direction and the dimension of the hole size to the size of the unit cell of the plain woven fabrics. Good agreement between the SCF for woven fabric composites subjected to an on-axis (weft direction) tensile load has been found with Lekhnitskii's model but not in the off-axis directions (i.e. 90^o, 45^o directions)[91]. In a similar manner, ESPI was used to investigate the tensile strain field of a composites plate in the presence of stress concentrations (measuring the field strain with sub-micrometer spatial accuracy). The experimental results were compared with the predictions of a theoretical model developed by Lekhnitskii and a finite element study. The SCF values obtained near the holes from the experiments were lower compared to the analytical and numerical models. The agreement between the models was again poor in the off-axis loading direction.

In Ref. [93] the moiré pattern of stress concentration around holes in graphite/epoxy composite laminate subjected to uniaxial tension was explored. The experimental results

were compared with Savin's elasticity theory and excellent agreement for the displacement obtained in the loading direction was obtained but was not the case for values of displacement obtained in the transverse direction.

6.3.4 Stress concentration for damaged composites

Interlaminar stresses occurring at the free edge of a hole or notch cause composite laminate to delaminate. After damage starts to occur at higher stress levels, the stress concentration factors are different from the strain concentration factor because the local stiffness of the laminate is not the same as for the undamaged laminate. It was shown in Ref. [77] that the SCF at the location of damage was reduced by about 18%, suggesting stress relaxation occurs due to microdamage in the laminate and redistribution of stress around the stress concentration site. These mechanisms involve a combination of matrix cracking, fibre debonding or fibre pull-out.

A finite-element approach is given in Ref. [94] for modelling the detailed damage development in notched composites using interface elements to include spitting and delamination. The method is applied to a cross-ply laminate with a centre crack in tension, predicted the development of delamination zone.

Microdamage also occurs during the machining of holes in composite laminates. It was shown in Ref. [95] that damage from the machining process can be characterised using TSA and a modified stress concentration factor is presented as a measure of damage parameter. However, the parameter was quantified using Equation 6.4 assuming the behaviour of the composite laminates are similar to an isotropic material. However, the ranking of severity of the damage based upon the SCF was in good agreement with the fatigue life of the specimen.

6.4 Derivation of the thermoelastic stress and strain concentration factors

In this section different ways of obtaining the stress/strain concentration at holes in orthotropic composite plates from thermoelastic data are developed. To achieve this, it is necessary to understand the nature of the thermoelastic response; three approaches are presented (as discussed in Chapter 3) to quantify SCF's from the thermoelastic data.

A stress concentration factor, SCF_σ, for a single hole in the centre of a strip of material loaded under uniform uniaxial loading is defined as follows:

$$SCF_\sigma = \frac{\sigma_{Hole}}{\sigma_{Far-field}} \tag{6.22}$$

where σ is the principal stress.

Figure 6.2 shows a strip of orthotropic material with a central circular hole loaded along the principal axes (Figure 6.2a) and loaded 'off axis' (Figure 6.2b). To relate the stresses at the hole to those in the plate it is simpler to define the stresses at the hole in a polar coordinate system (r and θ and the stresses in the far-field in a Cartesian system (x,y), as shown in Figure 6.2). In the polar coordinate system the laminate stresses are defined as: σ_{rL} (radial stress), $\sigma_{\theta L}$ (tangential stress) and $\sigma_{r\theta L}$ (shear stress). At the edge of the hole at the surface of the plate the radial stress and shearing stress are both zero, since no external tractions exist at the periphery of the hole.

Also, to satisfy the stress free boundary condition in the far-field, when considering the laminate as a homogeneous body, only the applied stress exists, so the SCF_σ is generally given as:

$$SCF_\sigma = \frac{\sigma_{\phi L}}{\sigma_{app}} \tag{6.23}$$

where $\sigma_{\phi L}$ is the laminate tangential stress at the hole and σ_{app} is the stress applied to the laminate.

The thermoelastic temperature change, ΔT, for a composite lamina (e.g. the surface ply of the laminate) is given by:

$$\begin{aligned} \Delta T &= -\frac{T}{\rho C_p}(\alpha_x\sigma_x + \alpha_y\sigma_y + \alpha_s\sigma_s) \\ &= -\frac{T}{\rho C_p}(\alpha_1\sigma_1 + \alpha_2\sigma_2 + \alpha_{12}\sigma_{12}) \\ &= -\frac{T}{\rho C_p}(\alpha_r\sigma_r + \alpha_\phi\sigma_\phi + \alpha_{r\phi}\sigma_{r\phi}) \end{aligned} \tag{6.24}$$

where the subscripts x,y denote the principal stress directions in the surface ply, 1,2 are in the principal material directions of the surface ply and r,ϕ denotes the system in the surface ply in polar coordinates. It is important to note that the bracketed term in Equation 6.24 is an invariant since ΔT is a scalar quantity (as explained in Chapter 3). Equation 6.24 deals with the surface ply. In this case the shear terms in the xy direction disappear as σ_s is zero in the principal stress directions and the shear terms in the 12 direction also disappear as α_6 is zero in the principal material directions. It is only in the last expression in Equation 6.24 that the shear terms need to be retained.

Even if the values are taken at the hole for a general laminate both the radial and shear stresses will exist. Equation 6.24 could be recast to denote the overall behaviour of the laminate, treating it as an orthotropic homogeneous block of material. Here the shear terms in the first and second expressions vanish to zero as before. In the third expression in Equation 6.24 the laminate radial stress and shear stress would also be zero.

It is possible to formulate the stress concentration factor from TSA data (as SCF_{TSA}) in three different ways. Firstly, and most conventionally, it is assumed that the thermoelastic response is purely from the surface ply, so that:

$$\frac{\Delta T_H}{\Delta T_F} = \frac{\alpha_r \sigma_r + \alpha_\phi \sigma_\phi + \alpha_{r\phi} \sigma_{r\phi}}{\alpha_1 \sigma_1 + \alpha_2 \sigma_2} \tag{6.25}$$

where σ_1 and σ_2 are the stress changes in the principal material directions (α_6=0) and ΔT_H and ΔT_F are the measured thermoelastic temperature changes at the edge of the hole and in the far-field region, respectively.

In the work in chapter 5, it was shown that the global response was unlikely to be relevant. However, for completion it is referenced here. Therefore,the second option is to define the thermoelastic response as a function of the global laminate behaviour to correspond with the definition given by Equation 6.23 so that SCF_{TSA} is defined as:

$$\frac{\Delta T_H}{\Delta T_F} = \frac{\alpha_{\phi L} \sigma_{\phi L}}{\alpha_{1L} \sigma_{1L}} \tag{6.26}$$

where the subscript L denotes the laminate behaviour.

For laminated composites with a low thermal conductivity (e.g. GFRP) under adiabatic conditions, the thermoelastic effect from the inner zones of the material is not able to affect the surface temperature. Therefore, the measured thermoelastic temperature change relies on the properties of the surface material. As explained in chapter 3, this assumption would simplify the stress analysis of composite laminates where the presence of the surface resin layer on a composite laminate can replicate the strain field of the laminate and serves as a strain witness, which provides the third case for comparison, where the thermoelastic temperature change can be expressed as the strain concentration factor, SCF_ϵ, that can be defined as follows:

$$SCF_\epsilon = \frac{\epsilon_\phi}{\epsilon_{app}} \tag{6.27}$$

where ϵ_θ and ϵ_{app} denote the local strain and applied strain, respectively. The SCF_ϵ is generally not equal to SCF_σ because of the difference in the directional modulus of the laminate, i.e.:

$$SCF_\epsilon = \frac{\epsilon_\phi(\phi = 90)}{\epsilon_{app}} = \frac{a_\phi \sigma_\phi(\phi = 90)}{a_L \sigma_{app}} = \frac{a_\phi}{a_L} SCF_\sigma \tag{6.28}$$

where a_ϕ and a_L are the compliances of the laminate. Therefore, SCF_ϵ is only equal to SCF_σ when a_ϕ=a_L.

Since the resin layer is isotropic, SCF_ϵ is equal to SCF_σ then a third formulation of the SCF_{TSA} is as follows:

$$\frac{\Delta T_H}{\Delta T_F} = \frac{\epsilon_\phi + \epsilon_r}{\epsilon_x + \epsilon_y} \tag{6.29}$$

6.5 Thermoelastic stress analysis of holes in laminated composites

In this section, an analysis of the effect of holes in a variety of laminated composite plates is presented to provide experimental SCF's based on TSA data. For composite specimens under uniaxial tensile load the SCF can be extracted from the temperature change, ΔT, data by taking a ratio of the highest thermoelastic signal adjacent to the hole to the average signal measured in the far-field region.

The validity of this approach is demonstrated by investigating four different finite width plates with a central hole under in-plane loading with different ply lay-ups for glass/epoxy composite orientations (UD(0), CP (0), QI, AP). Specimens containing a central circular hole were machined from the composite panels. All the specimens had a 10 mm central circular hole produced with a tungsten carbide drill to minimise machining damage. The dimensions of the specimens and the loading conditions are given in Table 6.1. To minimise the effect of signal noise, the applied loads for the TSA tests were chosen to give a strong thermoelastic response from each laminate; the effect of the mean load on the thermoelastic signal has previously been shown not to be significant (see Chapter 5). The principal strains in the far-field region were measured using strain gauges in the far-field region. The loading conditions and measured far-field strain readings are shown in Table 6.2.

A loading frequency of 10 Hz was used in these tests. The TSA data around the hole and the far-field region was collected from all four specimens. The TSA measurement provide directly the quantities in the left hand side of Equations 6.25, 6.26, 6.27 and 6.29. To populate the right hand side of these equations the stresses and strain were obtained from the analytical and finite element models which are described in the next

Table 6.1: Lay ups and dimensions of test specimens

Specimen	**Stacking sequence**	**Dimensions (mm)**		
		Length	Width	Thickness
UD(0)	$(0)_6$	251.0	39.3	1.50
CP(0)	$(0,90)_s$	249.2	40.8	1.00
QI(0/45)	$(0,\pm45,90)_s$	249.1	39.8	1.90
AP	$(\pm45)_s$	249.7	38.5	1.00

Table 6.2: Loading conditions and strain reading from the far-field region

Specimen	**Applied load (kN)**		**Far-field Strain**		**Strain sum**
	Mean load	Amplitude	ϵ_x	ϵ_y	$(\epsilon_x+\epsilon_y)$
UD(0)	3.0	1.0	0.000997	-0.000275	0.000722
CP(0)	2.0	1.0	0.002126	-0.000245	0.001881
QI(0/45)	3.0	1.0	0.001510	-0.000328	0.001182
AP	0.6	0.5	0.001907	-0.001036	0.000871

section. The different distribution of $\frac{\Delta T}{\Delta T_F}$ around the hole for different laminates are shown in Figure 6.5, where it is clear from these plots that the fibre orientation has a major effect on the stress distribution and the ±45 fibre orientation has the effect of 'spreading' the strains.

6.6 Edge effect

Depending on the size of the pixel, the TSA data at the boundaries are affected by the measurement region because the pixel only partially covers the area of interest on a test specimen. In this location the data will be influenced by the input from the specimen and from the background. This could lead to a reduction in the measured value of the thermoelastic signal. There have been several techniques suggested previously to improve the measured TSA data at the edge boundaries [96, 97, 98]. Barone developed a technique that works based on compatibility and implementation of an iterative procedure to smoothen the interior values which is used to correct the boundary values [97]. This method was applied to thermoelastic data to quantify the SCF around a hole in an Araldite plate and by applying the technique an increase of 16% of the measured value at the edge of the hole was demonstrated. In a similar manner, in Ref. [98], a technique was developed based on an effective iterative least-squares method for calculating reliable edge isopachic stresses from measured interior values. Galietti and Pappalettere [96] developed an algorithm, which performed polynomial smoothing and automatically

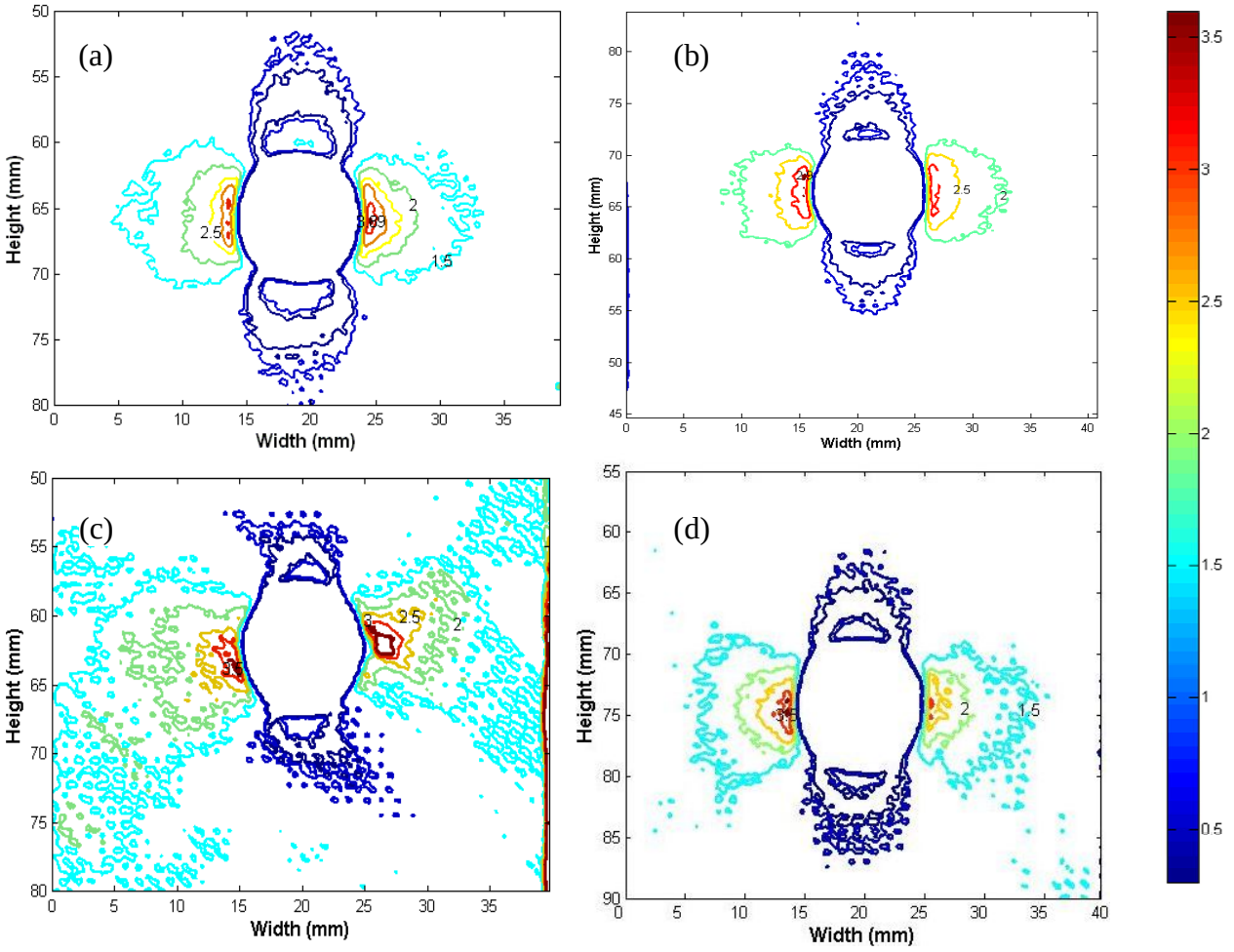

Figure 6.5: Distribution of $\frac{\Delta T}{\Delta T_F}$ around holes from TSA data for a) UD(0) b) CP(0) c) AP d) QI

located edges in the data set that allowed the SCF to be recalculated. All the approaches show that edge readings give a reduced value for the SCF and therefore it would be useful to apply one of these to the current data. However, the Cedip system used in this work has higher pixel resolution compared to the work given in Refs. [96, 97, 98] which actually reduces the length of edge efffect. Additional work was performed using higher resolution lens in a steel plate (300 x 40 x 6 mm) with 14 mm diameter hole. An infinite plate with an open hole under uniaxial load creates a stress concentration factor of 3. The SCF for an unloaded hole in the middle of a finite strip based on the geometry is given by [99] as:

$$k_t = 2 + (1 - d/w)^3 \tag{6.30}$$

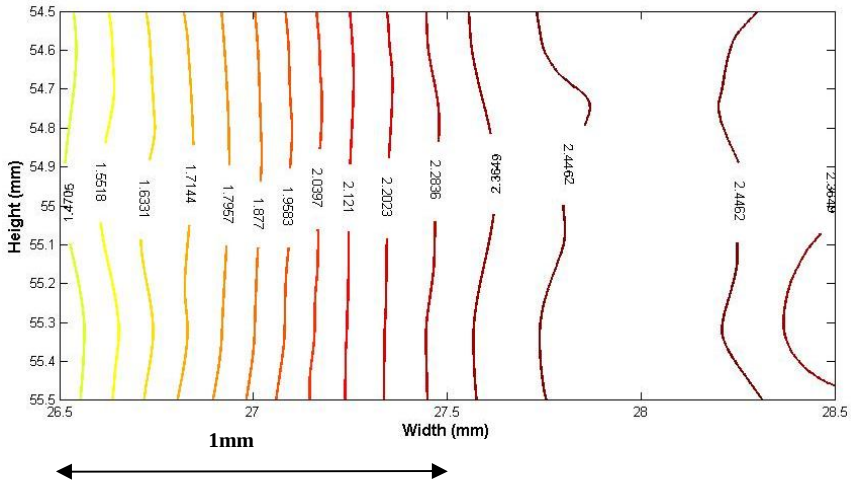

Figure 6.6: SCF contour plot from TSA data at the edge of the hole

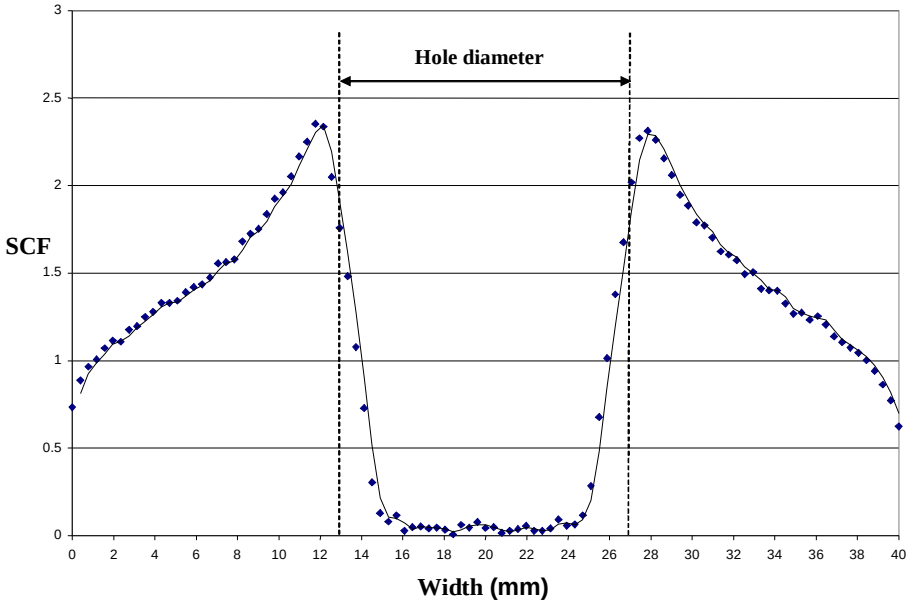

Figure 6.7: SCF line plot from TSA data

The value of maximum SCF in this experiment ($k_t = 2.27$) was found to be 2.42 (as shown in Figure 6.6). In a similar manner, by repeating the experiment with normal lens (i.e. 27 mm lens) the maximum SCF was found to be 2.39 (as shown in Figure 6.7). These results confirmed that, most likely the data is not influenced by edge effect, but indicating the possibility of non-adiabatic effect in the presence of high stress gradients.

6.7 Finite element analysis of composite laminates with holes

To aid the interpretation of the TSA data, Finite Element (FE) models of the specimens were produced using ANSYS commercial software [100]. The stress distribution in a rectangular laminated composite plate with central hole has been studied using 2D and 3D finite element methods. The effect of fibre orientation on stress concentration factor under in-plane static loading is assessed for the specimens mentioned in the previous section. The layered nature of composite materials means that only a limited type of elements can be used efficiently for FE analysis of composites. For laminates with a symmetric layups, 2D elements can be used by incorporating the global laminate properties. Such elements are widely used in composite analysis for modelling the in-plane behaviour of flat plates. In practice, it is more usual to utilise some form of plate or shell element. It would be possible to stack 3D brick elements with each layer of brick representing a single ply. Layering brick elements for relatively thin plates leads to an ill-conditioned set of equations [101]. Therefore, brick elements are only used where composite lay-ups are very thick and the geometry is more solid than a plate or where there is a 3D stress field such as can occur at the free edges (a 3D sub model can be used for such regions). In shell elements the standard bending theory assumption is made, that the strains only have a combination of constant and linear variations through the thickness of the shell. The ANSYS package for FE analysis was selected to model the different laminated plates with holes. The detailed description of the 2D and 3D FE analyses are given in following sections.

6.7.1 2D Finite element analysis

The 2D finite element model was developed using 8-node structural solid elements (PLANE82). The detail and geometry of the element is given in Ref. [100]. Firstly, a quarter of a thin orthotropic plate following same geometry and loading conditions provided in Table 4.1 is modelled for UD(0), CP(0), AP and QI laminates. This was done to verify the accuracy of the numerical modelling by comparing it to the measured in-plane strain. Next, a series of rectangular plates with the same geometry and loading conditions as the specimens tested in the experimental work have been modelled for the different laminate types. Due to the symmetric nature of the specimen, only quarter models have been considered, see Figure 6.8. The material properties assigned to the laminate were the same as in Table 4.2 and Table 4.4. A denser mesh was used close to the hole to capture the stress gradient accurately, as shown in Figure 6.9. Based on the results the SCF_{TSA} for an infinite orthotropic plate was calculated based on right

hand terms in Equations 6.25, 6.26 and 6.29. The strain sum in the far-field region was compared with the experimentally measured far-field strain in the plate.

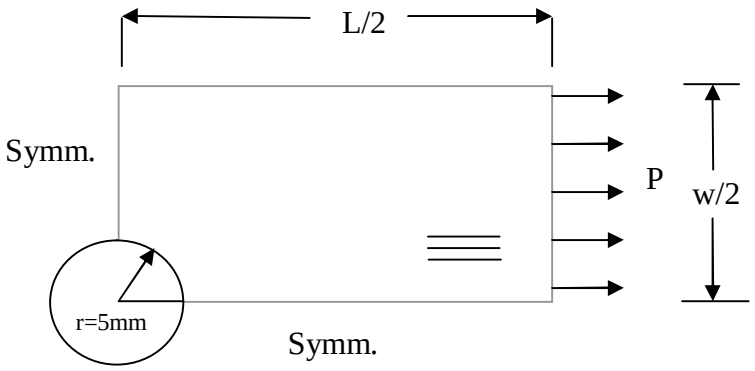

Figure 6.8: Orthotropic plate with a hole in the centre under uniaxial tension

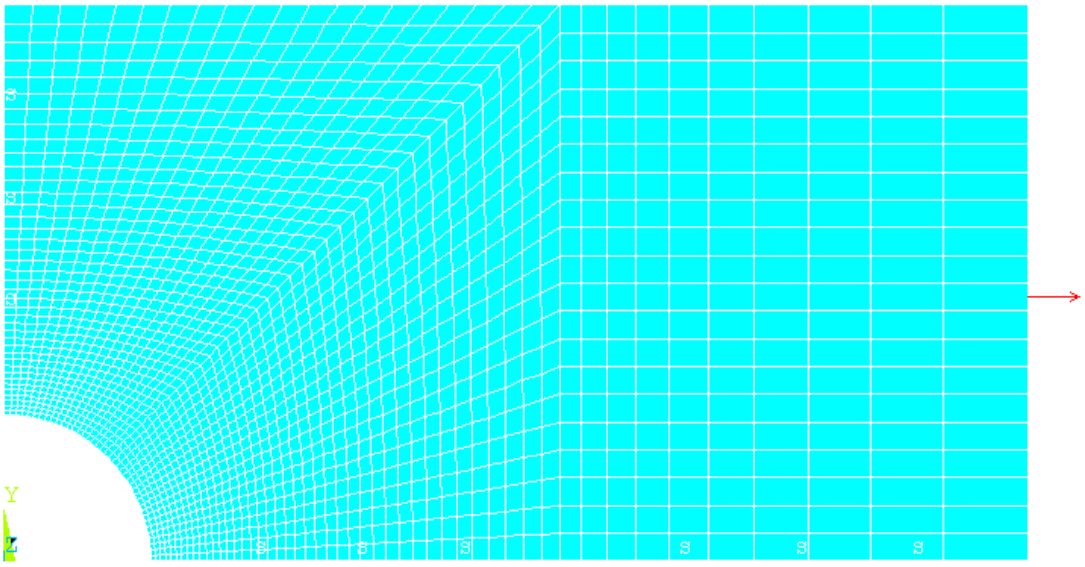

Figure 6.9: Typical mesh of the composite laminate

6.7.2 3D Finite element analysis

An eight noded linear layered structural 3-D Shell Element with six degrees of freedom at each node (specified as Shell99 in the ANSYS package [100]) was selected for the 3D analysis. In the layered element the fibre direction has to be specified in the input to the FE package as shown in Figure 6.10. In this case all the layers are at fixed known angles to each other (e.g. stacking sequence) and the thickness of each layer needs to be specified separately. In this case each ply is treated as an homogeneous, elastic

and orthotropic material. In order for the 3D model to exhibit the same stress as the 2D model, the applied force had to be recalculated to account for the difference in the thickness between the two models. The 3D mesh of the rectangular plate was built within the plane of the plate and layered sub-elements stacked together with one element in the through thickness direction to model the laminate. Figure 6.10 illustrates the stacking sequence of the $(\pm 45)_s$ laminate. The through thickness material properties given in Table 4.2 are incorporated in the model. The geometry and boundary conditions of the specimens with holes were similar to the 2D model (as shown in Figure 6.11). Based on the results the SCF_{TSA} for an infinite orthotropic plate was calculated following the left hand terms in Equations 6.25. The strain sum in the far-field region was compared with the experimentally measured far field strain to assess the accuracy of the model.

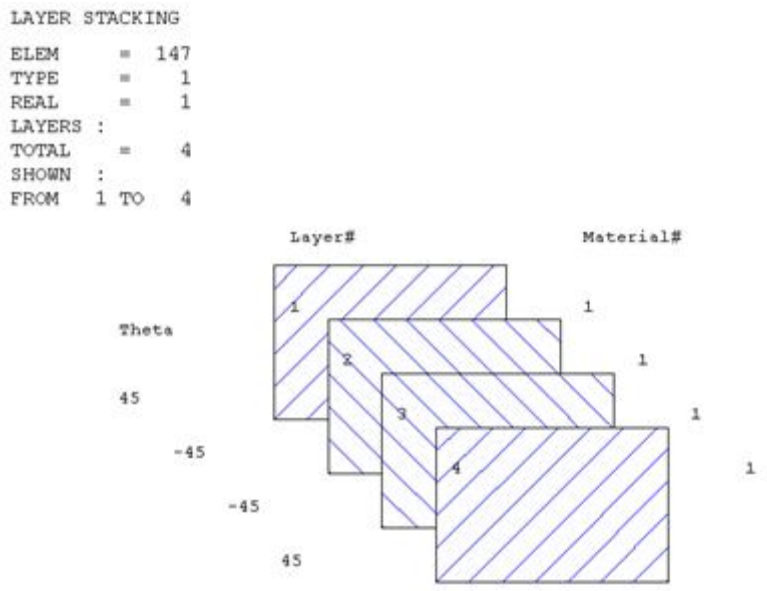

Figure 6.10: Defined laminate stacking sequence for AP laminate $(45/\text{-}45/\text{-}45/45)_T$

6.8 Validation of FE model

Firstly, to validate the 2D and 3D finite element results, the data obtained for strips without holes were used. The results are then compared to experimental results taken from strain gauges installed on actual test specimens (i.e. data collected in Chapter 5, see Table 5.1). Here the 2D model is a global model using material properties for the laminate given in Table 4.4. Table 6.3 presents both the measured strain, FE data and the calculated strain values based on the CLT. To aid interpretation Table 6.4 shows departures from the measured data. It can be seen that the 2D FEA corresponds well

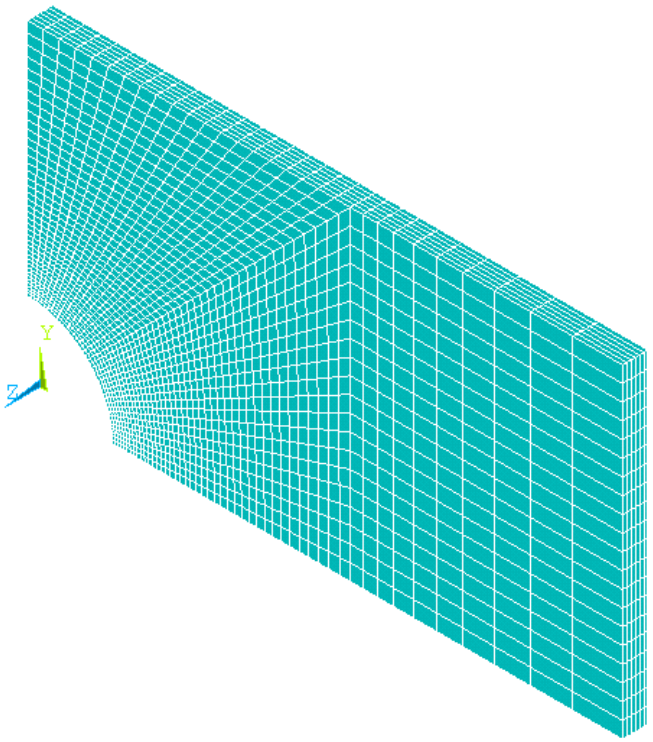

Figure 6.11: Typical mesh of 3D laminated plate

in all cases, with the greatest error being for the CP(0) specimen. The error in the 3D FEA is very similar to that of CLT. As the 3D FEA is based on CLT to combine the ply property to form a global behaviour it is not surprising that this is the case. However, the large errors shown, particularly in the angle-ply specimens, are a major cause for concern.

To further examine and confirm the measured results using a different test specimens, strain gauges were installed on specimens with holes. The results from these are shown in Table 6.5 and the departures in Table 6.6. A similar trend is observed here and confirms that the 3D FE result must be considered unreliable for the specimens that contain angle plies (i.e. AP and QI(0/45)). A possible error in the 3D FEA is the through thickness material properties, but it is expected that this will be similar in each lay-up. If this was the source of error, then results for the UD(0) would not should show such a good agreement. Therefore, the conclusion must be it is the limitation of CLT, which is beyond the scope of this work. A simple way to address this is to create a homogenised global model in 2D as has been done here; in all the cases the agreement is good.

Table 6.3: Comparison of strain ($\mu\epsilon$) in the composite strip for conditions given in Table 5.1

Specimen	**Measured strain**		**Strain (2D FEA)**		**Strain (3D FEA)**		**Strain (CLT)**	
	ϵ_x ($\mu\epsilon$)	ϵ_y ($\mu\epsilon$)	ϵ_x ($\mu\epsilon$)	ϵ_y ($\mu\epsilon$)	ϵ_x ($\mu\epsilon$)	ϵ_y ($\mu\epsilon$)	ϵ_x ($\mu\epsilon$)	ϵ_y ($\mu\epsilon$)
UD(0)	2264	-581	2316	-579	2316	-579	2300	-575
CP(0)	1949	-296	2109	-239	2121	-241	2119	-239
QI(0/45)	2281	-694	2237	-712	2133	-679	2235	-711
AP	3371	-1640	3438	-1615	3441	-2114	3510	-2161

Table 6.4: The comparison of the differences between the measured strain and the strain obtained using numerical and analytical approaches

Specimen	**Strain (2D FEA)**		**Strain (3D FEA)**		**Strain (CLT)**	
	ϵ_x ($\mu\epsilon$)	ϵ_y ($\mu\epsilon$)	ϵ_x ($\mu\epsilon$)	ϵ_y ($\mu\epsilon$)	ϵ_x ($\mu\epsilon$)	ϵ_y ($\mu\epsilon$)
UD(0)	52	2	52	2	36	6
CP(0)	160	57	172	55	170	57
QI(0/45)	-44	-18	-148	16	46	-17
AP	67	25	70	-474	139	-521

Table 6.5: Comparison of strain in the far-field region for conditions given in Table 6.2

Specimen	**Measured strain** ($\mu\epsilon$)		**Strain (2D FEA)** ($\mu\epsilon$)		**Strain (3D FEA)**($\mu\epsilon$)	
	ϵ_x	ϵ_y	ϵ_x	ϵ_y	ϵ_x	ϵ_y
UD(0)	997	-275	1026	-205	1145	235
CP(0)	2126	-245	2236	-209	2206	-191
QI(0/45)	1510	-328	1644	-477	1613	-493
AP	1907	-1036	2623	-1210	2686	-1632

Table 6.6: The comparison of the differences between the measured strain in the far-field region and the strain obtained using numerical and analytical approaches

Specimen	**Strain (2D FEA)**($\mu\epsilon$)		**Strain (3D FEA)**($\mu\epsilon$)	
	ϵ_x	ϵ_y	ϵ_x	ϵ_y
UD(0)	29	70	148	40
CP(0)	110	36	80	54
QI(0/45)	134	-149	103	-165
AP	716	-174	779	-596

6.9 Strength reduction factor

The composite laminates given in Table 6.1 were loaded to failure under tensile loading to determine the failure strength. The derived SCF_{TSA} were compared with strength reduction factors (SRF) obtained from failure tests, by taking the ratio of the failure

stress of notched (first noticeable failure) and unnotched specimens (following Equation 6.1). The failure strength of the notched specimens in comparison with the unnotched specimens (i.e. failure strength vs displacement curves) are given in Figure 6.12 and Figure 6.13. The comparison between the SCF_{TSA}, measured SRF and SCF based on raw FE data (following Equation 6.1) are shown in Table 6.7. Here the 2D model is a global laminate model. It is clear from Table 6.7 that the SCF_{TSA} does not correspond with the SRF and in all cases provides a smaller value than the SCF_{TSA} approach. When comparing the raw FE output (as a stress ratio) and analytical data, in most cases the SRF provided a more conservative value.

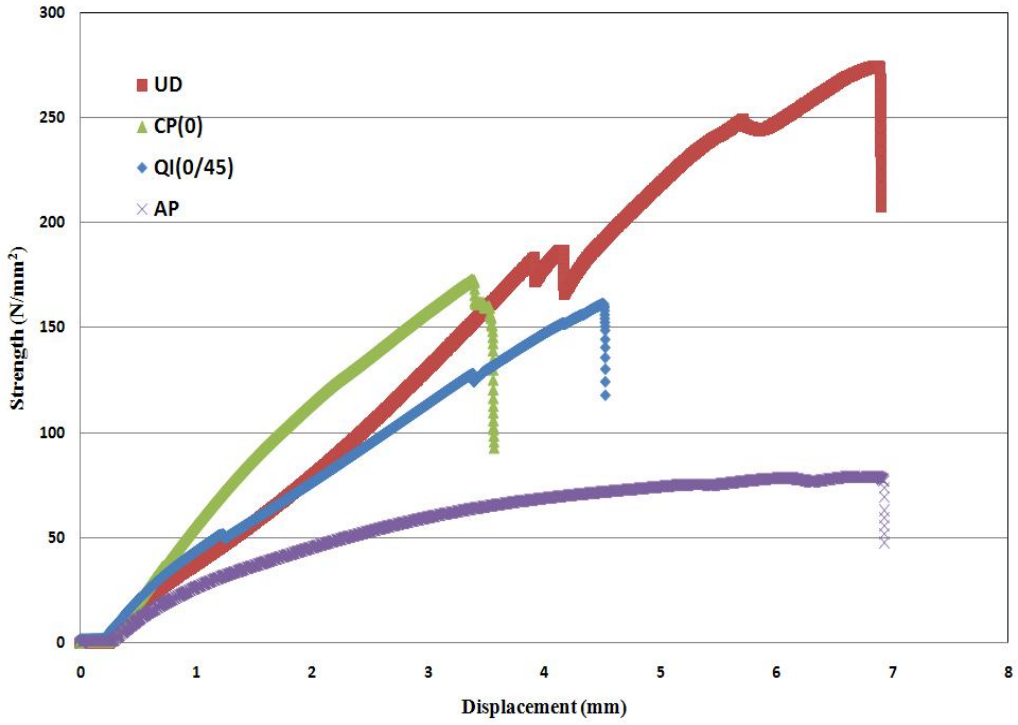

Figure 6.12: Comparison of notched failure strength of UD(0),CP(0),QI(0/45) and AP laminates

Table 6.7: SCF_{TSA}, SRF and SCF (from FEA and analytical work) for specimen with holes

Specimen	SCF_{TSA}	**Strength reduction factor(SRF)**	**Analytical**	**2D FEA**
UD(0)	3.83	4.51	5.21	5.18
CP(0)	2.81	2.29	4.03	5.04
QI(0/45)	3.38	2.33	2.93	3.03
AP	3.80	1.60	2.55	2.71

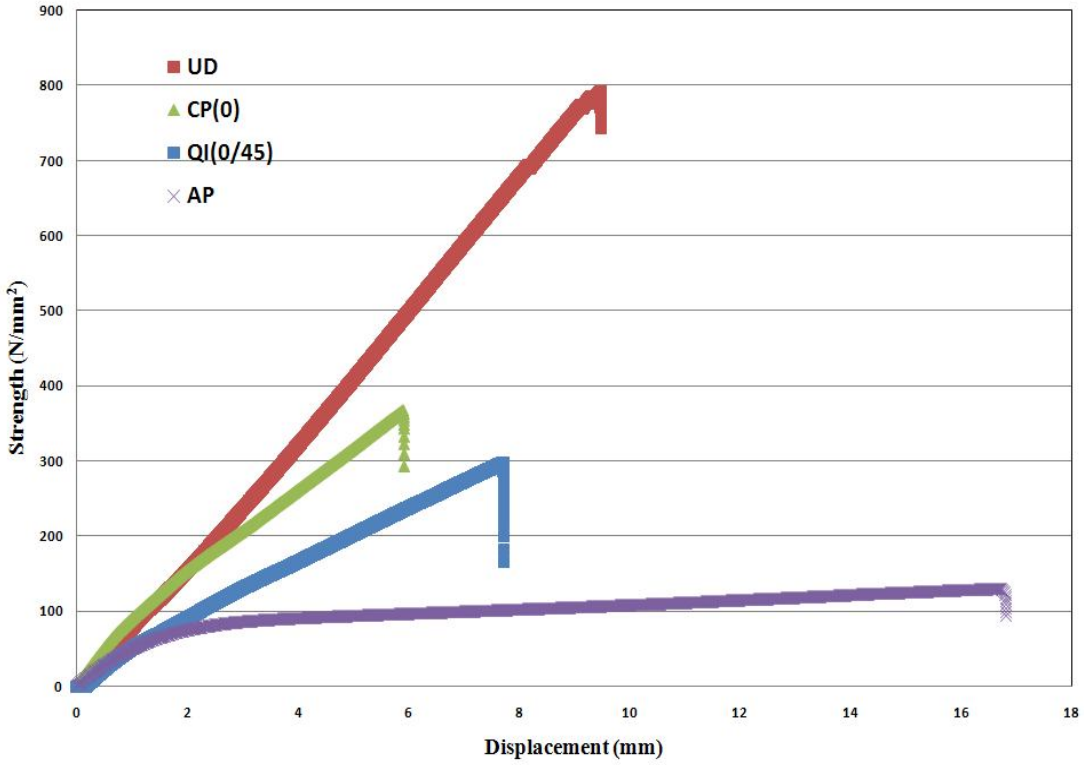

Figure 6.13: Comparison of unnotched failure strength of UD(0),CP(0),QI(0/45) and AP laminates

6.10 TSA Results and discussion

The SCF_{TSA} values for the orthotropic plates were calculated using Equations 6.25, 6.26, 6.27 and 6.29 from the raw FE output (i.e. stress and strain values) incorporating the measured CTE values. To evaluate SCF_{TSA} based on Equation 6.25 the 2D model (known as 2D FEA 6.25) for the surface ply only (i.e. the UD surface layer for the UD, CP, and QI models and the AP surface layer for the AP model) is modelled for a given applied load. For Equations 6.27 and 6.29 the stress and strain have been evaluated for the laminate as a whole. The 3D FEA results were modified to fit with Equation 6.25 (known as 3D FEA 6.25). Equation 6.5 was modified accordingly to a form similar to Equation 6.26 to provide SCF_{TSA} values.

The values of the maximum SCF_{TSA} values for the experimental, analytical and FEA data and the position around the hole are shown for the different lay-ups in Table 6.8.

By comparing the values of the maximum SCF_{TSA} it is difficult to identify a clear match between the experimental data using any of the treatments derived above. It is the case that in the presence of large stress gradients, such as those experienced local to the holes, non-adiabatic behaviour may occur. To investigate if the large mismatch in the

Table 6.8: Values and position of the maximum SCF_{TSA} for the different composite laminates

Specimen	**Experimental**		**Analytical (Equation 6.26)**		**2D FEA (Equation 6.25)**	
	SCF_{TSA}	$\theta(^0)$	SCF_{TSA}	$\theta(^0)$	SCF_{TSA}	$\theta(^0)$
UD(0)	3.83	0	5.21	0	4.57	0
CP(0)	2.81	170	4.04	0	4.56	0
QI(0/45)	3.38	180	2.93	0	4.52	0
AP	3.80	0	2.56	25	3.91	34

Specimen	**2D FEA (Equation 6.26)**		**2D FEA (Equation 6.29)**		**3D FEA (Equation 6.25)**	
	SCF_{TSA}	$\theta(^0)$	SCF_{TSA}	$\theta(^0)$	SCF_{TSA}	$\theta(^0)$
UD(0)	5.19	0	5.23	0	4.19	18
CP(0)	4.18	0	5.91	0	5.11	0
QI(0/45)	3.14	0	5.04	0	2.69	0
AP	2.73	0	5.08	0	5.54	0

derived SCF_{TSA} values could be attributed to non-adiabatic effects, values of SCF_{TSA} were obtained around the hole, away from the maxima, in increments of 10 degrees. These were compared with the values obtained from the FEA and analytical models for the three different treatments. The SCF_{TSA} data presented in Figures 6.14 to 6.17 are shown for a quarter of the region around the hole (i.e. from 0 to 90).

'Edge effects' are a common phenomena observed at the boundary of holes in TSA measurements [47]. However, these are not a concern in this work due to the relatively small applied strain, as demonstrated in Section 6.6. In all cases, the agreement improves away from the maximum stress concentration region, indicating that non-adiabatic effects could be the cause of the poor agreement in the SCF_{TSA} values given in Table 6.8. Another clear indication that the disagreement in the data is not due to the 'edge effect', as commonly reported.

It is clear from all the figures that the strain witness surface resin layer response approach given by Equation 6.29 shows the greatest deviation from the experimental data in all cases, which indicates that the strain witness assumption is not valid in this application. The analytical model (analytical (6.26)) and FEA model (2D FEA (6.26)) are in close agreement with each other and with the experimental data. This provides an indication that the thermoelastic response can be represented by the global laminate behaviour in the presence of in-plane stress gradient and not that of the surface ply as described in Chapter 5. In general, it can be concluded that the 2D FEA (6.26) assumption gives

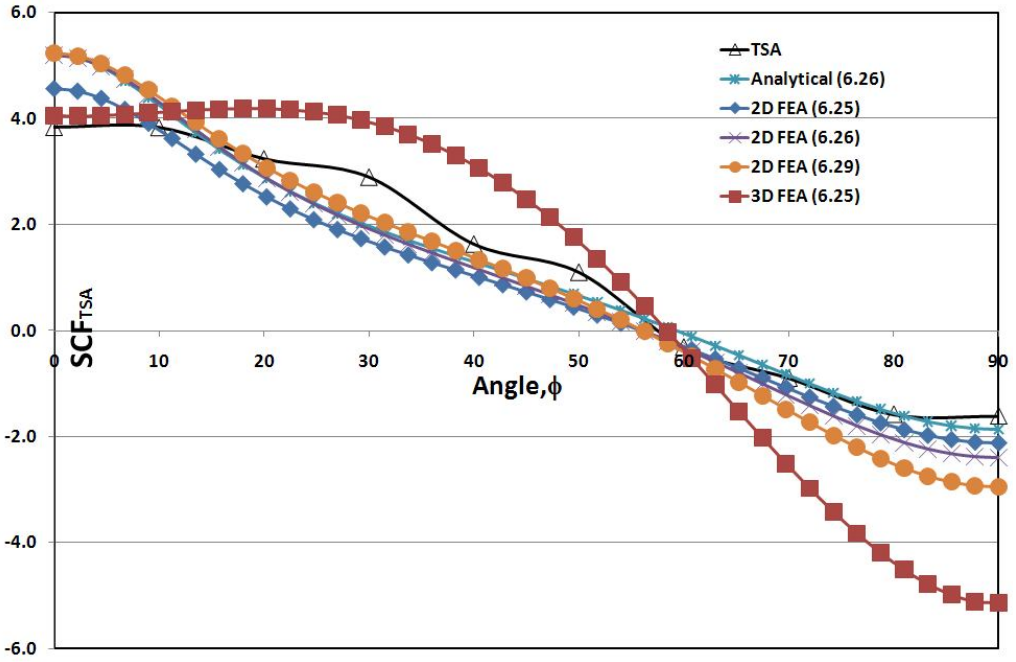

Figure 6.14: Comparison of experimental SCF_{TSA} with those from an analytical solution and FEA for an UD(0) laminate with a central circular hole

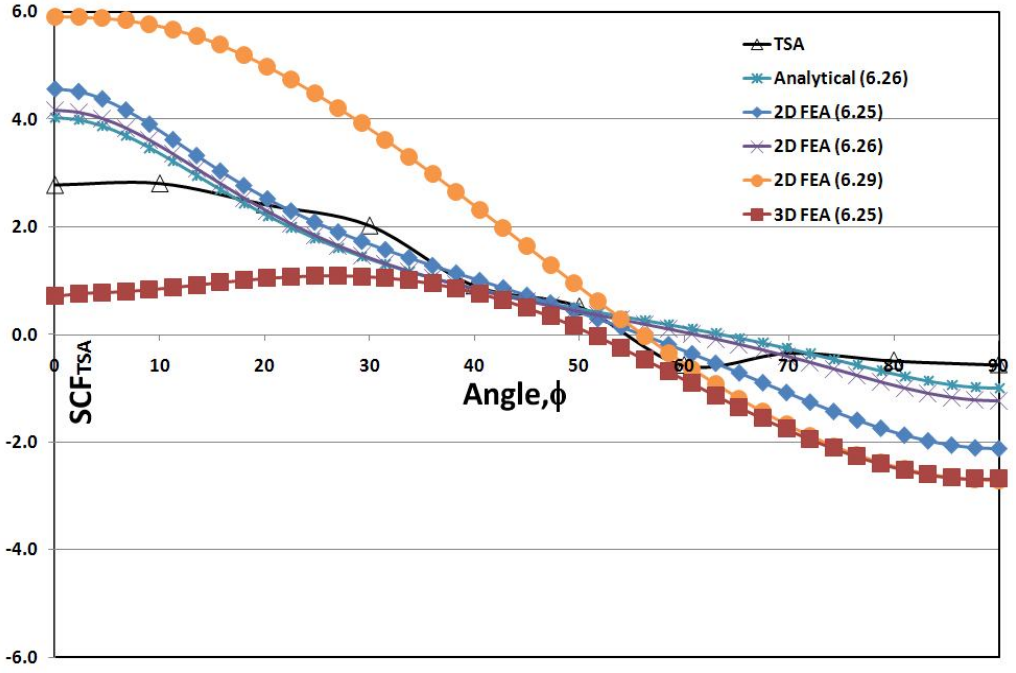

Figure 6.15: Comparison of experimental SCF_{TSA} with those from an analytical solution and FEA for a CP(0) laminate with a central circular hole

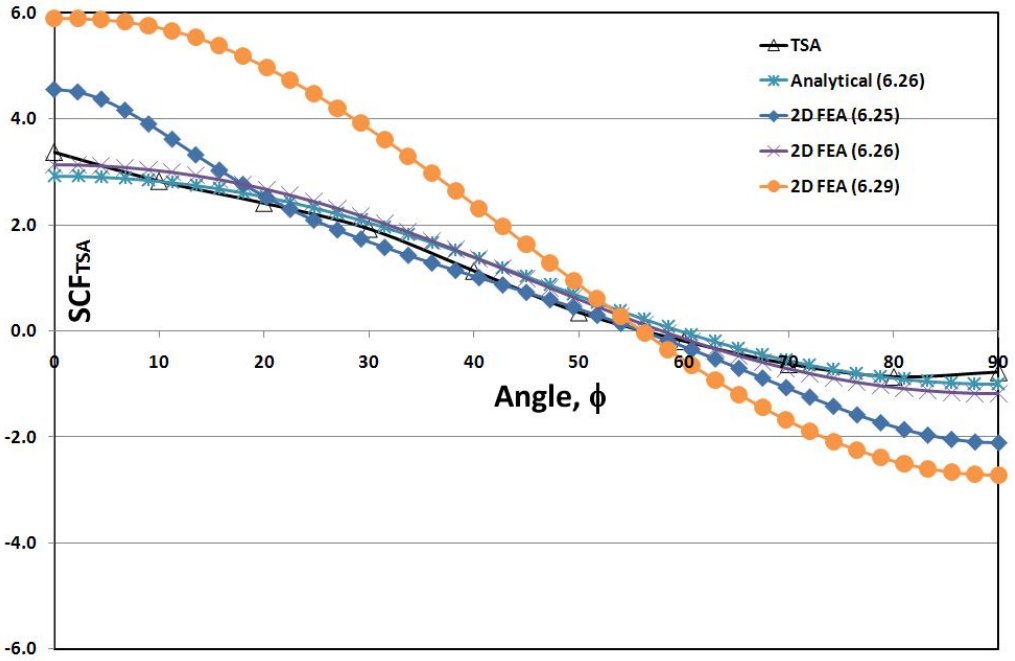

Figure 6.16: Comparison of experimental SCF_{TSA} with those from an analytical solution and FEA for a QI(0/45) laminate with a central circular hole

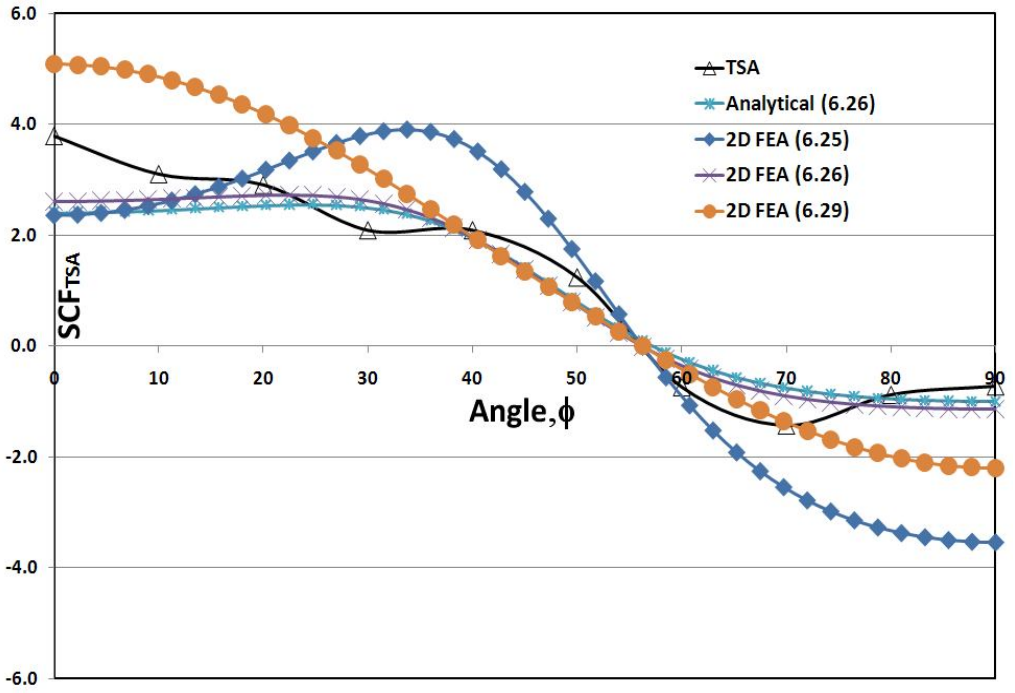

Figure 6.17: Comparison of experimental SCF_{TSA} with those from an analytical solution and FEA for an AP laminate with a central circular hole

the best agreement to the experimental data. This is exemplified for the QI laminate with very clear correlation between the experimental data and the analytical and FE model. It is also important to note that the 2D finite element model (i.e. 2D FEA (6.25)) neglects the influence from the adjacent plies. Therefore, there is a requirement for a 3D FE model to better simulate the ply-by-ply material behaviour. However, it is clear that the 3D FEA provides values that not corresponding to rest of the data showing probably the limitations shown in Table 6.5.

6.11 Summary

A novel attempt to examine different approaches in quantifying the thermoelastic response from the neighbourhood of holes in orthotropic composite laminates as an 'SCF_{TSA}' is detailed in this Chapter. The different approaches are compared with analytical and finite element models. In the presence of through thickness temperature gradient as well as in-plane temperature gradient caused by the discontinuity in the structure, the results show that the SCF_{TSA} derived for composite materials is best represented by global laminate behaviour. The effect of in-plane temperature gradient is apparent as better agreement between the measured SCF_{TSA} data and numerical models are observed away from the edge of the hole. The assumption that the thermoelastic response depends solely on the properties of the surface layer (i.e. the resin rich layer or the orthotropic surface ply) of composite laminates is not compelling in this analysis.

The results show that the TSA signal from composite materials is significantly affected by several factors which cause difficulties in stress analysis but also demonstrates the necessity and usefulness of experimental data in the design process. It has still not been shown that the routine for obtaining the thermoelastic data for quantitative prediction of stress/ strain are accurate for all lay-ups of composite laminates. The assumption that the surface resin rich layer masks the infrared emission generated by the sub-surface laminate is shown to be invalid for all the cases. However, a reliable calibration routine based on the surface resin layer (for materials for which the assumption is valid) could avoid extensive material testing in order to obtain SCF_{TSA} based on the two normalised temperature values.

In the next Chapter, the possibility of using TSA for analysing loaded holes, (pin-loaded joints) is explored. Bearing in mind the level of complexity involved in analysing this problem, the experimental work is done in two stages, firstly looking at an isotropic pin-loaded joint and perform experimental studies with numerical validation. Secondly, some preliminary experiments are performed to understand the possible application of TSA to composite pin-loaded joints. Despite the shortcomings mentioned in TSA so far

the following chapter will highlight the necessity of full-field experimental data in the design process.

Chapter 7

Stress analysis of pin-loaded joints

7.1 Introduction

Mechanical fastening and adhesive joints are the most common joining techniques for assembling structural components of similar or dissimilar materials. In comparison with adhesive joints mechanical fastening offers the following advantages: no surface preparation is required, the joined member can be disassembled easily for inspection and repair purposes and it is relatively inexpensive. However, the presence of holes for positioning of the fastener reduces the load bearing capability of the joint members. It is known that there will be localised increases in the stresses close to the edge of the hole. In order to maintain the structural integrity of a load bearing structure it is necessary to determine the stress concentration adjacent to the holes. The determination of the stress concentration factor (SCF) for a joint is complex, as many parameters need to be accounted for. Experimental methods therefore have a lot to offer in this difficult stress analysis problem.

Bolts and rivets are the preferred form of mechanical fasteners used in primary load bearing structures. However, the common method used to determine the strength of mechanically fastened joints is through pin-loading, where the bolt is replaced by a pin. The loss of clamping pressure reduces the fatigue life with reduction in the static strength. However, the clamping action should not be relied upon for design purposes because it would be difficult to detect a single untorqued fastener. The general representation of a pin loaded plate is shown in Figure 7.1.

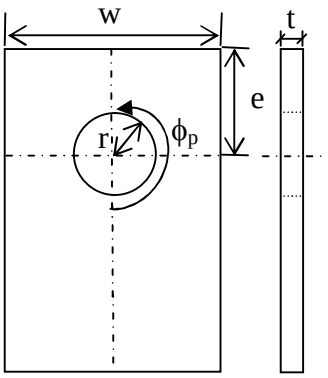

Figure 7.1: Lug nomenclature

The SCF in plates with central circular holes loaded through pins depends on the following parameters [6] :

1. The plate/pin geometry (dimensions and shape details)
2. The fit between the pin and the hole
3. The loading condition (i.e. through-thickness pressure, contact properties, static, dynamic)
4. The plate and pin material

The thermoelastic stress analysis method has been used to characterise experimentally composite structures in a quantitative manner, as given in previous chapters. However, the application of TSA to mechanical joints has been previously limited to pin-joints in isotropic plates [102]. The requirement of an optical path (for the infrared camera), which allows the stress distribution around the joints to be characterised limits the application to pinned joints rather than bolted joints. It should also be noted that, unlike pin-joints in metallic structures, the through thickness clamping mechanism provided by the bolt head and nut has a influence on the bearing strength of the composite laminates.

The literature survey has revealed that there are not many full-field experimental studies of mechanical fasteners in composite material available in the open literature. It is notable that only one study is available on the study of pin-loaded joints in composite materials, in which the stress analysis performed using TSA has been applied in a qualitative manner [103]. The intention of this chapter is to build on the findings of quantitative TSA data obtained from isotropic pin joints to assist in the development of better design procedure for mechanical fasteners in composite joints.

In this chapter, the behaviour of mechanically fastened joints is reviewed. The possibility of applying TSA to characterise mechanical joints is also discussed. The effect of different pin fits, namely snug and clearance and the pin/plate geometry is the main focus of this chapter. The aim of this Chapter is to show quantitative stress concentration data for isotropic (Aluminium) pin joints. Then demonstrate how this is applicable to composite joints. Finally, some initial results on pin-loaded joints in aluminium and composite plates are presented. The repeatability of the technique is also assessed by comparing it with previous work done using similar material and geometry parameters. Also, the importance of full-field experimental data is highlighted by detailing the limitation of available analytical solutions and comparison with 2D and 3D FE models.

7.2 Review of pin-loaded plate studies

The majority of early work on isotropic pin-loaded plates has used experimental methods, mainly strain gauges and photoelastic techniques. Most of it has concentrated on pin fit profiles and different plate geometries. Based on this, engineering design data as a function of joint or plate geometry for standard loading cases have been developed for isotropic pin-joints [104]. Hand calculations with reference to stress concentration design curves are useful to quickly assess simple joints. However, discrepancies occur for complex joints, as secondary effects such as the pin to plate stiffness ratio, friction and pin finish are neglected in these calculations. The need for a more universal design method, by incorporating various parameters, requires the analysis of pin and plate design using the finite element method. Detailed FEA can take into account secondary parameters and provide more accurate results. However, it requires high computational time and in the case of multiple fasteners, severe convergence problems are faced. In this section, a general review of defining SCF's for isotropic pin joints are discussed.

7.2.1 Stress concentration

In practice, engineering components tend to have discontinuities in section such as fasteners. Stress concentration values for pin-loaded holes are defined using either the original gross cross-section or the net cross-section. In some cases calculations are made with respect to bearing area. The theoretical stress concentration factor, k_{te}, for bolted joints on the net section immediately adjacent to the hole is given by [105]:

$$k_{te} = \frac{w}{d} + 1 - \left(1.5q\frac{(w/d-1)}{(w/d+1)}\right) \tag{7.1}$$

the parameter q, for e/w < 1,

$$q = 1.5 - \frac{0.5}{e/d} \tag{7.2}$$

and for e/w > 1, q is equal to zero

The stress in the plate, adjacent to the hole in the direction perpendicular to the load direction, is therefore given by:

$$\sigma_{max} = k_{te}\frac{P}{t(w-d)} \tag{7.3}$$

Equation 7.1 can be re-expressed with respect to the gross cross-sectional area in a similar manner to Equation 6.1 or as:

$$k_{tg} = \frac{k_{te}}{1-(d/w)} \tag{7.4}$$

Equation 7.1 can also be re-expressed with respect to the bearing area as:

$$k_{tb} = \frac{\sigma_{max}}{\left(\frac{P}{td}\right)} = \frac{k_{te}}{w-d} = \frac{k_{te}}{\left(\frac{w}{d}-1\right)} \tag{7.5}$$

In a similar manner, the experimental reference stress, or nominal stress, is defined using either the net cross-section or the original gross cross-section. In the first instance, the SCF is taken to be the ratio of the average stress on the minimum net section of the plate to the load at which the specimen failed [105]. The stress concentration factor based on the net cross-sectional area is given by:

$$k_{tn} = \frac{\sigma_{tu}}{\frac{P}{(w-d)t}} = \frac{\sigma_{tu}(w-d)t}{P} \tag{7.6}$$

P is the load at which the specimen failed and the numerator is the unnotched net section strength. The stress concentration factor based on the gross cross sectional area is given by Ref. [105]. The SCF is taken to be the ratio of the maximum bearing load to the ultimate tensile load remote from the fastener hole, as follows:

$$k_{tg} = \frac{P_{tu}}{P_B} = \frac{\sigma_{tu}wt}{\sigma_B dt} \tag{7.7}$$

where P_B is the bearing load transferred by the fastener to the plate and P_{tu} is the ultimate tensile load for the plate without a hole. In experimental work it is usually easier to use k_{tg} as the reference stress can be obtained simply from the specimen geometry. In order to use the value of k_{tn}, the net cross-sectional area is needed to calculate the reference stress. However, the stress in the net cross section is usually of more interest, and k_{tn} is more generally used [104] for design purposes. The value of k_{tn} can be related to k_{tg} as follows:

$$k_{tn} = \left(1 - \frac{d}{w}\right) k_{tg} \tag{7.8}$$

For specimens under uniaxial tensile load SCF determined from TSA data is equivalent to Equation 6.3, where it is the ratio of the maximum stress at the edge of the hole to the average stress over some distance ahead of the fastener hole. In Section 7.4.1, an experimental program on isotropic pin-joints is detailed to show the comparison between the different methods to obtain SCF to highlight the importance of TSA data.

7.3 Review of mechanical fasteners in composite structure

The behaviour of mechanical fasteners in carbon and glass fibre reinforced composite laminates have been extensively investigated by many researches by means of analytical, computational and experimental methods. A wide range of variables such as geometry parameters, lay-ups, fastener parameters and their influence on the joint strength and failure modes have been considered. A large part of the research has been concentrated on the determination of the influence of geometric factors on the joint strength, as this has been identified as the major governing parameter of the strength of the joint. This is mainly the case for the behaviour of the structure under static loads. The complex studies on the change in stress-strain relationship when joints are subjected to fatigue loading are still limited, especially in terms of experimental data.

More detailed experimental methods such as strain gauges and photoelasticity, have also been applied to the problem of obtaining strain concentration factors. A similar concept is applied to analytical methods, where analytical models are developed to predict the failure load based on the joint geometry and mechanical properties of the material. These methods give an indication of the safety factor that needs to be applied in the design of the joint, however, they do not provide any information of the stress distribution in the joints, which is essential in optimising and improving joint efficiencies. Computational methods do give an indication of the stress distribution around joints, as well as the SCF. Several numerical models have also been developed to predict failure of pinned and bolted

joints, and most of them are reviewed in detail by Camanho and Matthews [6] and a recent one by [106]. However, fine meshes or higher order interpolation polynomials are needed to capture the steep stress gradients for accurate predictions. For large 3D models and joints with multi-fasteners this could be a major obstacle. In order to overcome this problem, the analysis is usually performed in three different stages. Firstly, the global structural analysis is performed, followed by the load distribution analysis in the joint members and finally local stress analysis around the joint. In the case of joints with multi-fasteners, prior calculations (optimisation algorithms) are needed to identify the critical fastener before the single fastener is modelled in order to avoid the convergence problems. In general, to simulate final joint failure, progressive damage models have been developed and implemented in finite element codes. This procedure is repeated for increasing load levels until the material properties have been fully degraded, and the joint fails. In most cases, the FE programs often stop before the failure load is reached due to excessive element distortions.

The general parameters that influence the strength of mechanically fastened joints are presented in the following section. While the main part of the published work has focused on parametric studies on strength and failure of mechanical fasteners, there is limited work published regarding the manufacturing process to improve the joint performance. An insight into some of the development in manufacturing techniques to improve joint efficiency is also presented in next section.

7.3.1 Material parameters

For general engineering purposes there are 3 main types of reinforcement fibres in common use, E-glass, carbon fibres and aramid fibres (e.g. Kevlar 49). E-glass fibres are often used as random reinforcement (e.g. chopped fibres) or roving (e.g. bundles or parallel fibres). E-glass is the most cost effective reinforcement fibre available. Carbon fibres are used for higher integrity applications (e.g. aerospace industry), where their higher specific stiffness is required. The price ratio for general purpose resin is 1:2:4 for polyester, vinylester and epoxies. However, epoxy resins out-perform other resin types in terms of mechanical properties and resistance to environmental degradation (suitable for aircraft components). Composites manufactured using low temperature prepreg are of high quality and give good mechanical performance, as vacuum bagging and high pressure (using autoclave), eliminates the voids by compaction. On the other hand, the original advantages of using composites were room temperature curing and ambient pressure moulding. This method is widely used for manufacturing large structures. However, poor quality can arise as a result of mainly from uncontrolled fibre to resin ratios, large voids, dry reinforcement patches and under-cure.

One of the advantages claimed for fibrous composite structures is that orthotropic properties can be tailored for specific application. However, the desire to develop adequate strength tends to restrict the choice of fibre patterns to those that produce quasi-isotropic material. The overall intention is to show that material selection, manufacturing feasibility and material properties are strongly interrelated factors that have to be considered in the design process in order to achieve highly efficient composite joints. In this section, the effect of fibre orientation and laminate stacking sequence on composite joints and the methods to improve the efficiency of the joints are presented.

7.3.1.1 Fibre orientation and laminate stacking sequence

The fibre orientation has an influence on the position around the hole circumference at which failure is initiated and further influences the mode of failure. The quasi-isotropic pattern gives the highest structural efficiency (lowest SCF) for a composite joint. An increase in the strength associated with the 0 plies is almost nullified by the large increase in the stress concentration factor. Less homogeneous stacking sequences exhibit lower bearing strength due to the higher interlaminar shear stress presence in the laminate. The minimum values of w/d and e/d ratios to achieve full strength depend on the lay-up used. High w/d ratios are necessary to achieve full strength in ±45 and 0/90 laminates.

Okutan and Karakuzu [107] chose two different laminate configurations $(90,0)_{2s}$ and $(45)_{2s}$ in order to determine the significance of fiber orientation on bearing strength. It was evident from the load displacement curves that the $(\pm 45)_{2s}$ laminates failed in a more sudden fashion than $(90,0)_{2s}$ laminates. For this reason, the use of mechanically fastened joints in $(\pm 45)_{2s}$ laminates is not recommended. Hart-Smith [7] concluded that shear-out failures are frequent for laminates rich with 0 fibres and deficient in 90 fibres. As a general guide, it was also stated that there should not be more than 3/8 or less than 1/8 ratio of the fibres in any one direction (0,45 and 90) in the laminate. This means that the bearing strength is maximised for quasi-isotropic laminates, while the stacking sequence should be optimised in order to obtain highest strength and desired mode of failure.

The pin-bearing strength of glass/epoxy laminates for eight different stacking sequences of laminates with 0, 90 and 45 layers were studied by Quinn and Matthews [108]. The joint strength was clearly dependent on the stacking sequence. The study suggested that placing 90 fibres on the surface increases the bearing strength because this will produce a compressive through thickness direct stresses than can restrain delamination. Park [109] investigated the effects of stacking sequence and clamping force on the delamination

bearing strength and the ultimate bearing strength of pin and bolted joints in carbon/epoxy composite laminates. The results of the pinned joint test for orthotropic composite laminates with stacking sequences of $(90_6,0_6)_S$ and $(0_6,90_6)_S$, shows that both lay-ups have almost same ultimate bearing strengths. Thus, the stacking sequence with 90 fibres on the surface has a higher delamination bearing strength. The delamination failure was characterised using acoustic emissions (AE). The work also demonstrated that the increase in ultimate bearing strength for bolted joints results from the effect of lateral boundary constraint by bolt head, washer and nut, rather than the clamping pressure. The clamping pressure changes the failure mode from a catastrophic type to a progressive one. Hamada et. al. [110], reported that the quasi-isotropic laminates with had 0 plies on the outer surfaces, 90 plies next to the 0 plies, and ± 45 plies interspersed in the middle of the laminate $(0,90,\pm 45)_{2s}$ had the highest bearing and net-tension strength. It is clear that there are many options for selection of stacking sequence depending on the specific use and also including geometry and fastener parameters.

7.3.1.2 Manufacturing routes

Currently, there are few methods employed in industry to reduce stress concentrations in composite joints based on the general behaviour of the joints. For example, extra layers of material are incorporated at the fastener region to increase the bearing area. Also, a number of ± 45 plies are added to the laminate to promote delamination that behaves as a stress relief in the joint. There are other additional methods that can be found in the literature to reduce the stress concentration at the joint and improve the efficiency of the joint.

The conventional method of making a hole in a laminate is to drill a hole in a cured composite. However, this method destroys the continuity of the fibres in the structure leading to large stress concentrations. To improve the continuity in the laminate, Chang et. al. [111] used a steel punch to bypass the fibre around hole (also known as a moulded-in hole). The experimental result shows that specimens with moulded-in holes demonstrated higher failure strength than drilled specimens an increase of nearly 46% was reported. Similar experiments were done by Lin et al.[112] for woven fabric composite and the experimental results show that specimens of a $(0,90)_s$ lay-up with a moulded-in hole shows higher failure strength than the drilled hole specimen. However, significant differences were not observed for $(\pm 45)_s$ laminates with drilled and moulded-in holes. The local reinforcement in the moulded-in holes, changes the fibre content and fibre orientation in the laminates. Thus, owing to their anisotropic and inhomogeneous properties, the material strength also varies with direction and location. Therefore a suitable numerical method is needed to predict the failure of a laminate

with a moulded-in hole. Lin et. al. [112] used the modified rule of mixtures to define the material moduli of laminates with a moulded-in hole. The Hashin strength criteria and a material degradation model are incorporated in the finite element analysis, which demonstrated reasonable correlation with the experimental results.

Mechanical fasteners impose a compression load on the bearing surface of laminate causing microbuckling of the fibres at the bearing surface and delamination of plies under through-thickness stress. In order to improve the bearing strength of bolted joints the use of adhesively bonded metallic inserts is investigated by means of experimental and computational methods [113, 114, 115]. Manufacturing defects relating to hole machining can reduce the strength and fatigue life of pin-loaded joints in comparison to defect free laminates. Therefore metallic inserts can be used to decrease the stress concentration or to repair damage near the hole boundary. The insert provides a localised plastic zone, which provides stress relief in the joint. However, the drawback is that the method requires addition of extra weight around the loaded hole. Therefore, the shape of the inserts should be accounted to for in order to minimise the weight. This will provide optimised use of isotropic material and also the maximum possible stress reduction at the hole boundary. Camanho, et. al. [113] performed a 3D FE analysis by incorporating bolt-insert contact analysis, elastoplastic behaviour of the adhesive to evaluate the effects of the insert material and thickness on the performance of the joint. The results showed strength improvement when inserts are used. The prediction of stress concentration reductions around loaded holes employing photoelastic analysis showed a large reduction of stress concentration at the joints [115]. However, none of the mentioned research work indicates the size or shape of an optimum insert should be used.

The literature indicates that continuity of the fibres and strengthening of the bearing area could provide significant improvement in the joint efficiency. Based on that assumption, Li et al. [116] introduced fibre steering technique to enhance the bearing strength of bolted joints. The procedure requires dry tows of fibres to be placed precisely on a prepreg fabric following by both the tensile and compressive principal stress trajectories around the hole. An improvement in stiffness and strength is expected when the fibres are steered to match the path by which the load traverses the structure. The mechanical test on the joint indicates that fibre steering improved the ultimate failure strength by a factor of 1.36 for a specimen reinforced by 3k fibre tows in tensile principal stress patterns and 6k fibre tows in compressive principal stress patterns.

7.3.2 Geometry parameters

The design methodology for mechanical fasteners in metallic structures cannot be applied directly to joints in composites because of material anisotropy and the brittle nature of the material. Among the different geometry parameters considered in metallic joints the ratio of the width of the plate to the diameter of the pin (w/d) have gained the most attention in the literature. The lug nomenclature is same as shown in Figure 7.1. By tailoring other parameters, such as fibre orientation and the stacking sequence of the laminate, etc. with the increase in the w/d ratio, significant reductions in the stress concentration can be achieved. The other geometric parameters, i.e. e/d and t/d ratios, have smaller influences on the joint efficiency and become insignificant after certain limits. For example, by increasing the e/d ratio beyond 2 and increasing the w/d ratio beyond 3 does not have a significant effect on the load bearing capability of the connection [117]. Combination of different geometry parameters has a significant effect on the mode of failure of composite joints. Failure modes are characterised as bearing failure, shear failure, net tension failure, cleavage tension failure, fastener failure (e.g. bolt failure) and fastener pull through laminate failure. The failure stresses in composite joints are given as:

$$\sigma_b = \frac{P}{dt} \tag{7.9}$$

for the bearing stress, localised hole damage (due to delamination or matrix cracking)

$$\sigma_s = \frac{P}{2et} \tag{7.10}$$

for shear out stress (can be prevented by increasing e/d >3)

$$\sigma_{net} = \frac{P}{(w-d)t} \tag{7.11}$$

for net section stress (prevented by increasing w/d above a critical value)

When any one of the stresses reaches a critical value the joint will fail. Among these, only bearing failure and tension through the hole are considered desirable and the rest are considered as premature failures. Okutan [117] studied the behaviour of single hole pin-loaded specimens experimentally, by varying w/d and e/d ratios and concluded that net tension failure occurred for specimens that had small w/d ratios and large end distances. Also, when the width was increased, the specimens with small end distances failed in a shear out mode, while by increasing the end distance, bearing failure developed. It is also

evident that joints with higher w/d ratios increase the joint efficiency and that generally bearing failure is preferable (higher efficiency) as catastrophic failure is undesirable in composite joints. However, using small diameter fasteners could result in excessive bending and may lead to failure of the fastener. Therefore, it is important to optimise the geometry parameters to obtain joints with the highest joint efficiency.

In Ref. [118] it was reported that the optimum composite joint strength is obtained at w/d values close to 3, which are believed to be the transition point between bearing and tension failure. Similar geometry effects were also observed in woven glass laminates showing there was no large change in the SCF [118]. Liu et al. [119] investigated the relation between the efficiency of mechanical joints and the laminate thickness to pin diameter ratio (t/d) of material with a woven glass fabric and phenolic matrix by experimental and computational methods. It was reported that, as the composite joint thickness increases the contact interaction between the pin and the plate changes and it was concluded that thick plates with smaller pins and thin plates with larger pins have lower joint efficiencies. It was found that the t_2/d_2 ratio could be used to distinguish between the two failure modes, pin bending and bearing failure.

It can be concluded that, the distinction between bearing and net tension failure is largely established by the joint geometry. Scaling effects include both in-plane and thickness as the stress distributions and failure modes in thick section composites will be different from those of thin plates.

7.3.3 Fastener parameters

A wide range of fasteners (e.g. rivets, screws, bolts and pins) depending on the application are available to join metallic parts, but the particular characteristic of composite laminates limits the choice. Bolts are required in high load bearing structures and have been found to be the most efficient way of mechanically fastening composite members. Rivets are not efficient, as they can produce variable lateral clamping forces. Countersunk fasteners are also not preferable because of fastener rotation in a single lap joint. Due to the lower through thickness strength than the in-plane strength in composite material, the fastener head is less effective than the shank in transferring the bearing load [1].

There can be almost a factor of 2 difference between the strength of a pin-loaded joint, in which there is no lateral constraint (clamp-up) and a bolted joint. The bolt head and nut prevent any initial damage to the composite material by deflecting sideways when load is applied. The lateral clamping pressure suppresses the delamination and propagation of interlaminar cracks. A plain pin will give the lowest bearing strength and

a fully tightened bolt shows the highest joint strength. An increase in the temperature will decrease the strength of a laterally constrained joint. Care should be taken with the relief of clamp-up over the life of the joint. A common method used to determine the strength of mechanically fastened joints is through pin-loading, where the bolt is replaced by a pin. Especially in the case of analytical studies and 2D FE analysis, the through thickness pressure is not accounted for. In these cases the strength increases from changing from pin to a bolted joint should be accounted for in design purposes. However, the 2:1 ratio is a maximum and there is no general factor that can be applied, as this is dependent on the particular clamping force and other material properties for each particular joint considered.

An important manufacturing and assembly related issue is machining tolerance and fit between the fastener and the hole. Mechanically fastened joints in aerospace structures are characterised by tight tolerances on both the fasteners and the machined holes. In some non-aerospace applications, larger clearances are required to facilitate installation of the fasteners to the structural members. This can lead the connection to experience a loss of strength due to a more concentrated load distribution at a single location and higher stress concentration will lead to local deformation of the joint. The effect of clearance has been found to be significant in both the distribution and the magnitude of the stresses around a hole. Kelly et al. [120] showed, using a 3-D computational model that for carbon epoxy laminates, the magnitude and distribution of the stress depends on the level of the clearance. Clearance results in a shift in position of the maximum tangential stress from the net-section plane ($\phi = 90$) towards the bearing plane ($\phi = 180$) with increasing clearance. This is directly related to the reduction in the contact angle between the fastener and the hole, where the maximum stress is at the end of the contact angle. The contact area has found to increase with load in clearance fit joints, but not in neat-fit joints [121, 122]. However, these effects have not been validated using any full-field experimental method to date. Hyer et. al. [121] investigated the effect of pin elasticity, clearance and friction on the stresses in a pin-loaded orthotropic plate and concluded that the effect of friction and clearance was most significant on the joint strength. It was highlighted in his work that a 22% reduction in the contact arc can lead to a decrease in the joint strength about 12%. Most of studies that have considered clearance in the joints have been mainly used by analytical and computational methods. DiNicola and Fantle [123] performed experiments on the bearing strength of clearance fit fastener holes in graphite/epoxy woven laminates and measured hole deformations using a compressometer. Pierron et. al. [124] investigated woven glass/fibre epoxy pin-joints with clearance using both experimental and FE techniques. The load deflection curves were used to assess the effect of clearance on the joint strength. It is also notable that careful installation of an interference fit in composite structures can increase the static

tensile strength of the joint [7]. However, literature on the influence of the interference fit on the joint strength is not available.

The effect of friction on the stresses at a pin-loaded hole has mainly been analysed using analytical and computational models. Zhang and Ueng [125] developed an analytical model to evaluate the effect of different coefficients of friction for laminates of different configurations. It was concluded that a small increase in the value of the maximum hoop stress was noted with increasing boundary friction. Therefore, friction should be accounted for in numerical modelling of stress distribution in pin loaded holes, to avoid introducing error. In the same work, it was also reported that pin elasticity is not as important as friction and clearance as the effect of these parameters on the peak stress is not as significant.

7.3.4 Stress and strain concentration in composite joints

The methodology for mechanical fasteners in metallic structures cannot directly be applied to composites joints, yet Hart-Smith, [7] developed a methodology for composite joints analysis that correlates the isotropic stress concentration analysis with concentration relief that occurs in composite joints prior to the failure. The effective stress concentration factor experienced by composite laminates at loaded holes is given by:

$$K_{tc} = 1 + C(K_{te} - 1) \tag{7.12}$$

where C is the correlation factor.

C varies with both the fibre pattern and the hole size. The value of C has been found to be close to 0.25 for 6.5 mm bolts in three different carbon/epoxy quasi-isotropic laminates. It was noted that the fraction is same as the percentage of 0^o plies in the laminate. It is important to note that C can be justified only when net tension failure is observed. It is stated in Ref. [126], that C is not dependent on geometry and varies linearly with the 0^o fibre percentage.

Table 7.1: Pin and plate configurations

Pin-fit type	**Specimen**	**w/d**	**e/d**	**t/d**	$\lambda(\%)$
Snug	AlS10	5.0	2.5	0.6	-
	AlS20	2.5	1.25	0.3	-
Clearance	AlC10/1	5.0	2.5	0.6	0.695
	AlC20/1	2.5	1.25	0.3	0.695
	AlC10/2	5.0	2.5	0.6	0.990
	AlC20/2	2.5	1.25	0.3	0.498

7.4 Thermoelastic stress analysis of isotropic pin-loaded plates

7.4.1 Test specimens and loading arrangements

The effect of pin and plate geometry and fit types are the main focus of this section and the experimental SCF's for pin-loaded plates were obtained using TSA. The details of the pin and plate configurations are given in Table 7.1. The hole diameter in the lug was either 10 or 20 mm, giving w/d ratios of 5 and 2.5 respectively. For the snug fit type the pin diameter was made almost equal to the hole diameter (d_{pin}/d_{hole}=1). For the clearance fit the pin diameter was smaller than the hole diameter with clearance, λ defined as:

$$\lambda = \frac{d_{hole} - d_{pin}}{d_{hole}} \tag{7.13}$$

The lowest practical limit for λ is 0.1% which can be only be obtained in laboratory conditions. In most cases a larger clearance is desirable to facilitate installation of the pin, therefore λ values in this work are much greater.

The pin-loading condition is created by a double-lap joint configuration, where the effect of load eccentricity and secondary bending is omitted (as shown in Figure 7.2) and the surfaces of interest are optically accesible. Prior to testing, the specimen surfaces coated with two passes of RS matt black paint. The aluminium plates were loaded through two silver steel pins (ground close to tolerance) situated in the holes on the longitudinal centre line of the plate, using a servo hydraulic test machine. The dynamic loading frequency was set to 10 Hz, in order to maintain adiabatic conditions. Each specimen was loaded to 10 kN with a sinusoidal load variation of $\pm$7 kN about the mean value. Each arrangement provided two plate configurations, one at either end.

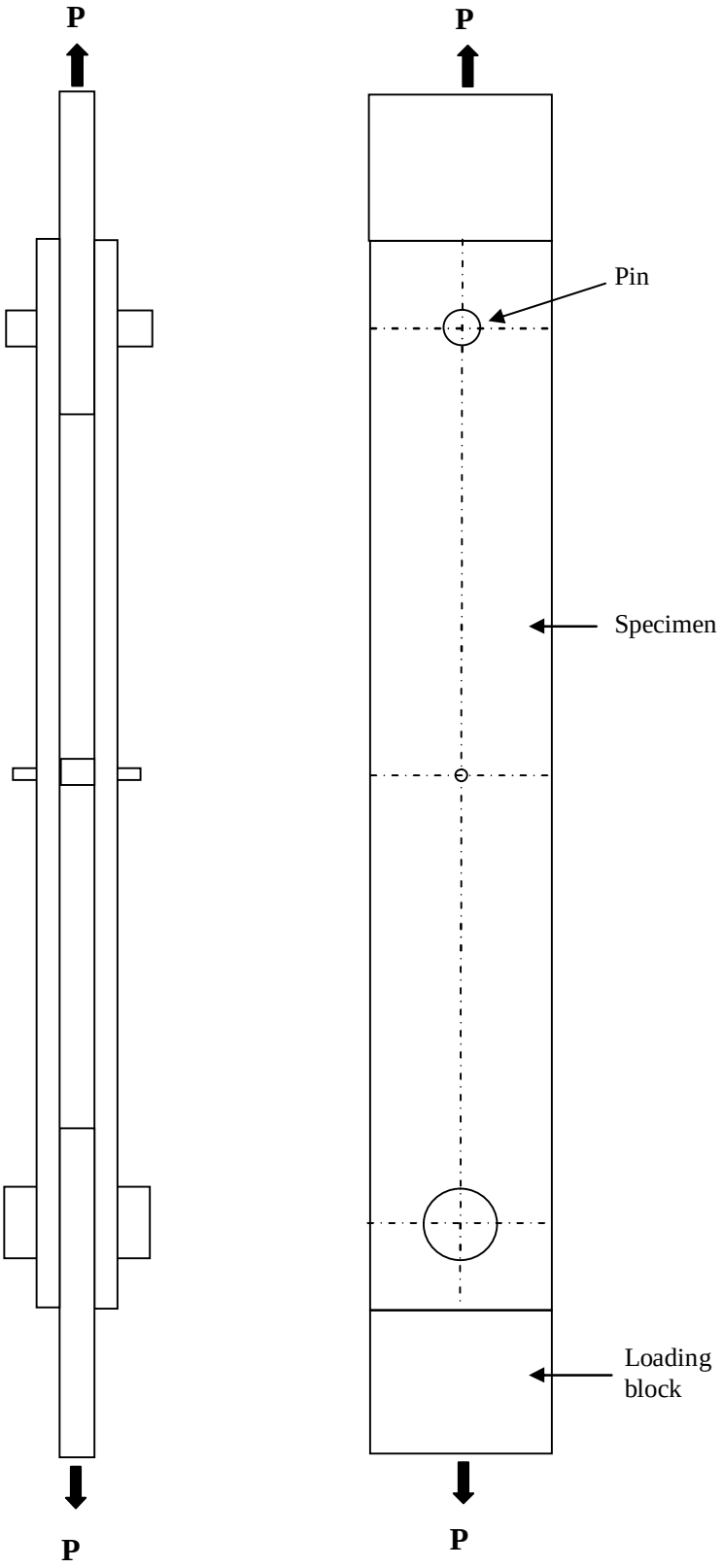

Figure 7.2: Test specimen and loading configuration

7.4.2 Analysis of isotropic pin-loaded plates

The stress concentration factors for the specimens described in Section 7.4.1 have been determined using TSA and the maximum SCF's are summarised in Table 7.2. Two positive peaks on either side of the pin (at $\phi_p = 90^o$ and 270^o) and two negative peaks above ($\phi_p = 0^o$) and below the pin ($\phi_p = 180^o$) are evident in Figure 7.3. In the case of pin-loaded plates, the 'edge effect' is small as there is a continuous transition from the plate to the pin. The equivalent line plot along the horizontal diameter of the hole is shown in Figure 7.3. However, the line plot is not symmetrical. The difference between the two maximum SCF's at the edge of the hole is approximately 17% (as shown in Figure 7.4). This is attributed to the quality of the pin/hole interface, which is dependent on the quality of the manufacturing process when the specimens were made and loading conditions. The average of these two values has been considered.

For the plate configurations with clearance fits there is an increase in the SCF with an increase in clearance. Comparison of the stress contours plot for a snug fit and clearance fit specimen (AlS10 and AlS10/01) is shown in Figure 7.5. For a snug-fitting pin the tangential stresses along the contact arc were found to be small. However, increasing the clearance resulted in a decrease in the contact arc and hence an increase in the tangential stresses. The position of the maximum SCF also changed as a result of the changes in the contact arc and this is clearly noticeable in Figure 7.5b.

Table 7.2: Stress concentration factor data for different plate configurations

Pin-fit type	**Specimen**	**w/d**	$\lambda(\%)$	**SCF**
Snug	AlS10	5.0	-	4.25
	AlS20	2.5	-	3.32
Clearance	AlC10/1	5.0	0.695	4.50
	AlC20/1	2.5	0.695	4.25
	AlC10/2	5.0	0.990	3.75
	AlC20/2	2.5	0.498	3.50

7.4.3 Non-linearity of the load-stress relationship at the contact arc

At the area around the non-contact region around the edge of the hole, only the tangential stress exists and along the contact arc both tangential and radial stresses are present. Unless friction between the pin and lug has been completely eliminated there will be a shear stress at the interface. In increasing the applied load, in the pin-loaded lug the hole in the lug will wrap around the pin, thus spreading the contact arc over a large area and dispersing the load. The degree of non-linearity in the stress-load relationship

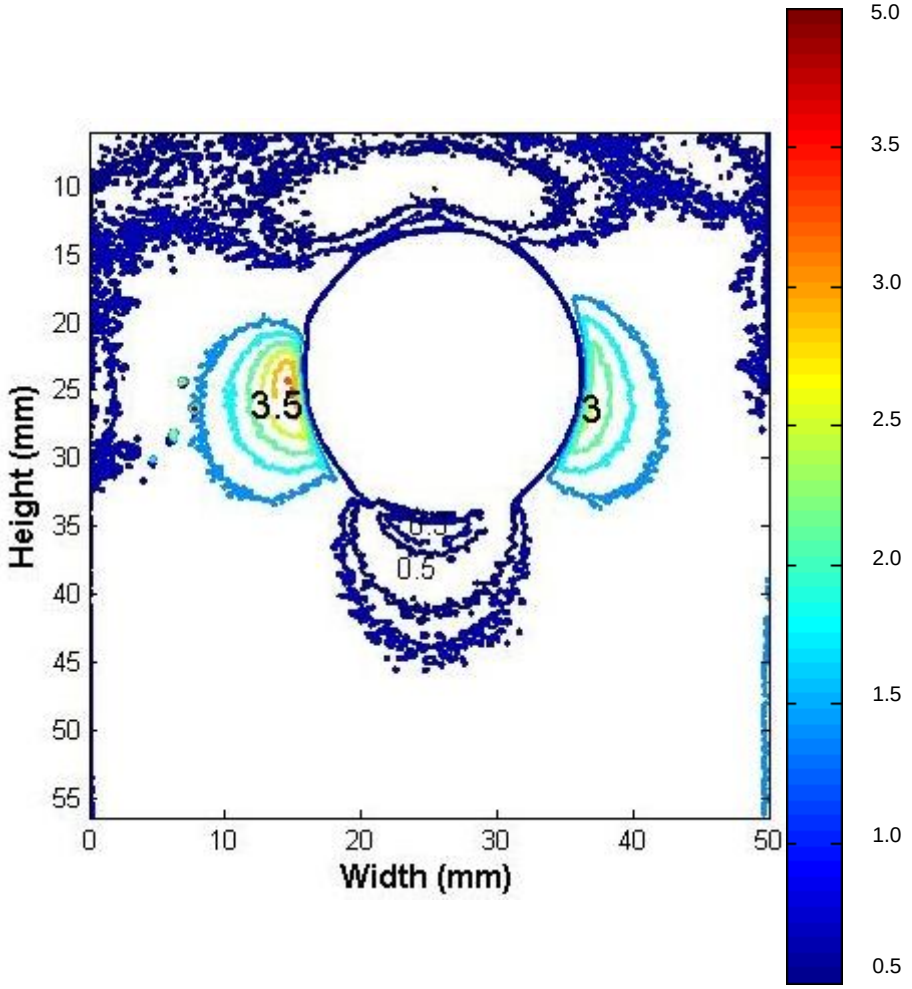

Figure 7.3: Contour plot around AlS20 joint

and the implication on thermoelastic effect is presented in Ref. [49]. It was concluded that the stress sum show slight non-linearity at θ=90 and 180 for snug fit specimen by increasing the load by 4 to 9%.

7.5 Finite element analysis of isotropic pin-loaded joints

In order to provide the full comparison of available SCF's values derived from analytical method, experimental data and FE work, a set of 2D and 3D FE work is presented in this section.

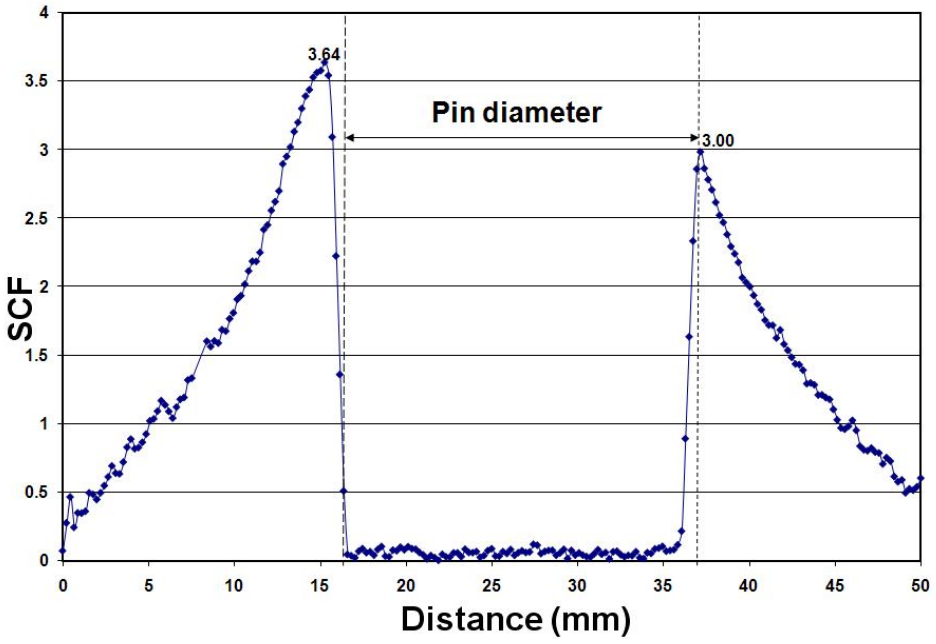

Figure 7.4: Line plot through the horizontal centre line of the pin for specimen AlS20

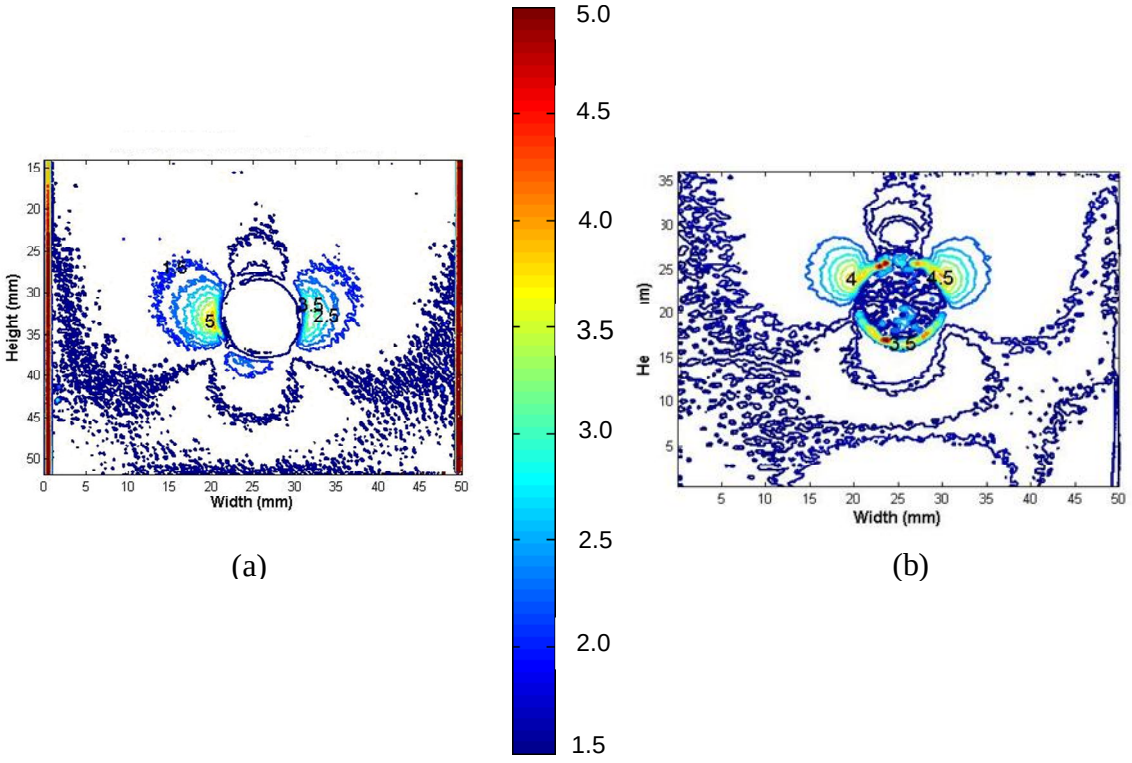

Figure 7.5: SCF contour plot for (a) specimen AlS10 (snug fit) (b) AlC10/1 (clearance fit)

7.5.1 2D finite element analysis

The double shear lap joint (as shown in Figure 7.2) containing a single pin joint is modelled using ANSYS [100]. The dimensions of the plate were taken to be L = 300 mm, W = 50 mm and thickness t = 6 mm. The radius of the hole are for the two types of the pin sizes, where r = 5 mm or 10 mm the distance from the upper edge to the center of hole is e = 25 mm. The material properties of the pin and the plate are given in Table 7.3. These material properties are incorporated in the model in defining element attributes. A two-dimensional, plane 183 [100] element which is suitable for modeling irregular meshes has been used. The element input data includes thickness for the plane stress condition. Due to the symmetric nature of the problem, only half of the geometry is modelled and the finite element mesh of the plate is also shown in Figure 7.6. Symmetric boundary conditions are applied along the length of the laminate. The pin is assumed to be rigid and radial boundary condition using the link element (link1) [100]. This technique is simple and no extra elements are required compared to contact method (explained in Section 7.5.2) and the time taken to reach to the solution is less.However, it is not possible to include friction and clearance effect in this technique.

The distribution of stresses around the pin hole (for r = 5 mm) from the 2D analysis is compared with the TSA plot in Figure 7.7. The two results compares well, but more realistic results can be obtained from 3D analysis which enables the secondary effects such as contact properties and friction can be included and this will be discussed in following section.

Table 7.3: Elastic properties of pin and plate

Component	**Material**	**Young's Modulus (GPa),** E	**Poisson's ratio,** ν
Pin	Silver steel	200	0.33
Plate	Aluminium	69	0.30

7.5.2 3D finite element analysis

The 3D model consist of a mesh of eight-noded, three-dimensional (SOLID185 [100]), finite elements for the pin and lug, with 3-D surface-to-surface contact elements (CONTA174) for the interface between the pin and the hole. A friction coefficient, of $\mu = 0.2$ was applied between the pin and the hole surfaces. Due to the symmetry, only half of the assembly was modelled with the application of the similar boundary condition to the 2D model (as shown in Figure 7.8). The material was assumed to remain as elastic. As the

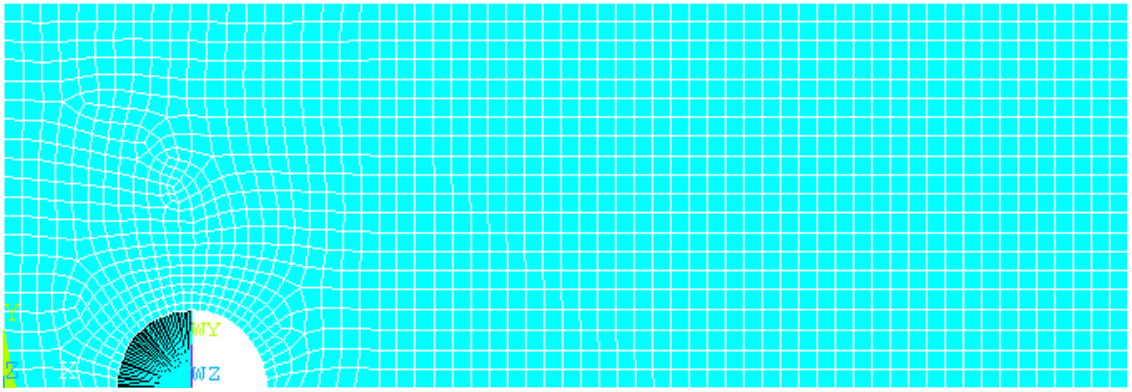

Figure 7.6: 2D mesh of the pin joint

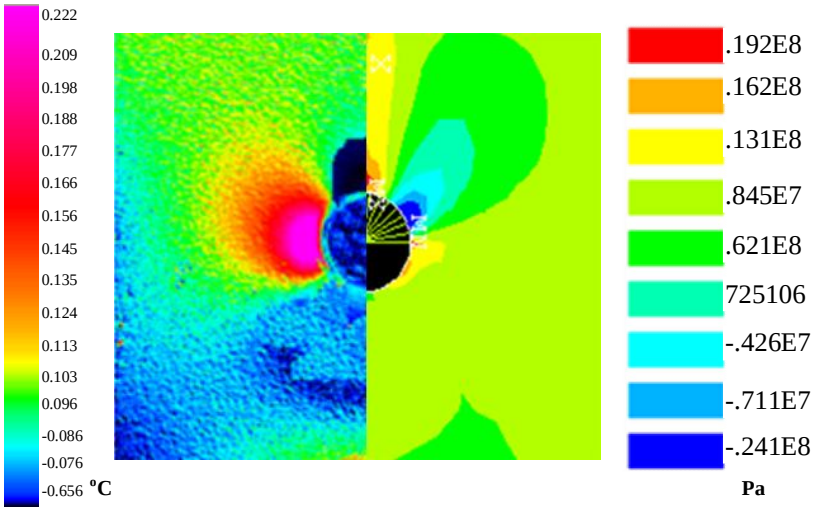

Figure 7.7: Comparison of TSA and FE results (r = 5 mm)

contact area between the pin and lug depends upon on the applied load, the model is solved by considering the geometric non-linear behaviour. The plate has been simulated to be loaded through the end of the loading plate by applying a uniform tension, with the rigid steel pin is being held fixed in position. An incremental-iterative analysis was done to apply the load into 1000 sub steps.

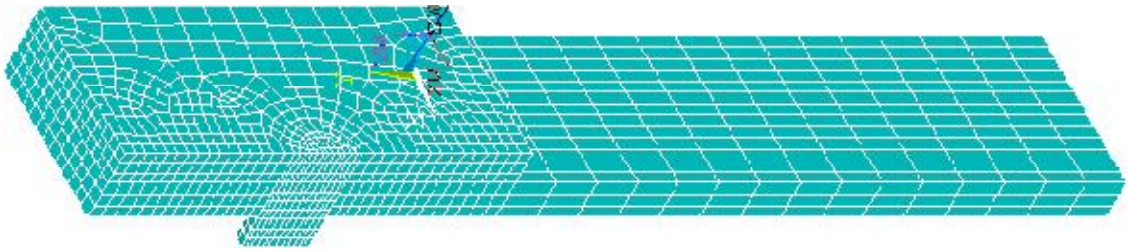

Figure 7.8: Finite element mesh of a geometry of pin-loaded lug

The stress distribution around the pin hole (for r = 10mm) from the 3D analysis is compared with the TSA plot (as shown in Figure 7.9). The two results compares well in a qualitative manner. Polar and Cartesian components of stresses have been presented.

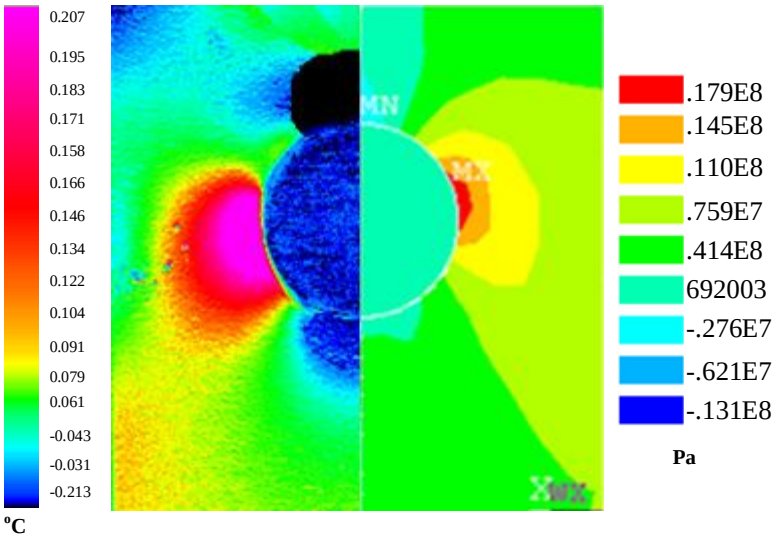

Figure 7.9: Comparison of TSA and FE results (r = 10 mm)

7.5.3 Results and discussion

Because of the symmetric nature of the assembly of pin-loaded lug, the discussion is limited to 0^o to 180^o along the edge of the hole. The comparison between the different values of SCF obtained for the 2D and 3D analysis together with the TSA data for the 2 different w/d ratios (for snug fit only) is presented in the Table 7.4. The SCF_{TSA} was obtained by taking the ratio of the maximum stress at ($\phi_p = 90$) divided by the average stress in the far-field region ($\frac{\sigma_{\phi h}+\sigma_{rh}}{\sigma_{\phi ff}+\sigma_{rff}}$). Based on the close replication (by incorporating most of the realistic features) made in the 3D modelling this provides a better match with the experimental data. However, the maximum SCF obtained from TSA is relatively smaller than the experimental value, which could be attributed to the heat transfer problem face in the regions close to the high stress gradient region (as reported in Chapter 6). To further evaluate this statement, the SCF at $\phi_p = 0$ to 180^o is shown in Figure 7.10 for r = 5mm and Figure 7.11 for r = 10 mm. It can be seen that the difference in the SCF's between the 3D model and TSA improves significantly as the value is taken away from the hole (similar observation was made in Chapter 6).

Figure 7.12 shows the comparison of different SCF values obtained based on analytical solutions, FEA and previous TSA work on isotropic pin lug. The average values of experimental SCF's obtained from this work is close to values available in previous TSA work (as shown in Figure 7.12). Figure 7.12 clearly demonstrates the scatter in the

Table 7.4: Comparison of SCF's obtained from experimental and numerical data

Specimen	w/d	Experimental	2D FEA	3D FEA
AlS10	5	4.25	3.21	5.35
AlS20	2.5	3.32	3.02	3.58

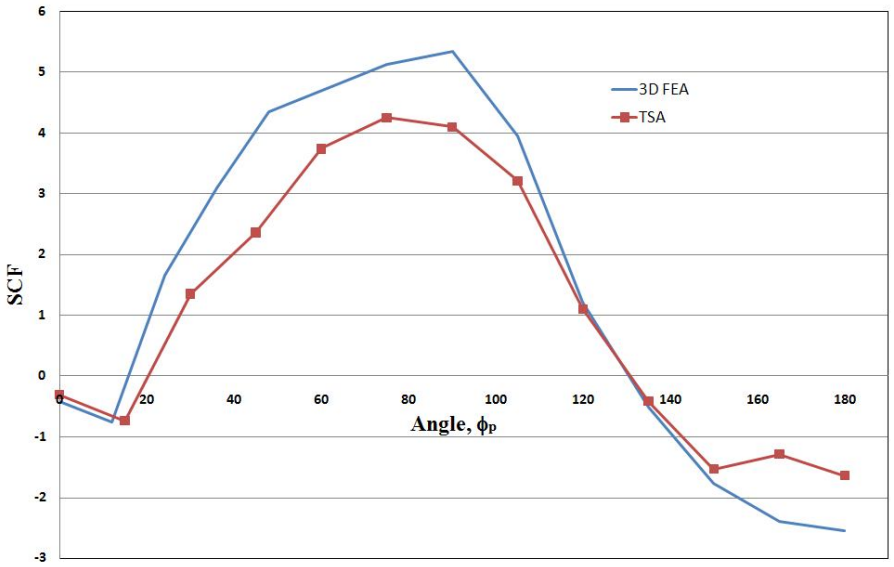

Figure 7.10: Comparison of TSA and 3D FEA results (r = 5 mm)

data available for the same plate pin/plate parameters and shows the importance of the experimental data so that less conservative design guidelines can be used. It is useful to note that Refs. [48, 127] represent steel specimens and also in Ref. [48] the joints are slightly lubricated for ease of assembly. The values for Refs. [104, 127] are based on net section SCFs.

A set of tests examining the effects of width to pin diameter ratio (w/d) and pin-fit has been described and the the experimental and results presented. It was found that SCFs decrease with an increase in the w/d ratio. The snug fitting pins induced smaller stresses at the edge of the hole than clearance fit pins. One of the important aspects of the study lies in the good agreement between the results of the thermoelastic tests and those obtained from the 3D numerical results and the comparison with previous results, which are generally good. This shows the potential in developing an accurate method to predict joint efficiency of axially loaded composite plates using this work as a starting point.

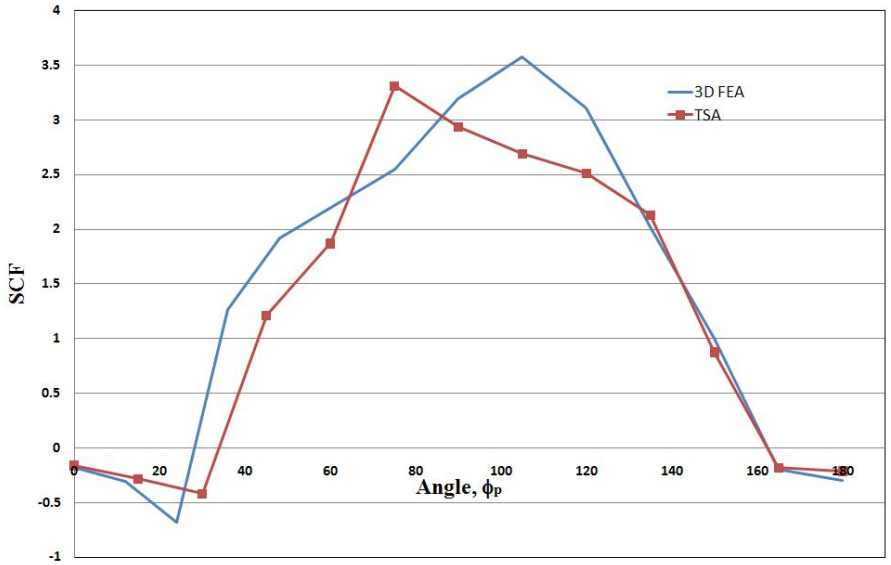

Figure 7.11: Comparison of TSA and 3D FEA results (r = 10 mm)

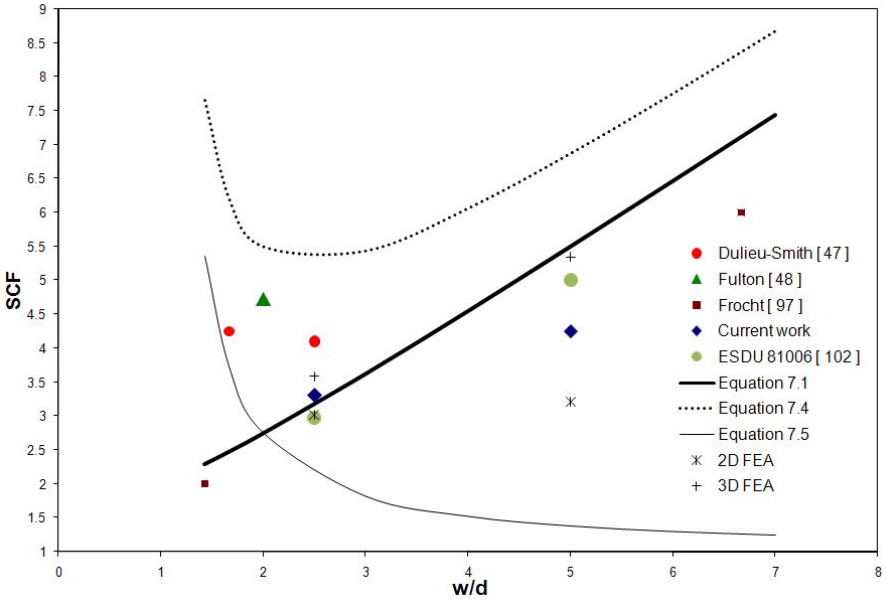

Figure 7.12: Comparison of stress concentration factors for snug fitting pins

Figure 7.13: Assembly of the composite pin-loaded joint

7.6 Thermoelastic stress analysis of composite pin-loaded joints

Based on the findings of the thermoelastic stress analysis of the isotropic pin-loaded joints, similar composite pin-loaded joints with similar geometry and applied loading conditions were designed manufactured. The assembly of the joint is shown in Figure 7.13. Two different type of composite pin-loaded joints are considered in this work, namely the UD(0) and QI(0/45) joints. Since the initial idea was to relate the work done in Chapter 6 on holes in the laminate, therefore the composite plate with pin holes of radius, r = 5 mm and r =10 mm were obtained from the same panel. However, the problem in using the thin plates obtained from the same panel is that at a very low applied load the thermoelastic signal from these joints are very noisy and unreliable (including the phase data). Therefore, it is not possible to obtain reliable thermoelastic data. In attempt to increase the applied load, the joint either fails or creates damage around the pin-loaded hole further increasing the difficulty in obtaining reliable data. This requires a new type (thicker specimen) specimen need to be designed and manufactured in order to obtain reliable thermoelastic data. However, the thermoelastic theory developed so far is based on the plane stress assumption, which is valid for thiner specimens and where the through-thickness stress between the different layers are negligible, (also plane strain assumption is valid).

7.7 Summary

The initial results from the isotropic pin-loaded joints shows potential in developing an accurate method for predicting SCF of axially loaded composite plates. There is a

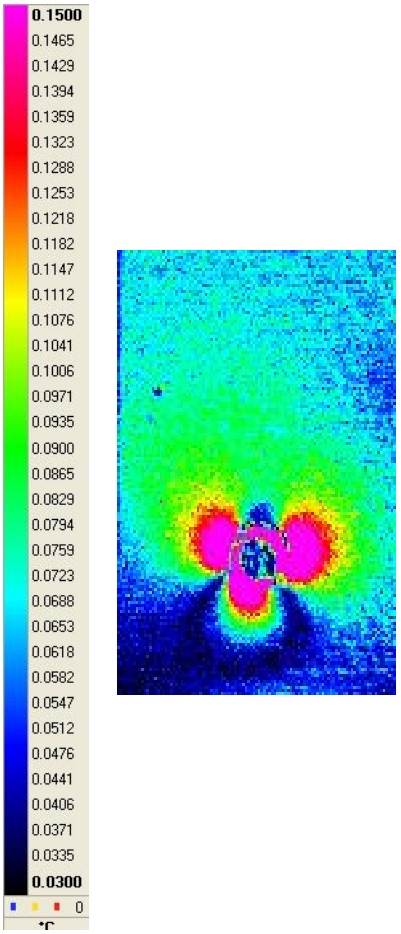

Figure 7.14: Thermoelastic temperature signal from UD laminate

clear match between the thermoelastic measurements and 3D FEA results. However, slight differences in the peak SCF are observed in the TSA data possibly due to the high temperature gradient at the location of maximum stresses. Although, the results are presented for a snug fitting pin, it is not possible to manufacture the pin and plate with such tight tolerance in reality (i.e. $\lambda = 0$). However, this is the actual condition modelled in the FEA analysis.

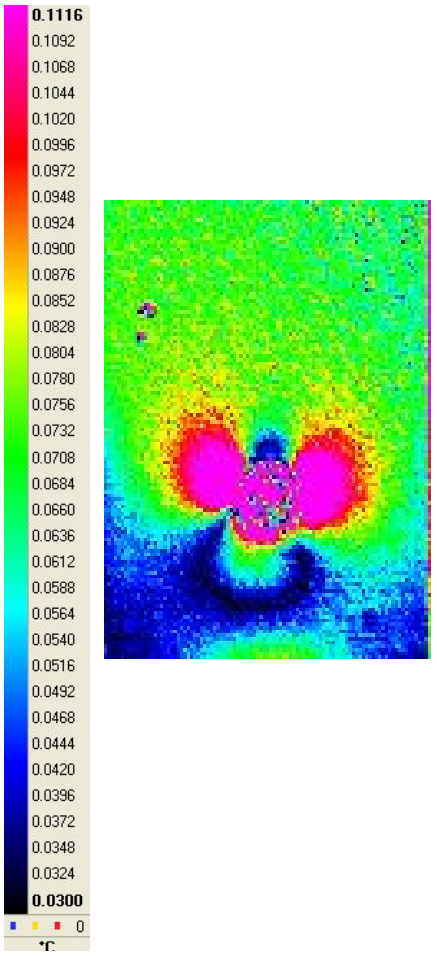

Figure 7.15: Thermoelastic temperature signal from QI laminate

Chapter 8

Recommendations for future work and conclusions

8.1 Future work

The primary focus of this research work as outlined in the objectives of this thesis, meant to provide a step forward in the application of TSA to laminated composite material in a quantitative manner have been fulfilled. At this stage of the research project it has became evident that there are areas that need further investigation to provide a deeper understanding in order to improve and widen the application of TSA to composite materials.

8.1.1 Numerical modelling of thermoelastic behaviour of composite laminate

The thermoelastic behavior of composite laminate depends on the fibres, resin, associated geometrical scales (i.e. yarn, fibre waviness, braided fabric) and stacking sequences. By introducing a homogenisation method, due to the limitation of the analytical solution (i.e. CLPT), to predict the thermoelastic behaviour the crucial parameter at micromechanical level are not possible to be incorporated. This limitation is even applicable to simple unidirectional materials considered in this work, where the surface variation, surface ply features, separation between the fibre and matrix regions and micro-cracks or in homogeneity present in the laminate are noticeable in the thermoelastic data. These minute effects need to be accounted for in the TSA data in order to obtain more accurate interpretation of the thermoelastic data.

Moving to the next level of complexity, where due to the stacking sequences of the laminate, there is concern for the fabrication stresses or residual stresses that develop due to the variations in coefficient of thermal expansion (CTE). These stresses superpose on mechanical loads and therefore influence the load capacity. There is still a lack of information available on the effect of residual stresses on thermoelastic response of composite material. Within the laminate the deformation of one ply is constrained by the other plies with different fibre orientations and residual stresses builds up in each ply. This will clearly have influence on the thermoelastic response and this effect is not taken in simple analytical models. Although the effect of residual stress on TSA has been investigated previously, in most TSA studies this is assumed to be negligible.

3D numerical models are needed to provide a better representation of the themoelastic behaviour in order to provide more information on the thermoelastic behaviour of the composite laminate. With the advances in the computational techniques and facilities it is possible to implement a thermoelasticity model in order to improve the fundamental understanding of the thermoelastic behaviour of the composite material.

8.1.2 Heat transfer analysis in composite medium

In order to analyse the thermoelastic behaviour of the laminate, the problem needs to be separated into two parts. First one deals with the periodic heat transfer within the composite medium. The second one is to deal with the thermoelasticity issues. The heat conduction effects in the composite material need to be modelled accurately in order to understand the heat transfer problem in a layered medium. The in depth understanding of the heat transfer issues, will allow possible development and implementation of routines that enable the TSA data to be compensated for analytically to represent the actual temperature measurements in the presence of through thickness temperature gradient as well as in the presence of in-plane temperature gradient. This will also allow the thermoelastic measurements to be taken at practical loading frequencies (between 2-5Hz).

With the level of complexity present at a the micro-structural level in composite material in mind, a control experimental model needs to be build up in order to understand the fundamental heat transfer issues. Therefore, simple representative model with well understood/ defined materials (e.g. a resin matrix and periodic metal rods) needs to be analysed to obtain the general understanding of periodic heat transfer problem in a simple laminate (i.e. a UD(0) and UD(90) configurations). This will provide the explanation for the possible heat transfer between the two distinct mediums (fibre and resin). This should be followed by incorporating the effect of stacking sequence to

account for the through thickness temperature gradient. Then, extend this work to account for the effect of geometry discontinuity in the specimen that leads to in-plane temperature gradient.

8.1.3 Material characterisation

It is well known that the mechanical and thermoelastic behaviour of E-glass is practically independent of temperature. However, taking into account the non-linear behaviour of the thermal strain of the resin as a function of temperature, more accurate characterisation methods (i.e. dilatometer or high resolution optical methods) of CTE is needed, which is a crucial parameter in defining the thermoelastic behaviour of the composite material.

8.1.4 Post processing of thermal data

It is absolutely crucial to a have clear understanding of the post-processing performed in the Cedip software in order to obtain the measured temperature change based on the acquired raw thermal data. This is particularly important since it has been shown that the thermoelastic response is possibly a combination of heat diffusion from the substrate and the thermoelastic temperature change of the surface coating. It is important to understand how the 'filtering' of the thermoelastic signal is done, since the FFT of the temperature data, will show the presence of two different loading frequencies (combination of temperature change due to the thermoelastic effect and diffusion). The two signals are not in phase. By combining the two sinusoidal temperature changes, there is a chance that either one might get removed randomly as noise in the thermoelastic data.

8.2 Conclusions

In the following section, conclusions based on the findings of Chapters 3, 4, 5, 6 and 7 are discussed.

In chapter 3, the theoretical background required to apply TSA to a composite material is presented. The important findings in this chapter are:

- Detailed analysis that shows the term $\alpha_1\sigma_1 + \alpha_2\sigma_2 + \alpha_6\sigma_6$ is an invariant, is documented in this Chapter. This is an important foundation for the following analysis

and clarifies the derivation of the thermoelastic relationship for orthotropic materials. This is particularly important when conducting quantitative analysis in components where the reference axes are not the principal stress or material axes. An example of where this is important is in Chapter 6 where the reference system is defined in polar coordinates.

- Four different theoretical approaches to define the source of the thermoelastic response from multi-directional laminates have been identified that provide the basis for the analysis in Chapter 6.
- In this chapter a strain based approach is devised for investigating the thermoelastic response from an orthotropic material.

The experimental procedures for obtaining the mechanical and physical properties of a composite material are detailed in Chapter 4.

- Material selection and the accurate material properties required for assessing the nature of the thermoelastic response is presented.

The validity and limitation of the theoretical models presented in chapter 3 are assessed in Chapter 5. The detailed analysis has shown that:

- An approach based on the 'strain witness' assumption is not suitable for calibrating the thermoelastic data for quantitative prediction of stress/ strain data.
- The thermoelastic response from a composite laminate is affected by the orientation of the surface lamina and is a function of a combination of the response from the orthotropic surface layer and the resin layer.
- Findings from the numerical analysis showed the necessity of including heat conduction properties in the thermoelastic analysis for accurate interpretation of thermoelastic signal.

In Chapter 6, analysis of the stress concentration in laminates with different fibre lay-up, focusing on circular hole is presented. In this Chapter:

- A novel attempt to examine different approaches in quantifying 'SCF$_{TSA}$' in the presence of holes in multi-directional composites is presented.
- The effect of in-plane temperature gradient on the thermoelastic response is identified with better agreement between the measured 'SCF$_{TSA}$' data and numerical models are observed away from the maximum stress concentration point.

Chapter 7 provides background for analysis of mechanical fasteners in composite joints.

- Initial experiments in isotropic material for addressing the application of TSA to characterise the stress concentration in pin-loaded joints have shown that the technique can be applied successfully to this problem.
- Due to the complex nature of the problem, the experiments need to be redesigned for composite joints to obtain stronger thermoelastic signal from TSA measurements.

Appendix A

List of publications

Sambasivam, S., Quinn, S., and Dulieu-Barton, J.M., "Thermoelastic stress analysis of composite components", Proc. of the 13th Postgraduate Conference in Engineering Materials, Southampton, 2007, 2pp.

Sambasivam, S., Quinn, S., and Dulieu-Barton, J.M., "Thermoelastic stress analysis of composite components", Poster presentation at the Novel Applications of Surface Modification (NASM 2007) Conference, University of Southampton, 2007.

Sambasivam, S., Quinn, S., and Dulieu-Barton, J.M., "The surface resin layer for strain analysis of laminated composites", Proc. SEM XI International Congress and Exposition on Experimental and Applied Mechanics, Orlando, 2008, Paper Reference 435.

Sambasivam, S., Quinn, S., and Dulieu-Barton, J.M., "Thermoelastic stress analysis of holes in laminated composite materials", Proc. SEM XI International Congress and Exposition on Experimental and Applied Mechanics, Orlando, 2008, Paper Reference 69.

Frehmann, R.K., Sambasivam, S, Dulieu-Barton, J.M., and Quinn, S., "Material properties for quantitative thermoelastic stress analysis of composite structures", Applied Mechanics and Materials, Vols. 13-14, 2008, 99-104.

S. Quinn, S. Sambasivam and J.M. Dulieu-Barton, "Derivation of the stress concentrations at holes in orthotropic plates using thermoelastic stress analysis", SEM Annual Conference and Exposition on Experimental and Applied Mechanics, Alburquerque, June 2009, Paper Reference 503.

Sambasivam, S., Quinn, S., and Dulieu-Barton, J.M., "Identification of the source of the thermoelastic response from orthotropic laminated composites", Proc. of the 17th, International Conference on Composite Materials, UK, 2009, 12pp.

References

[1] L.J. Hart-Smith. *Design and analysis of bolted and riveted joints in fibrous composite structures.* Recent advances in structural joints and repairs for composite materials. Kluwer academic publishers, 2003.

[2] J.M. Dulieu-Barton. Introduction to thermoelastic stress analysis. *Strain*, 35: 35–38, 1999.

[3] P. Bremond. New developments in thermoelastic stress analysis by infrared thermography. In *IV Pan-American conference for non-destructive testing*, 2007.

[4] K. McKenzie. Effects of surface coatings on infrared measurements of thermoelastic responses. In P Stanley, editor, *Stress and vibration: developments in industrial measurement and analysis*, volume 1084, pages 59–71, London, 1989.

[5] G. La Rosa and A. Risitano. Thermographic methodology for rapid determination of the fatigue limit of materials and mechanical components. *International journal of fatigue*, 22:65–73, 2000.

[6] P.P. Camanho and F.L. Matthews. Stress analysis and strength prediction of mechanically fastened joints in frp: a review. *Composites*, 28A:529–547, 1997.

[7] L.J. Hart-Smith. *Joints in: Engineered materials handbook*, volume 1. ASM International, Metal park, 1987.

[8] P. Stanley and W.K. Chan. Stress studies in composite cylinders based on measurement of infra-red emmisions due to cyclic loading. In *Proc. Int. Symp. on Mechanics of Polymer Composites*, 1986.

[9] P.R. Cunningham, J. M. Dulieu-Barton, A.G. Dutton, and R.A. Shenoi. Thermoelastic characterisation of damage around a circular hole in a grp component. *Key Engineering Materials*, 204-205:453–463, 2001.

[10] R. El-Hajjar and R Haj-Ali. A quantitative thermoelastic stress analysis method for pultruded composites. *Composites Science and Technology*, 63:967–978, 2003.

[11] T.R. Emery, J.M. Dulieu-Barton, J. S. Earl, and P.R. Cunningham. A generalised approach to the calibration of orthotropic materials for thermoelastic stress analysis. *Composites Science and Technology*, 68(3-4):743–752, 2008.

[12] G. Pitarresi, A. Conti, and U. Galietti. Investigation on the influence of the surface resin rich layer on the thermoelastic signal from different composite laminate lay-ups. *Applied Mechanics and Materials*, 3-4:167–172, 2005.

[13] R.K. Fruehmann, S. Sambasivam, J.M. Dulieu-Barton, and S. Quinn. Material properties for quantitative thermoelastic stress analysis of composite structures. *Applied Mechanics and Materials*, 13-14:99–104, 2008.

[14] W. Weber. Uber die specifische warme fester korperinsbesondere der metalle. *Ann d Physik u Chemie*, 96:177–183, 1830.

[15] W. Thompson. On the thermoelastic, thermomagnetic and pyroelectric properties of matter. *Trans R Soc*, 5:4–27, 1851.

[16] M. H Belgen. Infrared radiometric stress instrumentation application range study. Technical report, NASA, 1967.

[17] P. Stanley and W. K. Chan. Quantitative stress analysis by means of the thermoelastic effect. *Journal of Strain Analysis*, 20(3):93–104, 1985.

[18] J.M. Dulieu-Barton and P. Stanley. Development and applications of thermoelastic stress analysis. *Journal of strain analysis*, 33(2):93–104, 1998.

[19] G. Pitarresi and E. A. Patterson. A review of the general theory of thermoelastic stress analysis. *Journal of strain analysis*, 38(5):405–417, 2003.

[20] S. P. Timoshenko and J. N. Goodier. *Theory of elasticity*. McGraw-Hill, New York, 3 edition, 1970.

[21] G.F.C. Rogers and M. Yon. *Engineering Thermodynamics: S.I.Units: Work and Heat Transfer*. Longman, 1992.

[22] A.K. Wong, R. Jones, and J.G. Sparrow. Thermoelastic constant or thermoelastic parameter. *Journal of Physics and chemistry of solids*, 48(8):749–753, 1987.

[23] A.S. Machin, J.G. Sparrow, and M.G. Stimson. Mean stress dependence of the thermoelastic constant. *Strain*, pages 27–30, 1987.

[24] S. Quinn and J.M. Dulieu-Barton. Identification of the sources of non-adiabatic behaviour for practical thermoelastic stress analysis. *Journal of Strain Analysis for Engineering Design*, 37(1):59–71, 2002.

[25] J. McKelvie. Consideration of the surface temperature response to cyclic thermoelastic heat generation. In B.C. Gasper, editor, *Stress analysis by thermoelastic technique*, pages 56–67, London, 1987.

[26] A. Salerno and S. Desiderati. Procedure proposal for the correction of nonadiabatic thermoelastic stress analysis results. *Review of Scientific Instruments*, 75(2):507–514, 2004.

[27] I.A. Vasko. *Infrared radiation.* London: Iliffe Books Ltd, London, 1968.

[28] D.A. Scribner, M.R. Kruer, and J.M. Killiany. Infrared focal plane array technology. *IEEE*, 79(1):66–85, 1991.

[29] *SPATE/VPI 9000 series, Operators Manual*, 1992.

[30] *DeltaTherm operation manual*, 2001.

[31] J.A. Jamieson, R.H. McFee, G.N. Plass, R.H. Grube, and R.G. Richards. *Infrared Physics and Engineering.* McGraw-Hill, New York, 1963.

[32] M. G. Dreyfus. Spectral variation of blackbody radiation. *Applied optics*, 2:1113–1116, 1963.

[33] J. M. Dulieu-Barton, T. R. Emery, S. Quinn, and P. R. Cunningham. A temperature correction methodology for quantitative thermoelastic stress analysis and damage assessment. *Measurement Science and Technology*, 17(6):1627–1637, 2006. 0957-0233.

[34] *DL003U-I Altair LI user manual.* Cedip Infrared System, 2006.

[35] J.M. Dulieu-Smith. Alternative calibration techniques for quantitative thermoelastic stress analysis. *Strain*, 30:9–16, 1995.

[36] D. E. Oliver and J. M. B Webber. Absolute calibration of the spate technique for non-contacting stress measurements. In *Vth International Congress on Experimental Mechanics*, page 539546, 1984.

[37] M. J. Zickel and C. S. Welch. Thermal coating characterization using thermoelasticity. *Review of Progress in Quantitative Nondestructive Evaluation*, pages 1849–1855, 1993.

[38] P. Stanley and W.K. Chan. Spate stress studies of plates and rings under in-plane loading. *Experimental Mechanics*, 1:57–77, 1986.

[39] P. Stanley and W.K. Chan. The application of thermoelastic stress analysis techniques to composite materials. *Journal of Strain Analysis*, 23:137–143, 1988.

[40] J. M. Dulieu-Smith and P. Stanley. Developments in the interpretation of the thermoelastic response of composite materials. In *2nd Int. Symp. on Experimental Techniques and Design in Composite Materials*, pages 120–140, 1994.

[41] J.M. Dulieu-Smith and P. Stanley. The thermoelastic response of a thinwalled orthotropic cylinder loaded in torsion. In *Proc. SEM spring conference and exhibits*, pages 498–506, 1994.

[42] R.T. Potter. Stress analysis in laminated fibre composites by thermoelastic emission. In *Proceedings of the 2nd Int. Conference on Stress Analysis by Thermoelastic Techniques*, volume 731, pages 110–120, London, 1987.

[43] C.E. Bakis and K.L. Reifsnider. The adiabatic thermoelastic effect in laminated fiber composites. *Journal of composite material*, 25:809–830, 1991.

[44] A.K. Wong. A non-adiabatic thermoelastic theory for composite laminates. *Journal of Physics and chemistry of solids*, 52(3):483–494, 1991.

[45] R.T. Potter and L.J. Greaves. The application of thermoelastic stress analysis technique to fibre composites. In *Proceedings of the Conference on Optical and Opto-electronic Applied Science and Engineering*, volume 817, pages 134–146, 1988.

[46] D. Zhang, N.F. Enke, and B.I. Sandor. Thermographic stress analysis of composite materials. *Experimental Mechanics*, pages 68–73, 1990.

[47] S. Quinn. *Thermoelastic stress analysis of oblique holes in flat plates and cylinders.* PhD thesis, University of Liverpool, 2000.

[48] J.M. Dulieu-Smith. *Development and application of thermoelastic stress analysis.* PhD thesis, University of Manchester, 1993.

[49] M.C. Fulton. *Advanced topics in thermoelastic stress analysis.* PhD thesis, University of Liverpool, 1998.

[50] E. A. Patterson and R. E. Rowlands. Determining individual stresses thermoelastically. *The Journal of Strain Analysis for Engineering Design*, 43(6):519–527, 2008.

[51] J.M. Dulieu-Barton and P. Stanley. Applications of thermoelastic stress analysis to composite materials. *Strain*, 35(2):41–48, 1999.

[52] P. Stanley and C. Garroch. Improvements in the prediction and characterization of the thermoelastic response of glass-fibre reinforced composite products. *International Journal of Mechanical Sciences*, 39(2):163–172, 1997.

[53] D. Zhang and B.I. Sandor. Thermographic analysis of stress concentrations in a composite. *Experimental Mechanics*, 29(2):121–125, 1989.

[54] D. Zhang and B.I. Sandor. Advances in thermographic stress analysis and evaluation of damage in composites :testing and design. *American Society for Testing and Materials*, 10:428–443, 1992.

[55] R.A. Tomlinson and G.C. Calvert. Industrial application of tsa. *Journal of applied mechanics and materials*, 2:165–170, 2004.

[56] S.W. Boyd and J.M. Dulieu-Barton. Stress analysis of finger joints in pultruded grp material. *International journal of adhesion and adhesive*, 26(7):498–510, 2006.

[57] R.J. Greene and E.A. Patterson. Integrating thermoelastic and numerical stress method for reliable analysis. *Journal of strain analysis*, 38(4):303–312, 2003.

[58] U. Galietti, D. Modugno, and L. Spagnolo. A novel signal processing method for tsa applications. *Measurement science and technology*, 16, 2005.

[59] S.T. Lin, J.P. Miles, and R.E. Rowlands. Image enhancement and stress separation of thermoelastically measured data under random loading. *Experimental Mechanics*, 37(3):225–231, 1997.

[60] R.M. Jones. *Mechanics of composite materials*. Taylor & Francis Inc., 1998.

[61] ASTM D2584 -08 Standard test method for ignition loss of cured reinforced resins, 2008.

[62] ASTM D638-03: Standard test method for tensile properties of plastics, 2003.

[63] ASTM D7291: Standard test method for through-thickness flatwise tensile strength and elastic modulus of a fibre-reinforced polymer matrix composite material, 2007.

[64] S. W. Tsai and H. T. Hahn. *Introduction to Composite Materials*. Westport: Technomic, 1980.

[65] P.K Mallick. *Composite Materials Technology: Processes And Properties*. Marcel Dekker, 1993.

[66] Measurement of thermal expansion coefficient using strain gages. Technical report, Vishay micro measurements, 2007.

[67] ISO 11357-4 Differential scanning calorimetry (DSC) - part 4: Determination of specific heat capacity, 2005.

[68] G. Kalogiannakis, D.V. Hemelrijck, and G.V. Assche. Measurements of thermal properties of carbon/epoxy and glass/epoxy using modulated temperature differential scanning calorimetry. *Journal of Composite Materials*, 38:163–175, 2004.

[69] The pressure, strain, and force handbook, 1996.

[70] Biodata Ltd. Thermocouple accuracy. Technical report, Microlink, UK, 1996. URL `http://www.microlink.co.uk/tctable.html`.

[71] Instron. 2525-800 series load cells. Technical report, Instron Industrial Products, 2005.

[72] K. Kishore and V. Gayathri. Uncertainties in the measurements in differential scanning calorimeter and thermomechanical analyser. *Journal of Defence Science*, 31:63–71, 1981.

[73] S.A. Dunn. Analysis of thermal conduction effects on thermoelastic temperature measuraments for composite. *Journal of Applied Mechanics - Transaction of the ASME*, 59:552–558, 1992.

[74] A.K. MacKenzie. Effects of surface coatings on infrared measurements of thermoelastic responses. In *Stress and vibration: developments in industrial measurement and analysis*, volume 1084, pages 59–71, 1989.

[75] H.S. Carslaw and J.C. Jaeger. *Conduction of heat in solids.* Oxford University Press, USA, 1959.

[76] S.R. Hallett, B.G. Green, W. Jiang, K.H. Cheung, and M.R. Wisnom. The open hole tensile test: a challenge for virtual testing of composites. *International Journal of Fracture*, 158:169–181, 2009.

[77] S.C. Tan. *Stress Concentrations in Laminated Composites.* Technomic Publishing Co, 1994.

[78] G. Savin. *Stress distribution around holes.* Naukova duruka press. 1968.

[79] V.G. Ukadgaonker and D.K.N. Rao. A general solution for stresses around holes in symmetric laminates under in-plane loading. *Composite structures*, 49:339–354, 2000.

[80] Y.C. Pao and T.A. Huang. On stress-concentration analysis of laminated composite plates. In *Developments in Mechanics, 13th Midwestern mechanics conference*, volume 17, Pittsburgh, 1973.

[81] C. Kassapoglou and W.A. Townsend. Failure prediction of composite lugs under axial loads. *AIAA JOURNAL*, 41(11):2239–2243, 2003.

[82] S.G Lekhnitskii. *Theory of Elasticity of an Anisotropic Elastic Body*. Gordon and Breach Science Publishers, 1967.

[83] J.M. Whitney and R.J. Nuismer. Stress fracture criteria for laminated composites containing stress concentrations. *Jornal of Composite Material*, 8(3):253–265, 1974.

[84] R.J. Nuismer and J.M. Whitney. Uniaxial failure of composite laminates containing stress concentrations. In *ASTM special technical publication*, pages 117–142, 1975.

[85] X.P. Hana, L.X. Lib, X.P. Zhua, and Z.F. Yuea. Experimental study on the stitching reinforcement of composite laminates with a circular hole. *Composites Science and Technology*, 68(7-8):16491653, 2008.

[86] A. Russo and B. Zuccarello. An accurate method to predict the stress concentration in composite laminates with a circular hole under tensile loading. *Mechanics of Composite Materials*, 43(4):359–376, 2007. 10.1007/s11029-007-0033-z.

[87] H. Wu and B. Mu. On stress concentrations for isotropic/orthotropic plates and cylinders with a circular hole. *Composites Part B: Engineering*, 34(2):127–134, 2003.

[88] H. J. Konish and J. M. Whitney. Approximate stresses in an orthotropic plate containing a circular hole. *Journal of Composite Materials*, 9:157–166, 1975.

[89] K. Bakhshandeh and I. Rajabi. Orthotrophy and geometry effects on stress concentration factor for short rectangular plates with a centred circular opening. *The Journal of Strain Analysis for Engineering Design*, 42(7):551–555, 2007.

[90] Y. Zheng, C. Bookim, C. Cho, and H. G. Beom. The concentration of stress and strain in finite thickness elastic plate containing a circular hole. *International Journal of Solids and Structures*, 45:713–731, 2008.

[91] S.D. Pandita, K. Nishiyabu, and I. Verpoest. Strain concentration in a circular hole in composite plate. *Composite structures*, 68:361–368, 2003.

[92] S.M. Chern and M.E. Tuttle. Displacement fields around a circular hole in composite laminates. *Recent Advances in Experimental Mechanics*, 8:701–712, 2004.

[93] T. Lotfi, K. Moussa, and B. Lorrain. Stress concentration in a circular hole in composite plate. *Composite structures*, 68:31–36, 2005.

[94] M.R. Wisnom and F.K. Chang. Modelling of splitting and delamination in notched cross-ply laminates. *Composites Science and Technology*, 60:2849–2856, 2000.

[95] G.P Horn, Mackin T.J., and P. Kurath. Composite machining damage quantification using thermoelastic stress analysis. *Polymer Composites*, 23(2):193–200, 2002.

[96] U. Galietti and C. Pappalettere. Discontinuities location and assessment of scf from thermoelastic data. In *Proc. 11th Int. Conf. on Expl. Mech.*, pages 469–474, 1998.

[97] S. Barone. A technique for smoothing interior thermoelastic data and enhancing boundary information. *Strain*, 33(1):9–14, 1997.

[98] B. Rauch and R. Rowlands. Determining reliable edge isopachic data from interior thermoelastic measurements. *Experimental Mechanics*, 35(2):174 –181, 1995.

[99] R.B. Heywood. *Designing by photoelasticity.* Chapman and Hall, 1952.

[100] *ANSYS Manual (Release 9.0).* Ansys, Inc., November 2004.

[101] F.L. Matthews, G.A.O. Davies, D. Hitchings, and C. Soutis. *Finite element modelling of composite materials and structures.* Woodhead Publishing Limited, Cambridge, England, 2000.

[102] P. Stanley and J.M. Dulieu-Smith. Thermoelastic study of pin loaded lugs. In *Sixth national symposium on exp. stress analysis and matl. testing*, pages 160–169, Craiova, Romania, 1992.

[103] J. H. Hemann, R.E. Martin, and D.G. Mandic. Thermoelastic stress analysis of a pultruded composite double lap joint. In *Nondestructive evaluation of aging materials and composites III*, pages 68–72, Newport Beach, CA, 1999.

[104] Data item 81006: Stress concentration factor of axially loaded lugs with clearance-fit pins. Technical report, ESDU, 1982.

[105] W.D. Pilkey. *Petersons stress concentration factors.* Wiley-Interscience, 1997.

[106] D. Srinivasa, F. Joana, and F. Ronald. Mechanics of mechanically fastened joints in polymer-matrix composite structures - a review. *Composites Science and Technology*, 69(3-4):301–329, 2009.

[107] B.L. Okutan and R. Karakuzu. The strength of pinned joints in laminated composites. *Composites Science and Technology*, 63(6):893–905, 2003.

[108] W.J. Quinn and F.L. Matthews. The effect of stacking sequence on the pin-bearing strength in gfrp. *Journal of composite materials*, 11:139–145, 1987.

[109] H.J. Park. Effects of stacking sequence and clamping force on the bearing strengths of mechanically fastened joints in composite laminates. *Composite structures*, 53: 213–221, 2001.

[110] H. Hamada, K. Haruna, and Z. Maekawa. Effects of stacking sequences on mechanically fastened joint strength in quasi-isotropic carbon-epoxy laminate. *Journal of Composites Technology & Research*, 17:249–259, 1995.

[111] L.W. Chang, S.S. Yau, and T.W. Chou. Notched strength of woven fabric composites with moulded-in holes. *Composites*, pages 233–241, 1987.

[112] H.J. Lin, C.C. Tsai, and J.S. Shie. Failure analysis of woven-fabric composites with moulded-in holes. *Composites Science and Technology*, 55:231–239, 1995.

[113] P.P. Camanho and F.L. Matthews. Bonded metallic inserts for bolted joints in composite laminates. *IMECHE Part L Journal of Materials: Design and Applications*, 214:33–44, 2000.

[114] V. Kradinova, E. Madenci, and D.R. Ambur. Bolted lap joints of laminates with varying thickness and metallic inserts. *Composite Structures*, pages 75–85, 2005.

[115] A.R. Rispler, G.P. Steven, and L. Tong. Photoelastic evaluation of metallic inserts of optimised shape. *Composites Science and Technology*, 60:95–106, 2000.

[116] R. Li, D. Kelly, and A. Crosky. Strength improvement by fibre steering around a pin loaded hole composite structures. *Composite Structures*, 57(1-4):377–383, 2002.

[117] B. Okutan, Z. Aslan, and R. Karakuzu. A study of the effects of various geometric parameters on the failure strength of pin-loaded woven-glass-fiber reinforced epoxy laminate. *Composite Science and Technology*, 61(10):1491–1497, 2001.

[118] B. Okutan. Behaviour of pin-loaded laminated composites. *Journal of experimental mechanics*, 46:589–600, 2006.

[119] D. Liu, B.B. Raju, and J. You. Thickness effect on pin joint composites. *Journal of composite materials*, 33(1):2–21, 1999.

[120] G. Kelly and S. Hallstram. Bearing strength of carbon fibre/epoxy laminates: effects of bolt-hole clearance. *Composites Part B: Engineering*, 35:331–343, 2004.

[121] M. W. Hyer, E.C. Klang, and Cooper. D.E. The effects of pin elasticity, clearance, and friction on the stresses in a pin-loaded orthotropic plate. *Journal of Composite Material*, 21:190–206, 1987.

[122] R.A. Naik and J.H. Crews. Stress analysis method for a clearance-fit bolt under bearing loads. *AIAA JOURNAL*, 24:1348–1353, 1986.

[123] A.J. DiNicola and Fantle S.L. Bearing strength behavior of clearance-fit fastener holes in toughened graphite/epoxy laminates. *American Society for Testing and Materials*, 1206:220–237, 1993.

[124] F. Pierron, F. Cerisier, and M. Grediac. A numerical and experimental study of woven composite pin-joints. *Journal of Composite Materials*, 34(12):1028–1054, 2000.

[125] K. Zhang and C. Ueng. Stresses around a pin-loaded hole in orthotropic plates. *Journal of Composite Materials*, 18(5):432–446, 1984.

[126] A. Ruiz. Bolted joints in composites primary structures, 1988.

[127] M.M. Frocht and H.N. Hill. Stress-concentration factors around a central circular hole in a plate loaded through pin in the hole. *J. Appl. Mech.*, 7:A5–A9, 1940.